Investigating the Hydrodynamics of Potato NBLRR Rx1 Using Fluorescence Anisotropy

ALEXANDER JAMES LLEWELYN

INVESTIGATING THE HYDRODYNAMICS OF POTATO NBLRR RX1 USING FLUORESCENCE ANISOTROPY

ALEXANDER JAMES LLEWELYN

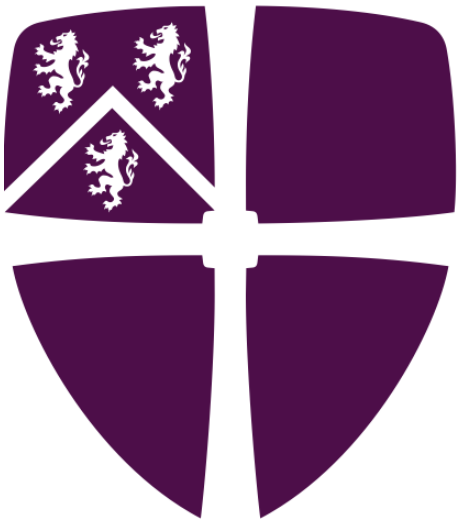

PhD Thesis

Department of Biosciences
Durham University
2020

ABSTRACT

The NBLRR family of proteins forms a vital component of the plant immune system but have poorly characterised activity and signalling. Potato NBLRR protein Rx1 confers extreme resistance to Potato Virus X and is known to exhibit DNA binding behaviour. Fluorescence anisotropy is a phenomenon characterised by the unequal emission of light by fluorophores along its axes of polarisation. This property can be exploited using polarised laser light to extract information about rotational velocity and hydrodynamic size. This thesis presents work to construct a time-resolved fluorescence anisotropy microscope system to study Rx1 *in vivo*, as well as a new method of analysing the data as a distribution of lifetimes. Lumazine Protein (LumP) was shown to be a suitable protein for these kinds of experiments, with superior properties compared to GFP. Additionally, LumP was found to act as a solubilisation factor for Rx1 *in vitro*. Anisotropy measurements using a LumP fusion demonstrated an increased size and wider distribution of sizes for Rx1 CCNBARC when bound to ATP compared to ADP. *Nb*Glk binding previously observed was confirmed by this independent method, while *Nb*DBCP was shown to abolish this binding. The solubilised LumP fusion was also shown to restore some phosphatase activity not observed in the refolded protein. Several putative protein interactors were investigated using VIGS, and EIL5 was found to be a promising hit, with silencing shown to enhance Rx1-induced immunity. Plant NBLRR NRC1 was shown to move to

DNA in response to Rx1 *in planta*. Putative SUMO binding site K506R in Rx1 was shown to be essential for Rx1 function. Rx1-LumP was shown to be functional *in vivo*, although no LumP fluorescence was observed.

The imagination of nature is far, far greater than the imagination of man.

— Richard Feynman

ACKNOWLEDGMENTS

Many people have been instrumental in bringing me to this point. The eternal optimism and pragmatism of my supervisor, Prof Martin Cann, is something to behold and got me through some difficult parts of the process. I would also like to thank Dr Lars-Olof Pålsson for acting as 'honorary' second supervisor and for patiently providing me his expertise in the mysterious art of laser microscopy.

Everyone in CG234 was great to work alongside, but thanks go especially to Vicki for providing a constant stream of ridiculous anecdotes and Buzzfeed quizzes, while taking on the responsibility of lab tyrant after the departure of Phil, who kept us all in line and whose cloning skills shall go down in legend for years to come. Thanks also go to Dave for all the late-night company in the lab and absurdist post-watershed comedy and to Chris for laying the groundwork for my PhD. Thank you also everyone that made Durham such a great place to be for so long, at Trevs, Castle, NUAS and much else besides.

Finally, thank you, of course, to my family, Liz, Ian and Abbie. You've all been incredibly supportive, never lost faith in me and I couldn't have done it without you.

DECLARATION

The work presented in this thesis is my own work, except where indicated by statement or citation and has not been submitted for any other degree. The copyright of this thesis rests with the author. No quotation from it should be published without the author's prior written consent and information derived from it should be acknowledged.

CONTENTS

LIST OF FIGURES

ACRONYMS

AC Adenylyl Cyclase

ACC Acetyl-CoA Carboxylase

ADP Adenosine Disphosphate

ARC Apaf-1, R proteins and Ced-1

ATP Adenosine Triphosphate Phosphatase xxi

ATPase Adenosine Triphosphatase

CAF1 Chromatin Assembly Factor Complex 1

cAMP Cyclic Adenosine Monophosphate

CC Coiled Coil

CFD Constant Fraction Discriminator

COP9 Constitutive Phosomorphogenesis 9

DAMP Damage-associated Molecular Patterns

DMRL 6,7-dimethyl-8-(1'-D-ribityl) lumazine

DMSO Dimethyl Sulphoxide

DOG1 Delay of Germination Protein 1

DsRed Discosoma Red

DTT Dithiothreitol

EDS1 Enhanced Disease Suscepibility 1

EDTA Ethylenediaminetetraacetic Acid

EF-Tu Elongation Factor Thermo Unstable

EGF Epidermal Growth Factor

EIX2 Ethylene-induced Xylanase

ETI Effector-triggered Immunity

ETR1 Ethylene Receptor 1

FRET Fluorescence Resonance Energy Transfer

GFP GreenFluorescence Protein xxii

GSH Glutathione

GSSG Glutathione Disulphide

GTP Guanosine Triphosphate

GTPase Guanosine Triphophate Phosphatase

HopZ ETI-deficient 1

HR Hypersensitive Response

HSP90 Heat Shock Protein 90

LB Lysogeny Broth LRR Leucine-Rich Repeat

LSD1 Lysine-specific Histone Demethylase 1

LumP Lumazine Protein

LysM Lysin Motif

MAMP Microbe-associated Molecular Patterns

MAPK Mitogen-activated Protein Kinase

MES 2-(N-morpholino)ethanesulfonic acid

NACHT Neuronal Apoptosis Inhibitor Protein, MHC Class II Transcription Activator, Heterokaryon Incompatibility Factor and Telomerase-associated Protein

NADPH Reduced Nicotinamide Adenine Dinucleotide Phosphate

NB-ARC Nucleotide-binding domain-ARC

NBD Nucleotide-binding Domain

NbGlk Nicotiana benthamiana Golden-like Kinase xxiii

NBLRR Nucleotide-Binding Leucine-Rich Repeat

NLR Nod-like Receptor

NLR-ID Nod-like Receptor Integrated Domain

NLS Nuclear Localisation Sequence

NTPase Nucleotide Triphosphate Phosphatase

PABP Poly(A)-binding Protein

PAMP Pathogen-associated Molecular Patterns

PEN1 Penetration Resistance Protein 1

Pep-13 Peptide 13

PIPES 1,4-Piperazinediethanesulphonic Acid

PTI PAMP-triggered Immunity

PVX Potato Virus X

RanGAP Ran GTPase Activating Protein

RBOH Respiratory Burst Oxidase Homologue

RLK Receptor-like Kinase

RLP Receptor-like Protein

RNP1 RNA-binding Protein 1

sAC Soluble Adenylyl Cyclase

SCF Skp, Cullin, F-box Containing

SEC Size-Exclusion Chromatography

SLiCE Seamless Ligation Cloning Extract xxiv

SOB Super Optimal Broth

SOC Super Optimal Broth with Catabolite

STAND Signal-transduction ATPases with Numerous Domains

SUMO Small Ubiquitin-like Modifiers

SWACOS STAND with Adenylyl Cyclase or Serine/Threonine Protein Kinase

TAC Time-Amplitude Converter

TAE Tris Base, Acetic Acid and EDTA

tagRFP Tag Red Fluorescence Protein

TALE Transcription Activator-like Effector

TCSPC Time-correlated Single Photon Counting

TE Tris, EDTA

TEMED N,N,N′,N′-Tetramethylethane-1,2-diamine

TIR Toll/interleukin-1 Receptor

Tris tris(hydroxymethyl)aminomethane

TRV1 Tobacco Rattle Virus 1

VAP Vesicle-associated membrane protein-associated Protein

VIGS Viral-induced Gene Silencing

VPg Viral Protein Genome-linked

WAK Wall-associated Kinase

WT Wild Type

Y2H Yeast 2-Hybrid YEB Yeast Extract Broth

ZAR1 HopZ-activated Resistance 1

ZED1 HopZ ETI-deficient 1

ZRK1 ZED-related Kinase 1

ZRK3 ZED-related Kinase 3

1

INTRODUCTION

Protein-protein interactions, oligomeric state and nucleotide binding behaviour combine to modulate the behaviour of plant R proteins. Rx1 is an R protein found in *Solanum tuberosum* that confers extreme resistance to Potato Virus X. The primary aim of this project has been to develop a fluorescence-based system to study the hydrodynamics and interactions of Rx1 *in vitro* and *in vivo* and to corroborate these findings with conventional biochemical techniques.

This chapter will cover the background of the plant immune system. Chapter 2 will discuss the mathematical basis and development of a fluorescence microscopy system that uses anisotropy to measure hydrodynamic radius. Chapter 3 will cover the background work that has been conducted on Rx1 *in vitro* and the work conducted on recombinantly expressed Rx1 during this project. Chapter 4 will cover the previous work and experiments conducted on Rx1 *in vivo.*

1.1 THE PLANT IMMUNE SYSTEM

Plants face a variety of biotic threats at the cellular level. Among the most prolific pathogens, with over 19,000 known examples (Jain et al., 2019), are fungi, as well as the fungus-like oomycetes of the Chromista kingdom, which are common sources of infection in plants and may be transported from plant to plant as spores dispersed by wind, water, soil and animal hosts. Entire crops can therefore be rapidly infected, causing devastating losses. For example, *Magnaporthe oryzae* causes

rice blast disease (Choi et al., 2013), which may lead to losses of up to 30% in annual rice yield (Talbot, 2003). With half the population of the world's primary food source being rice (Gnanamanickam, 2009), outbreaks of the disease can have devastating consequences and it has become a common model for plant fungal infections. Specialised hyphal structures called appressoria penetrate through plant cuticles and cell walls by force using turgor pressure (Ryder and Talbot, 2015) and haustoria are used to feed on intracellular components. A variety of enzymes, including glycoside hydrolases, glycosyltransferases, polysaccharide lyases, carbohydrate esterases and redox enzymes may also be used to break down plant defences and provide nutrient sources for growth (Lombard et al., 2014).

Bacteria are not commonly pathogenic to plants and the existence of pathogenic bacteria was not firmly established until long after pathogenic fungi were identified (Burkholder, 1948). Many are able to live in the apoplastic space, accessed through stomata or wounds, without significant harmful effect on the host plant. However, around 150 pathogenic species are known and typically employ enzymes and toxins to break down the cell wall. *Agrobacterium* species cause tumours to form in the host plant through horizontal gene transfer, a property which has led to their use in genetic modification experiments (Kannan, Bastas and Antony, 2015).

Viruses typically require a vector such as an insect, nematode or fungus for initial infection (Whitfield, Falk and Rotenberg, 2015). Often very simple, only a replicase, a coat protein, and a movement protein are typically required, though other more specialised genes may be present to facilitate transmission and infection (Asurmendi et al., 2004). *Tobamovirus* (Tobacco Mosaic Virus) was the first pathogen of any kind

to be identified as a virus (Beijerinck, 1898) and causes leaf discolouration and stunted growth in a variety of species, including tobacco, tomato and pepper (Creager et al., 1999). Plants can also be susceptible to infection by some protozoa (Dollet, 1984) and algae (Ponmurugan, Saravanan and Ramya, 2010), parasitisation by nematodes (Cotton et al., 2014) and other plants, as well as predation by insects and other animals.

Despite the diverse nature of these threats, plants are unable to adapt to pathogenic attacks through acquired immunity as vertebrates are, as they lack the circulatory systems to transport mobile immune cells, as well as the dedicated tissues for the production of antibodies to discriminate self and non-self. Instead, a robust innate immune system, coupled with genetically encoded resistance to specific diseases, is used to respond to infections (Nurnberger et al., 2004). Plants do not typically destroy pathogens directly, but rather employ generic resistance mechanisms that limit the spread and damage of the disease. There are two main types of immune response in plants: PAMP-Triggered Immunity (PTI) and Effector-Triggered Immunity (ETI) (J.D. Jones and Dangl, 2006).

1.2 PAMP-TRIGGERED IMMUNITY

1.2.1 *MAMPs and DAMPs*

Pathogen-Associated Molecular Patterns (PAMPs) are chemical motifs found only in, or generated only as a result of contact with, micro-organisms. These may be divided into Microbe-Associated Molecular Patterns (MAMPs) and Damage-Associated Molecular Patterns (DAMPs). MAMPs are typically macromolecules found in non-plant

microorganisms such as lipopolysaccharides in the outer cell membrane of gram-negative bacteria (Meyer, Pühler and Niehaus, 2001), and chitin in fungal cell walls (Baureithel, Felix and Boller, 1994). A key trait of MAMPs is that they are highly conserved within each group of microorganisms, with high functional importance that precludes mutation as a method of resistance. For example, Pep-13, found in an oomycete transglutaminase (Nürnberger et al., 1994), and RNP-1, a cold-shock protein in gram-negative bacteria (Felix and Boller, 2003), have regions that are highly conserved across all known orthologues and are necessary both for the proper functioning of the protein and for the elicitation of PTI.

DAMPs, by contrast, are passively generated in the host plant as a result of injury and pathogen-associated damage or released actively in response to stress. For example, plant cell walls contain linearly polymerised galacturonic acid, which is otherwise found only as a monomer under normal conditions. However, physical injury or pathogen-induced hydrolysis can release oligogalacturonides, which are known to trigger an immune response (Denoux et al., 2008). Similarly, a hormone called systemin, found in many Solanaceous species, is degraded in the initial immune response to wounding. The degraded peptide acts as a ligand for further immune signalling in other parts of the plant.

The use of Pattern-Recognition Receptors (PRRs), often Receptor-Like Kinases (RLKs) and Receptor-Like Proteins (RLPs) (Boller and Felix, 2009), allows plants to distinguish self from non-self in a similar way to antibodies in the mammalian adaptive immune system. While many MAMPs are polymeric or intracellular, plants are able to detect these signals in a variety of ways. Hydrolytic enzymes in

the apoplast attack fungal and oomycete cell walls, liberating fragments that may be detected at the plant cell surface (Liu et al., 2014), lipopolysaccharide-binding proteins can remove liphophilic acids from bacterial cell membranes (Ranf, 2016), and outer membrane vesicles containing many intracellular proteins are shed by bacteria and can be incorporated into plant cells by endocytosis (Bahar et al., 2016).

The extracellular domains of PRRs can vary wildly, with a diverse array of domains including Leucine-Rich Repeats (LRR), Lysine Motifs (LysM), Epidermal Growth Factor (EGF)-like domains, and other structures, to facilitate binding to a wide variety of molecular patterns (Yu et al., 2017). Upon binding of a PAMP to a PRR, a signalling cascade causes a systematic change in the cellular environment that reduces the virulence and spread of the invading pathogen. This is a generalised response, with very similar changes in biochemistry and gene expression observed for a wide variety of PAMPs. (Boller and Felix, 2009).

1.2.2 *Early Signalling*

Immune signalling can be rapid, with a decrease of intracellular pH within 0.5–2 minutes following PAMP exposure (Nicaise, Roux and Zipfel, 2009). This is associated with an influx of H^+ and Ca^{2+} and efflux of Cl^- and NO_3^- (Wendehenne et al., 2002) and the resulting membrane depolarisation (Mithöfer, Ebel and Felle, 2005). The exact chain of events in the early stages of signalling is poorly characterised and may vary for different receptors; however, phosphorylation appears to be the initial trigger. PRRs dimerise in a ligand-dependent way with structurally similar co-receptors (Ranf, 2017). A phosphorylation cascade leads to the activation of calcium import channels, while

calcium-dependent kinases and calmodulin trigger further downstream signalling as well as regulation of Respiratory Burst Oxidase Homologues (RBOH) (Zipfel and Oldroyd, 2017) and salicylic acid signalling, a key hormone in the plant immune response (Du et al., 2009). Elevated Reactive Oxygen Species (ROS) can be observed within 2 minutes of elicitation (Chinchilla et al., 2007) and are associated with direct antibiotic action, active defence measures by cell-wall cross-linking and downstream signalling of stress signals (Apel and Hirt, 2004).

Independently, Mitogen-Associated Protein Kinase (MAPK) pathways have been shown to be activated within 1–2 minutes of MAMP exposure (Nühse et al., 2000), leading to the activation of WRKY-type transcription factors in response to both MAMPs (Asai et al., 2002) and DAMPs (Huffaker, Pearce and Ryan, 2006). Radioactive phosphate labelling and 2D electrophoresis have demonstrated dozens of proteins, including RBOH, are phosphorylated within minutes of exposure to flg22, found in bacterial flagella (Benschop et al., 2007).

1.2.3 *Intermediate and Late Signalling*

Ethylene is used by plants as a hormone to trigger fruit ripening, flower opening and leaf shedding, and is also released in response to salt stress. l-aminocyclopropane-1-carboyxlate (ACC) synthase activity is elevated within 10 minutes of PAMP exposure (Spanu et al., 1994) and leads to a rise in ACC, the precursor, followed by ethylene. This has the effect of hastening development and senescence (Crocker and Knight, 1935) in response to infection. PRR receptors undergo endocytosis within 10–20 minutes of induction. It is unknown whether

this leads to further signalling or if it is simply a negative feedback function (Robatzek et al., 2007)

Two different MAMPs, flg22 and elf26 (from EF-Tu) were found to activate the upregulation of 1,000 genes and downregulation of 200 genes in *Arabidopsis* in almost identical patterns (Zipfel, Kunze et al., 2006), including the induction of RLK receptors as positive feedback (Zipfel, Robatzek et al., 2004). This has also been observed for both chitin (Libault et al., 2007) and the DAMP oligogalacturonic acid (Ferrari et al., 2007), indicating a common signalling pathway across a wide variety of elicitors.

Longer term effects of pathogenic infection include callose deposition to reinforce the cell wall (Gómez-Gómez, Felix and Boller, 1999), stomatal closure (Melotto et al., 2006), the production of antimicrobial compounds (Ahuja, Kissen and Bones, 2012) and seedling growth inhibition as a result of the downregulation of auxin-sensitive proteins (Navarro et al., 2006).

1.3 EFFECTOR-TRIGGERED IMMUNITY

PAMPs are highly conserved, biologically essential, and display a high degree of redundancy—many separate examples are typically found within any one species. Consequently, pathogens are rarely able to develop virulence to a host plant by gene deletion or mutation. Successful pathogens therefore must evolve methods to evade or inhibit the innate immune system (J.D. Jones and Dangl, 2006). Pathogenic bacteria typically use effector proteins to increase virulence using a type III secretion system: (S.R. Grant et al., 2006)—a protein appendage used by gram-negative bacteria to detect eukaryotic organisms and secrete proteins to aid in infection.

Two primary effector strategies exist:

1. Small molecule effectors. These are typically used to counter specific plant defences. For example, bacterial toxins can disrupt plant cellular processes such as protein synthesis and cell membrane integrity (Tamura et al., 2002). Plant hormones such as auxin can be used to reverse the effects of PTI (Abramovitch, Anderson and Martin, 2006). Exopolysaccharides can be expressed during infection to protect the cell from antimicrobial compounds (Leigh and Coplin, 1992).

2. Secreted proteins. There is a huge diversity of protein effectors used by bacterial pathogens — over thirty are employed by *Pseudomonas syringae* alone (Chang et al., 2005). Many effectors are poorly characterised; however, among the roles that have been identified are enzymes that degrade the cell wall (pectinases, endoglucanases and cellulases) (Jha, Rajeshwari and Sonti, 2005), proteases to degrade plant host proteins (Shao et al., 2002), ubiquitin ligase to disrupt host signalling processes and mark proteins for degradation (Abramovitch, Anderson and Martin, 2006) and phosphatases to disrupt kinase signalling (Espinosa et al., 2003). *Agrobacterium tumefaciens* uses a type IV secretion system to incorporate a plasmid containing hormones that induce tumorigenesis into the host's chromosomal DNA (Aguilar et al., 2010).

The evolution of these methods to evade the innate immune system has resulted in an evolutionary arms race wherein plants have developed receptors that detect effector molecules and initiate a stronger

immune response. The physiological effect of this typically resembles an extreme form of PTI, as well as a Hyper-sensitive Response (HR), leading to cell death to prevent further spread of infection (Truman, De Zabala and M. Grant, 2006). Nucleotide-Binding Leucine-Rich-Repeat (NB-LRR) proteins encoded by R genes typically recognise effectors on a 'gene-for-gene' basis that are unique to one or a handful of pathogens, unlike the many-to-one correspondence found in PTI, which responds to chemical signatures occurring in a wide variety of pathogenic and non-pathogenic microbes. Consequently, there is an enormous diversity of R proteins—over 125 are encoded in *Arabidopsis* Col-0 alone—most of which are species-specific and the signalling events that lead to ETI are poorly characterised (J.D. Jones and Dangl, 2006).

1.4 R PROTEINS

There are around 14,000 plant NB-LRR– (or NLR–) encoding genes currently identified, with many species containing hundreds of unique examples (Sarris, Cevik et al., 2016); however, the vast majority are uncharacterised, with only 191 having been identified as R genes. There are a further 123 identified R genes encoding proteins in a variety of different families. Of these 314 R genes, only 128 have a proposed mechanism, with an even smaller number being experimentally verified (Kourelis and R.A. Van Der Hoorn, 2018). Nine primary response mechanisms have been identified, with examples given in Table 1.1.

1.4.1 *Mechanisms*

1.4.1.1 *Direct intracellular detection*

The most common R protein mechanism is intracellular detection by NLRs. Direct interactions with effector proteins have been identified for several NLRs (Goritschnig et al., 2016; Zhu et al., 2017). This detection can be extremely specific. For example, NLR Recognition of *Peronospora parasitica* 1 (RPP1), which directly interacts with oomycete pathogen *Hyaloperonospora arabidopsidis* effector *Arabidopsis thaliana* Recognised 1 (ATR1), has several different alleles with distinct specificities for different alleles of the elicitor (Steinbrenner, 2015). Flax contains three allelic genes, L5, L6 and L7, which bind the fungal pathogen *Melampsora lini* effector AvrL567. These variants have differing specificities for variants in the effector, allowing for greater coverage of pathogens (Dodds et al., 2006).

This specificity is conferred by changes in the LRR domain, but activity is also affected by polymorphisms in other domains, suggesting a mechanism in which intramolecular interactions compete with effector binding (Ravensdale et al., 2012). Furthermore, effector binding has been shown to stabilise the 'on' state of the receptor, while unbound receptors exist in an equilibrium (Bernoux, Burdett et al., 2016). In particular, the interaction between the LRR and the NB-ARC domain may be key: binding of viral movement protein NSm^{21} to tomato NLR Sw-5b destabilises this interaction to trigger ETI (Zhu et al., 2017).

Sw-5b is also an example of a plant NLR with homologues possessing very different affinities. While the L5/L6/L7 family of proteins recognise variants of the same effector, the potato homologue of Sw-5b, R8, recognises a sequence-unrelated oomycete effector (Vossen et al.,

2016). This suggests very small changes in sequence can create large changes in specificity, though it is unknown whether these changes are only possible due to these sequence-unrelated effectors adopting a similar fold. In any case, interactions between the NLR and its effector, as well as intra-domain interactions, are finely balanced to enable highly specific immune responses to a wide variety of threats.

Two main categories of NLR are identified, featuring at their N-terminus either a Toll/Interleukin-1 Receptor (TIR) or a Coiled Coil (CC) domain (J.D. Jones and Dangl, 2006). The structure and function of NLR proteins are discussed in greater detail in 1.4.3.

1.4.1.2 *Indirect intracellular detection*

A number of plant NLRs are dependent on the expression of specific accessory proteins for an effector-induced immune response. While the function of these accessory proteins is not always clear, one model predicts they function as 'guard' proteins, which may allow the detection of multiple effectors by a single R protein by acting as adaptors (Dangle and J.D.G. Jones, 2001). In the guard model, rather than binding an effector directly, which may be evolutionarily circumvented in a successful pathogen by a mutation in the binding surface, an R protein instead recognises a change induced in an accessory protein upon effector binding. Central to this model is that the effector function (and pathogen virulence) is dependent upon this binding and the conformational change induced. This drastically reduces a pathogen's ability to develop resistance to a plant's immune system, because the conformational change in the host protein triggered by binding is essential for effector function, and allows the R protein to detect the presence of several different effectors with the same mode of action (J.D. Jones and Dangl, 2006).

More recent evidence has led to the development of the 'decoy' model. This is due to the contradictory evolutionary pressures implicit in the guard model: in the absence of a compatible R protein, a guard is pressured to reduce binding affinity with a pathogen effector in order to reduce its virulence effect. However, in the presence of an R protein, this pressure is reversed, in order to optimise detection of the pathogen. This results in evolutionary instability inconsistent with the long-term survival of both the R protein and guard in a population. Decoy proteins evolve to mimic the effector target (such as by gene duplication), but lack other functionality in disease resistance. This serves to both competitively inhibit binding to the functional target by sequestering the effector and optimise decoy binding to the R protein (R.A.L. Van Der Hoorn and Kamoun, 2008).

ZAR1 (HopZ-Activated Resistance 1) is an *Arabidopsis* CC-NLR that confers ETI in response to a number of effectors. ZED1 (HopZ ETI-Deficient 1) is a pseudo-kinase that is acetylated by HopZ1a, an effector from *Pseudomonas syringae*, whereupon it binds ZAR1 and triggers ETI. As a *ZED1* gene knockout does not itself impair pathogen virulence (Lewis et al., 2013), it may be acting as a biosensor to monitor pathogenic acetylation of other related kinases. ZED-1 Related Kinases, ZRK1 (also known as RKS1), and ZRK3 are also involved in ZAR1-triggered resistance. Upon its uridylation by AvrAC from *Xanthomonas campestris*, PBL2 (PBS1-Like kinase 2) binds ZRK1, which in turn binds ZAR1 (G. Wang et al., 2015). ZRK3 meanwhile acts similarly for an unidentified kinase upon its ADP-ribosylation by HopF2a (Seto et al., 2017). This demonstrates how a variety of strategies may be combined in one R protein: ZED1 is a decoy, its homologues ZRK1 and ZRK3 act as simple adaptor proteins, while PBL2 is likely a classical guard

protein as it is involved in the detection of certain PAMPs such as flg22 and elf18 (Zhang et al., 2010), suggesting it is a direct target of immune suppression by the pathogen.

1.4.1.3 *Integrated domains*

NLRs may contain Integrated Domains (NLR-IDs) that are important in effector recognition. RRS1 is an *Arabidopsis* TIR-NLR containing an WRKY DNA binding domain at its C-terminus. Acting as an in-built decoy, this facilitates detection of AvrRps4 from *P. syringae*, which interacts with a variety of WRKY proteins, leading to heterodimerisation with TIR-NLR Rps4 and an associated immune response. A secondary effector appears to have evolved later: PopP2 acetylates WRKY proteins and abolishes recognition of AvrRps4 in the RRS1-S allele. However, the RRS1-R allele has developed the ability to initiate an immune response following this acetylation; it appears this is triggered by the inhibition of DNA binding upon acetylation as an inhibitory Leucine insertion at the DNA binding site triggers a constitutive immune response in the RRS1-R allele only (Sarris, Duxbury et al., 2015). Integrated domains are therefore able to carry out the function of a separate decoy protein and the evolutionary arms race between plants and pathogens is clearly demonstrated in the sequential development of pathogenic effector→host receptor→receptor inhibitor→receptor adaptation.

1.4.1.4 *Executor genes*

Executor genes are a rare form of plant defence in response to Transcription Activator-Like Effectors (TALEs), produced by *Xanthomonas* species. These effectors bind to DNA promoter sequences to promote pathogenic susceptibility. Executor genes function as a decoy, with resistance genes being activated by promoter traps. Bs3 is controlled

by such a promoter trap and encodes a flavin monooxygenase, homologues of which have been shown to be involved in the plant immune response, either by detoxification of pathogen virulence factors (Schlaich, 2007) or modulating the redox state of the plant, which has been shown to be important in regulating defence responses (Mou, Fan and Dong, 2003).

1.4.1.5 *Direct perception at the cell surface*

RLKs and RLPs are the primary receptors for PTI (Boller and Felix, 2009); however, there are also a variety of these proteins involved in ETI. The terms RLK and RLP describe a wide variety of proteins characterised by an extracellular ligand-binding domain, a transmembrane domain and a cytoplasmic domain, which is a kinase in the case of RLKs. The extracellular domain is frequently an LRR: LeEIX2 is an example of an LRR-RLP and binds directly to Ethylene-Inducing Xylanase, which is an effector produced by *Trichoderma viride* that breaks down cell walls (Walia et al., 2017). The signal transduction mechanism of LeEIX2 and other RLPs is not known; however, it may occur by an interaction with a conjugate RLK upon ligand binding (Tör, Lotze and Holton, 2009). In addition to the more common LRR-RLK structures, there are known to be several RLKs with different extracellular domains, including a G-Lectin–S-Domain (Catanzariti, Lim and D.A. Jones, 2015), Wall-Associated Kinase (WAK) (Zhong et al., 2017) and a cysteine-rich domain (Zhou et al., 2007). It is not known whether any of these other types of RLK bind their ligand directly or indirectly.

1.4.1.6 *Indirect perception at the cell surface*

As well as direct ligand binding, a decoy or guard protein may be used. Rcr3 is an extracellular papain-like cysteine protease that is in-

hibited by the *Cladosporium fulvum* effector Avr2. The inhibited protein is detected by the R protein Cf-2, triggering an immune response. A strength of this method of detection is illustrated by the fact that a protein found in the secretions of the nematode *Globodera rostochiensis*, Gr-VAP, which has no sequence similarity to Avr2, triggers a similar response upon inhibiting Rcr3 (Lozano-Torres et al., 2012). This therefore enables the plant to respond to a particular pathogenic strategy rather than the structure of a specific protein, which may vary between species or evolve to evade detection.

1.4.1.7 *Active Loss of Susceptibility*

Also known as S genes (Schie and F.L. Takken, 2014), it is possible for plants to adapt to pathogen attack by the evolution of mutant proteins or variable expression of key genes that reduces a pathogen's virulence. There are three main types of loss-of-susceptibility mechanisms. Active loss of susceptibility describes the expression of proteins that directly disrupt a pathogen's ability to infect the host. *Hm1* was the first cloned R gene and falls into this category. The gene controls the expression of an NADPH-dependant reductase in maize that specifically detoxifies the HC toxin produced by the fungus *Cochliobolus carbonum* (Johal and Briggs, 1992)

1.4.1.8 *Passive Loss of Susceptibility*

Passive loss of susceptibility describes the loss of an interaction of a pathogen effector important for virulence with a host protein. In principle, any cellular genes that are involved in pathogen infection may act as recessive R genes. The vast majority of such genes are involved in translation and the initiation factors of the 4E/4G family are the most well-characterised (Schmitt-Keichinger, 2019). eIF4E factors bind to the 5'-end of an mRNA transcript (a 7-methylated guanosine

cap), while Polyadenosine Binding Protein (PABP) binds to the Poly-A 3'-end. Both proteins bind to eIF4G, leading to circularisation of the transcript and the resulting complex is responsible for recruiting further factors including the eIF4A helicase and the 43S preinitiation complex (Merrick and Pavitt, 2018). Viral RNA molecules lacking a 5'-cap require effector proteins for translation to take place; the VPg protein in potyvirids has been demonstrated to play such a role in its interaction with eIF4E. This factor was the first known example of a recessive R gene, with a mutant in pepper lacking VPg interaction conferring resistance to Potato Virus Y (Ruffel et al., 2002) and Lettuce Mosaic Virus (Duprat et al., 2002).

1.4.1.9 *Host Reprogramming*

Host reprogramming describes recessive or dominant-negative traits conferred by alleles of genes involved in cell signalling. For example, the Mildew Locus O (MLO) gene acts as a negative regulator of cell death in response to biotic and abiotic stresses. In particular, it negatively regulates pathways activating PEN1 (a syntaxin involved in vesicle-associated defence), and PEN2 (a myrosinase) and PEN3 (an ATP-Binding Cassette transporter), involved in efflux of toxic secondary metabolites. A loss of function allele in the MLO gene leads to resistance to a variety of powdery mildews in both monocots and dicots (Humphry et al., 2010).

Table 1.1: Examples of R proteins with different mechanisms

MECHANISM		PROTEIN	HOST	PATHOGEN	TRIGGER	KINGDOM	
Extracellular							
Direct	LRR-RLP	LeEIX2	Tomato	*Trichoderma viride*	EIX	Fungi	[1]
	LRR-RLK	XA21	Rice	*Xanthomonas oryzae* pv. *oryzae*	RaxX	Bacteria	[2]
Indirect	LRR-RLP	Cf-2 (guard: Rcr3)	Tomato	*Cladosporium fulvum* & *rostochiensis*	Avr2 & GrVAP1	Fungi/Nematode	[3]
Unknown	G-Lectin–S-RLK	I-3	Tomato	*Fusarium oxysporum* f.sp. *lycopersici*	Avr3	Fungi	[4]
	WAK-RLK	Stb6	Wheat	*Zymoseptoria tritici*	AvrStb6	Fungi	[5]
	Cysteine-rich-domain–RLK	TaRLK-R1/2/3	Wheat	*Puccinia striiformis* f.sp. *tritici*	Unknown	Fungi	[6]
Intracellular							
NLR, direct	TIR-NLR	RPP1	*Arabidopsis*	*Hyaloperonospora arabidopsidis*	Atr1Ndwsb	Oomycete	[7]
	CC-NLR	Sw-5b	Tomato	Tomato spotted wilt virus	Nsm	Virus	[8]
NLR, indirect	TIR-NLR	N (guard: NRIP1)	Tobacco	Tobacco mosaic virus	p50	Virus	[9]
	CC-NLR	Rx1 (guard unknown)	Potato	Potato Virus X	CP105	Virus	[10]
	NLR-ID						
NLR-ID	TIR-NLR-ID	RPS4/RRS1	*Arabidopsis*	*Pseudomonas syringae* pv. *pisi* & pv. *tomato*	AvrRps4 & PopP2		[11]
	CC-NLR-ID	RGA4/RGA5	Rice	*Magnaporthe oryzae*	Avr-Pia	Fungi	[12]
	Executor	Bs3	Pepper	*Xanthomonas campestris* pv. *vesicatoria*	AvrBs3	Bacteria	[13]
	Loss of susceptibility						
	Active	Hm1	Maize	*Cochliobolus carbonum*	HC toxin	Fungi	[14]
	Passive	Mo-1	Lettuce	Lettuce mosaic virus	N/A	Virus	[15]
	Reprogramming	Mlo	Barley	*Erysiphe graminis* f. sp. *hordei*	N/A	Fungi	[16]

[1]Ron and Avni (2004) [2]Pruitt et al. (2015) [3]Lozano-Torres et al. (2012) [4]Catanzariti, Lim and D.A. Jones (2015) [5]Zhong et al. (2017) [6]Zhou et al. (2007) [7]Goritschnig et al. (2016) [8]Zhu et al. (2017) [9]Caplan et al. (2008) [10]W.I.L. Tameling and Baulcombe (2007) [11]Sarris, Duxbury et al. (2015) [12]Okuyama et al. (2011) [13]Römer et al. (2007) [14]Johal and Briggs (1992) [15]Nicaise, German-Retana et al. (2003) [16]Büschges et al. (1997)

1.4.2 *NLR Classification*

1.4.2.1 *STAND proteins*

NLRs are part of the Signal-Transduction ATPases with Numerous Domains (STAND) family of proteins found in all kingdoms of life. STAND proteins are characterised by their large size and core P-loop ATPase domain, referred to as the Nucleotide-binding Oligomerisation Domain (NOD), bound to a sensor domain and a signalling domain. STAND proteins are related to the large AAA+ family of ATPases, which are typified by:

Nucleotide Binding Domain	Walker A—Also known as the P-Loop, binds the β-phosphate of ATP
	Walker B—Coordinates Mg^{++}, essential in ATP hydrolysis
	Sensor I—Coordinates a water molecule for nucleophilic attack on ATP
	Arginine finger
Four-helix 'lid' Domain	Sensor II—Binds to the γ-phosphate of ATP

(Erzberger and Berger, 2006)

These two domains mediate oligomerisation, with the nucleotide bound by the Sensor I & II and Walker A & B domains of one protein and the arginine finger of another. AAA+ proteins function as molecular switches, with conformational changes inducing oligomerisation upon ATP binding. Modulating this process can allow diverse

signalling behaviour ranging from slow, highly regulated bimodal switching, to continuous cycles of binding and hydrolysis with associated molecular motor behaviour. While retaining sequence and structural similarity, some AAA+ proteins lack ATP-binding activity altogether—Orc4 and Orc5 act as signal modulators within oligomeric complexes of active ATPases in the eukaryotic Origin Recognition Complex (Erzberger and Berger, 2006).

The NOD domain in STAND proteins derives from this AAA+ core, with a C-terminal Winged-Helix Domain (WHD), but lacks sensor II and, typically, the arginine finger. Most diagnostic of this family is an hhGRExE motif N-terminal of Walker A and a GxP motif C-terminal of the NOD domain. There are five classes of STAND proteins (Leipe, Koonin and Aravind, 2004).

1.4.2.2 *AP-ATPase*

This class contains plant NLRs as well as animal apoptosis regulators Apaf-1 and CED-4, and bacterial AfsR-like and CalR2 transcriptional regulators. AP-ATPase proteins frequently contain C-terminal superstructures such as LRRs or WD40 domains, while the N-terminus often features DNA-binding Helix-turn-helix domains or protein-protein interaction domains such as TIR and death-like domains.

1.4.2.3 *NACHT*

Named after its representatives, neuronal apoptosis inhibitor protein NAIP, MHC class II transcription activator CIIA, heterokaryon incompatibility factor HET-E, and telomerase-associated protein TLP1, the NACHT class of STAND proteins are also regulators of apoptosis in animals and frequently show a preference for GTP over ATP. Like AP-ATPases, the C-terminus is typically a repeating superstructure, while the N-terminus shows a great degree of diversity.

1.4.2.4 *SWACOS*

Standing for STAND With Adenylyl Cyclase or Ser/Thr protein kinase, SWACOS do not contain repeating C-terminal structures. One subfamily contains soluble Adenylyl Cyclase (sAC), distinct from the majority of ACs that are membrane-bound. Mammalian sAC is responsible for the capacitation of sperm by way of cAMP accumulation. LipR is a bacterial transcriptional activator with a C-terminal LuxR-type helix-turn-helix domain and lacks any N-terminal domain. The DhkG family is characterised by an N-terminal Ser/Thr kinase and a C-terminal HupT-type histidine kinase.

1.4.2.5 *MalT*

The MalT class is characterised by a C-terminal superhelical peptide repeat. MalT is responsible for regulating the maltose operon, while AlkS regulates an alkane-utilisation operon.

1.4.2.6 *MNS*

The MNS class is characterised by the lack of a arginine in strand 4 of the NOD found in all other STANDs, and the presence of an arginine in strand 5 at the location of the arginine finger of AAA+ ATPases. These proteins typically lack both an effector and sensor domain, but may act in conjunction with partner proteins (Danot et al., 2009; Leipe, Koonin and Aravind, 2004).

1.4.3 *NLR Structure and Function*

The four domains of NLR proteins, the CC and TIR (which are interchangeable), the NBD, and the LRR, each evolved separately before the prokaryote-eukaryote split but are only found together as part of the same protein in land plants (Yue et al., 2012); however, the

fusion is nonetheless ancient, being found in primitive bryophytes that branched off from the rest of the kingdom 450 million years ago (Xue et al., 2012).

1.4.3.1 *CC Domain*

A coiled coil comprises two or more α-helices forming bundles that supercoil around each other (Crick, 1953). They typically contain a Leucine-rich heptad of residues: the first and fourth positions are usually hydrophobic, forming the hydrophobic core of the coiled coil, while the fifth and seventh are usually charged residues that form salt bridges and electrostatic interactions to stabilise the structure. Considerable diversity exists, with bundles of 2, 3, 5, 7 and 12 helices having been observed, and functions include DNA binding and repair, protein-protein interactions, structural and cytoskeletal roles and motor protein activity (Testa, Moutevelis and Woolfson, 2009).

The CC domain within NLRs displays significant sequence diversity, with the exception of the EDVID consensus sequence found in most CC-NLRs (Rairdan et al., 2008). A smaller class of coiled coil, denoted $CC_{R,}$ is found in an ancient clade of NLRs (Collier, Hamel and Moffett, 2011). The crystal structure for the Mla10 CC has been solved and consists of two antiparallel α-helices connected by a short loop. These dimerise and form an elongated four-helix bundle (Maekawa, Cheng et al., 2011). A different arrangement was observed in the crystal structure of the Rx1 CC in complex with its cofactor RanGAP, indicating a compact monomeric four-helix structure (Hao et al., 2013). As sequence similarity is low (18%), this may represent a genuine difference in structure or an effect of cofactor binding. However, the NMR structure of Sr33 indicates a similar structure to Rx1, indicating RanGAP2 binding is not necessary for the compact structure.

Furthermore, size-exclusion chromatography (SEC) multiangle light scattering techniques indicate that the CCs of Sr33, Rx1 and Mla10 are all monomeric in solution, while SEC small-angle X-ray scattering suggested similar shapes consistent with the more compact four-helix structure (Casey et al., 2016).

Other work has shown $Sr33^{6\text{-}120}$and $Mla10^{5\text{-}120}$ do not dimerise *in planta* nor induce cell death, but longer 1-160 constructs both dimerise and induce cell death (Cesari et al., 2016). *In vitro* work has confirmed some dimerisation of $Sr33^{6\text{-}144}$ and $Mla10^{5\text{-}144}$(Casey et al., 2016). These data suggest that CC dimerisation may be important in its functionality.

1.4.3.2 *TIR Domain*

The Toll-Interleukin Receptor (TIR) takes the place of the CC in many NLRs. Its structure comprises a flavodoxin-like fold of a five-stranded parallel β-sheet surrounded by five α-helices. Its primary function is as a protein scaffold, particularly in the formation of homotypic interactions with other TIR domains (Ve, Williams and Kobe, 2015). For plant R proteins, homodimerisation has been observed for L6 (Bernoux, Ve et al., 2011) and AtTIR (Chan et al., 2010), while heterodimerisation has been observed for RRS1 with RPS4 (Williams, Sohn et al., 2014). The interface surface differs between the L6 homodimer and the AtTIR and RRS1/RPS4 dimers.

1.4.3.3 *NB-ARC Domain*

The central NB-ARC domain contains a nucleotide-binding domain, ARC1 and ARC2 (standing for Apaf-1, R proteins and Ced-4). The NB domain contains a parallel β-sheet P-loop NTPase that coordinates a Mg^{++} ion and water molecule as well as an ATP molecule (Leipe, Koonin and Aravind, 2004). ARC1 contains the diagnostic GxP motif

characteristic of STAND proteins, while the ARC2 domain is the winged-helix domain. Both ARC domains coordinate the adenine of the nucleotide (Danot et al., 2009). Homology modelling suggests the domain as a whole adopts a compact globular structure forming a closed nucleotide-binding pocket (Sela et al., 2012). ATPase activity in this domain may control signalling in some R proteins (W.I.L. Tameling, Elzinga et al., 2002). The standard model for this entails an auto-inhibited state while bound to ADP. Binding to an effector molecule is thought to trigger the exchange of ADP for ATP, putting the protein in an 'on' state (F.L.W. Takken and W.I.L. Tameling, 2009).

1.4.3.4 *LRR Domain*

The LRR is the most variable part of many NB-LRR proteins, containing repeats of different lengths and various non-canonical motifs (F.L.W. Takken and Goverse, 2012), with positive selection acting on a large number of very variable solvent-exposed amino acid residues (Sela et al., 2012), suggesting involvement in effector recognition. Structural modelling suggests a horseshoe-like structure with cationic residues on the LRR N-terminus interacting with the C-terminus of the NBARC domain, while aromatic residues on its C-terminus may interact hydrophobically with the EDVID region of the CC domain (Rairdan et al., 2008), maintaining an autoinhibited structure. Mutations in these regions that may disrupt these interactions can result in constitutive activation or inhibition, which is suggestive of a finely balanced equilibrium (F.L.W. Takken and Goverse, 2012).

1.4.3.5 *Interactors*

HSP90, Rar1 and SGT1 are important chaperone proteins that may be involved in the maintenance of this equilibrium. HSP90 and Rar1 interact with a number of NLRs, and their suppression results in com-

promised immunity (Kadota, Shirasu and Guerois, 2010). SGT1 plays a complex role in regulating the folding and degradation of NLRs, binding NLRs to the HSP90-Rar1 chaperone complex to facilitate proper folding (Kadota, Amigues et al., 2008), while also binding the SCF (Skip1–Cullin–F-Box) complex, a ubiquitin E3 ligase that promotes protein degradation (Catlett and Kaplan, 2006). SGT1-Rar1 also interacts with the COP9 signalosome, which regulates the SCF. Together, these proteins appear to regulate the proper folding and turnover of R proteins. Several negative regulators of NLRs have also been identified, including CRT1 (Compromised Recognition of TCV) (Kang et al., 2010) and SRFR1 (Suppressor of'RPS4-RLD1) (Li et al., 2010).

1.4.3.6 *Signalling*

Whether by direct interaction with an effector or by interaction with a guard/decoy protein, activation of R proteins appears to be transduced by lifting of autoinhibition by the LRR. In the inhibited state, the NBARC domain is bound to ADP in a wide variety of R proteins (W.I.L. Tameling, Elzinga et al., 2002; Williams, Sornaraj et al., 2011). Comparisons of the crystal structures of related animal STAND proteins Apaf-1 bound to ADP and CED-4 bound to ATP indicate a conformational change occurs upon effector binding whereby the NB/ARC1 domain rotates with respect to the ARC2 domain, creating a more open structure to enable binding of ATP. This is consistent with experiments that have shown that ATPase-deficient I-2 is constitutively active (W.I. Tameling, Vossen et al., 2006) and an autoactive mutant of M co-purifies with ATP (Williams, Sornaraj et al., 2011).

Downstream signalling of R proteins is poorly understood and the necessary domains appear to vary between R proteins, with some resulting in an immune response with only the N-terminal CC or TIR

domain in MLA10 (Maekawa, Kufer and Schulze-Lefert, 2011) and RPS4 (Bernoux, Ve et al., 2011) respectively, while for others, such as Rx1, the NB is necessary and sufficient (Rairdan et al., 2008). Dimeric and oligomeric assemblies have also been observed both before (Gutierrez et al., 2010) and after (Bernoux, Ve et al., 2011) activation. Cryo-EM experiments have revealed the inactive state of ZAR1 is maintained by the LRR domain, which maintains a monomeric state by interaction with NB-bound ADP and the CC domain: RKS1 binds to the LRR and is activated and stabilised by interactions with uridylated sites on PBL2, while steric clashing between the ADP-bound NB domain and the activated RKS1 protein triggers a conformational change that results in the release of ADP (J. Wang, J. Wang et al., 2019). Full activation is triggered by ATP binding which results in the formation of a cyclic pentamer, maintained by interactions of all the domains of ZAR1 (J. Wang, Hu et al., 2019). This suggests oligomerisation may be a vital part of R protein signalling.

2

CONSTRUCTION OF A FLUORESCENCE ANISOTROPY MICROSCOPE SYSTEM

2.1 INTRODUCTION

Fluorescence anisotropy may provide a useful method to investigate the structure and interactions of Rx1 and other proteins under various conditions both *in vitro* and *in vivo*. The central aim of this method is to calculate a rotational correlation time, ψ. This provides a measure of the speed of rotation of a molecule in solution. This value can be defined by the Stokes-Einstein equation (O'Reilly and Peterson, 1970):

$$\psi = \frac{V\eta}{kT}, \tag{2.1}$$

where

- η viscosity
- T temperature
- V particle volume
- k Boltzmann constant

This relationship makes a number of assumptions that are not strictly true at the molecular level, including that all particles are perfectly spherical. Nonetheless, the rotational lifetime provides a qualitative indication of a protein's volume or moment of inertia. This may be useful for determining protein binding, oligomerisation and structural changes.

Anisotropy refers to a type of metric that measures how a property of a sample depends on direction, such as how the properties of a magnet depend on its orientation. In the case of fluorescence anisotropy, anisotropic properties must usually be introduced into an otherwise isotropic (randomly orientated) sample. This may be achieved by excitation of a fluorophore using polarised light (such as a laser) in a process known as photoselection. This preferentially excites those molecules whose fluorescence dipoles are parallel to the polarisation of the excitation. After a fluorophore is excited, energy is released in the form of light polarised parallel to the emission dipole. Measuring the extent of polarisation of the emitted light allows for the calculation of the rotational lifetime (Jabłoński, 1960).

2.1.1 *Calculating r_0*

Consider a single stationary molecule. The orientation of such a molecule may be described by terms denoting the angle of its dipole relative to an arbitrary coordinate system, in this case its angle with respect to the Z-axis, θ, and the angle of its projection in the XY plane with respect to the Y-axis, φ as seen in 2.1. As the dipole is radially symmetrical, only two terms are required to fully described its orientation. The projections of the electric field of an emitting fluorophore modelled as a radiating dipole along the Z and Y axes are therefore $\cos\theta$ and $\sin\theta \sin\varphi$.

The intensity of fluorescence emission polarised along an axis is proportional to the square of the electric field's projection on that axis, while its polarisation is perpendicular to the dipole moment. Thus the relative intensities of light emitted by a fluorophore parallel, $I_{\parallel}$, and

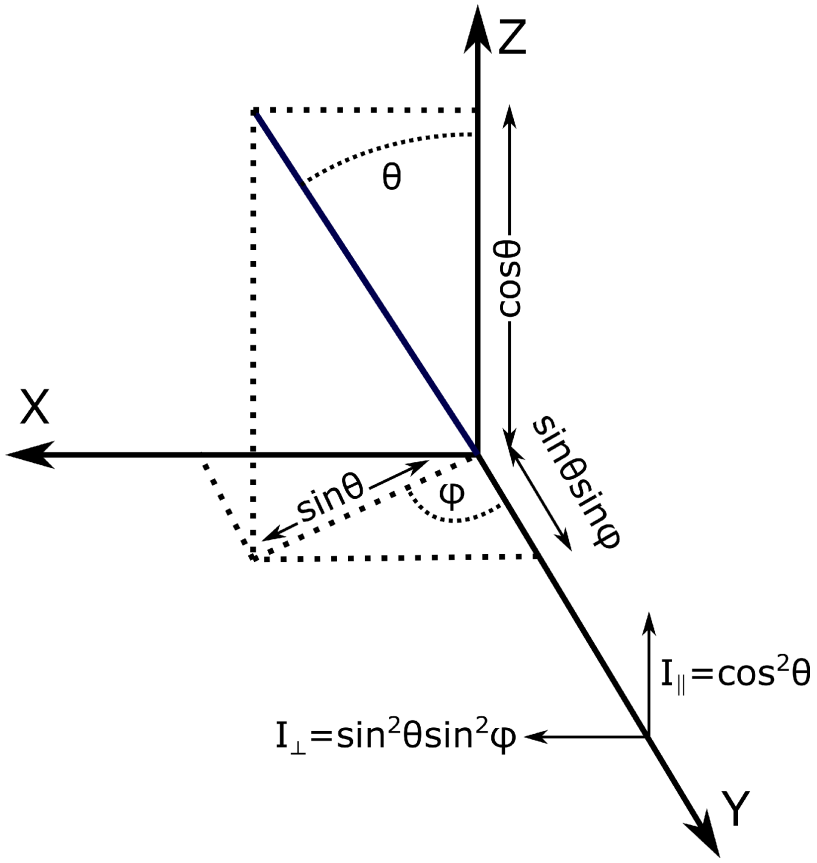

Figure 2.1: The orientation of a fluorophore can be described by two angular parameters, θ and φ.

perpendicular, $I_\perp$, to the Z-axis can be written (Melville, Lucieer and Aryal, 2006):

$$I_\parallel(\theta, \varphi) = \cos^2\theta \tag{2.2}$$

$$I_\perp(\theta, \varphi) = \sin^2\theta \sin^2\varphi. \tag{2.3}$$

Now consider a system of fluorophores oriented randomly about the Z-axis for a given value of θ. The number of molecules with an angle between φ and $\varphi + \mathrm{d}\varphi$ is proportional to $\mathrm{d}\varphi$ and thus has probability density function

$$p(\varphi) = \mathrm{d}\varphi. \tag{2.4}$$

The expected value of a function $f(x)$ over a range $k < x < k + i$ is

$$\langle f(x) \rangle = \frac{\int_k^{k+i} f(x)p(x)}{\int_k^{k+i} p(x)}, \tag{2.5}$$

per (Papoulis, 1984). Thus

$$\left\langle \sin^2\varphi \right\rangle = \frac{\int_0^{2\pi} \sin^2\varphi d\varphi}{\int_0^{2\pi} d\varphi} d\varphi = \frac{1}{2} \qquad \text{by 2.5} \tag{2.6}$$

$$I_\perp(\theta, \varphi) = \frac{\sin^2\theta}{2}. \qquad \text{by 2.2, 2.3 and 2.8} \tag{2.7}$$

Note that both $I_{\parallel}$ and $I_{\perp}$ are now independent of φ. We define fluorescence anisotropy per (Jabłoński, 1960):

$$\begin{aligned} r &= \frac{I_{\parallel} - I_{\perp}}{I_T} \\ &= \frac{I_{\parallel} - I_{\perp}}{I_{\parallel} + 2I_{\perp}}. \end{aligned} \tag{2.8}$$

The total intensity is equal to $I_{\parallel} + 2I_{\perp}$ because there are two orthogonal directions perpendicular to the plane of excitation.

For an excitation polarised in the Z-direction, this becomes:

$$\begin{aligned} r(\theta) &= \frac{\cos^2\theta - \frac{1}{2}\sin^2\theta}{\cos^2\theta + \sin^2\theta} && \text{by 2.3 and 2.7} \\ &= \frac{3\cos^2\theta - 1}{2}. && \text{using the identity } \sin^2\theta + \cos^2\theta = 1 \end{aligned} \tag{2.9}$$

Now permit θ to vary. Note that this is not a uniform distribution as with φ, because the number of molecules at an angle between θ and $\theta + \mathrm{d}\theta$ is proportional to the surface of the sphere sector it inscribes (see 2.2), so

$$p(\theta) = \sin\theta \mathrm{d}\theta. \tag{2.10}$$

Thus in a randomly orientated system of fluorophores,

$$\begin{aligned} \left\langle \cos^2\theta \right\rangle &= \frac{\int_0^{\frac{\pi}{2}} \cos^2\theta \sin\theta \mathrm{d}\theta}{\int_0^{\frac{\pi}{2}} \sin\theta \mathrm{d}\theta} && \text{by 2.5 and 2.10} \\ &= \frac{1}{3}. \end{aligned} \tag{2.11}$$

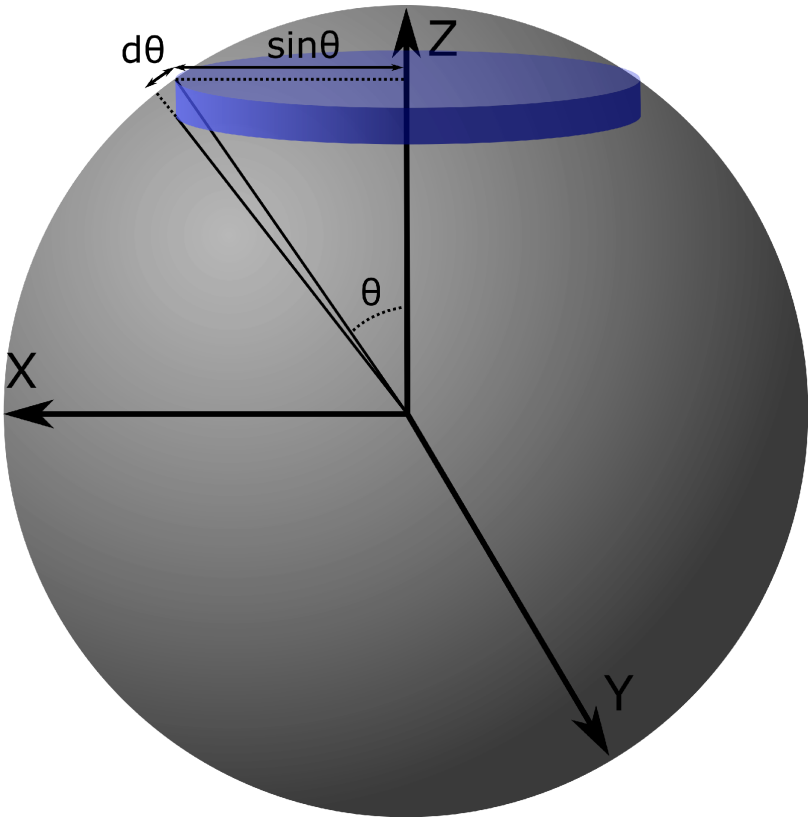

Figure 2.2: In terms of calculus, this can be considered as a cylinder with radius $\sin\theta$ and height equal to the circumference of the sector $d\theta$

So $r = 0$ for a perfectly isotropic system, while $r = 1$ for a population aligned perfectly with the Z-axis. Exciting a randomly orientated population of fluorophores with polarised light introduces anisotropy to a system, because the probability that a photon is absorbed is higher for a dipole aligned with the axis of excitation. For light polarised along the Z-axis, this is proportional to $\cos^2\theta$ (Lakowicz and Gryczynski, 2002), hence the distribution of fluorophores excited by polarised light is:

This also has the consequence that fluorescence emission measured at an angle of 54.7° has an anisotropy of zero because $\cos^2 54.7° = \frac{1}{3}$. This is known as the magic angle.

$$p^*(\theta) = \cos^2\theta \sin\theta \mathrm{d}\theta \tag{2.12}$$

and

$$\left\langle \cos^2\theta \right\rangle^* = \frac{\int_0^{\frac{\pi}{2}} \cos^4\theta \sin\theta \mathrm{d}\theta}{\int_0^{\frac{\pi}{2}} \cos^2\theta \sin\theta \mathrm{d}\theta} \qquad \text{by 2.5 and 2.12} \tag{2.13}$$

$$= \frac{3}{5}. \tag{2.14}$$

Thus $r = \frac{2}{5}$ for a photoselected sample where the absorption and emission dipoles are parallel and molecules are stationary. Anisotropy measurements are concerned with the extent of depolarisation of this emission over time. In practice, while absorption and emission dipoles are typically close to parallel, each fluorophore will have a fundamental anisotropy equal to

$$r_0 = \frac{2}{5}\left(\frac{3\cos^2\beta - 1}{2}\right), \tag{2.15}$$

where β is the angle between the excitation and emission dipoles. This puts r_0 in the range $-0.2 \leq r_0 \leq 0.4$. For a static fluorophore, the measured value for anisotropy will be $r = r_0$; however, as there is a delay between excitation and emission (the fluorescence lifetime), other factors may decrease this value, such as energy transfer and rotational diffusion.

2.1.2 *Calculating ψ*

We now consider a population of freely rotating fluorophores. Assuming molecules to be perfect spheres, it has been shown (Einstein, 1905) that the mean rotation of a molecule due to diffusion, ω, at time t can be written as

$$\langle \cos^2 \omega \rangle = \frac{1}{3}\left(1 + 2e^{-\frac{kTt}{V\eta}}\right). \tag{2.16}$$

Therefore,

$$\begin{aligned} r(t) &= r_0 \left(\frac{3\cos^2 \omega - 1}{2}\right) \\ &= r_0 e^{-\frac{kTt}{V\eta}}. \end{aligned} \qquad \text{by 2.9 and 2.13} \tag{2.17}$$

A quantity $\psi = \frac{V\eta}{kT}$ can be defined such that

$$r(t) = r_0 e^{-\frac{t}{\psi}}. \qquad \text{by 2.1 and 2.17} \tag{2.18}$$

It is possible to define a term r_s, the steady-state anisotropy, which is effectively the expected value of the function $r(t)$, where t varies with the distribution $I(t) = e^{-\frac{t}{\tau}}$:

$$r_s = \frac{\int_0^\infty I(t)r(t)\mathrm{d}t}{\int_0^\infty I(t)\mathrm{d}t}. \tag{2.19}$$

Substituting in $I(t)$ and $r(t)$ and rearranging gives

$$\frac{r_0}{r_s} = 1 + \frac{\tau}{\psi}, \tag{2.20}$$

where τ is the fluorescence lifetime. In other words, if $\tau \ll \psi$, $r \approx r_0$ and as $\psi \to 0$, $r_s \to 0$. In the context of proteins, ψ may be related to the mass of the protein:

$$\psi = \frac{V\eta}{kT} = \frac{\eta M}{RT}(\bar{v} + h), \tag{2.21}$$

where

M	molecular mass of protein in $\mathrm{g\,mol^{-1}}$
R	gas constant, $N_\mathrm{A}k = 8.314 \times 10^6 \mathrm{g\,cm^2\,s^{-2}\,K^{-1}\,mol^{-1}}$
η	viscosity in $\mathrm{g\,cm^{-1}\,s^{-1}}$
$\bar{v}$	specific volume of protein. Typical value $0.73\,\mathrm{cm^3\,g^{-1}}$
h	hydration volume of protein. Typical value $0.23\,\mathrm{cm^3\,g^{-1}}$

This gives units of s for ψ. Using this information it is possible to calculate an approximate mass of a fluorophore. For a fluorescently labelled protein, this may give indications of oligomerisation state, con-

formational changes and protein-protein interactions Melville, Lucieer and Aryal, 2006.

2.1.3 *Time Resolved Fluorescence Anisotropy*

While τ_c may be calculated using steady-state methods, time-resolved anisotropy measurements can be acquired on the picosecond timescale using pulsed lasers. This generates an exponentially decaying anisotropy signal that may be analysed to calculate more accurate values of r. Additionally, it is possible to extricate multiple anisotropy values, that may provide information about non-spherical fluorophores, segmental mobility and different coexistent populations in solution as well as being compatible with multiple exponential intensity decays.

Time-Correlated Single Photon Counting is the current state-of-the-art approach to collecting time-resolved fluorescence data. In TCSPC, a sample is excited with a pulse of light, typically from a picosecond pulsed diode laser operating in the 10-100 MHz range. An electrical pulse is sent as a reference signal from the laser every time the laser is activated. This pulse is modulated by a Constant Fraction Discriminator (CFD), which in turn sends a normalised pulse to a Time-to-Amplitude Converter (TAC). This acts as a start trigger. A photo-detector in turn sends an electrical pulse to a second CFD upon detection of a photon. The normalised signal from the second CFD acts as a stop signal to the TAC. The output signal from the TAC is proportional to the time between the start and stop triggers. Finally, the signal is amplified and sent to an Analogue-to-Digital Converter (ADC), which calculates the time between the start and stop signals.

TCSPC systems are designed such that the probability of the detection of a single photon in any given excitation window is low. This

is because a maximum of one photon may recorded at a time, so if multiple photons are detected, the signal becomes biased towards shorter timescales. Instead, a distribution of photon counting events is built up over many thousands of excitations, allowing for an extremely accurate and precise fluorescence decay to be detected.

Anisotropy decays exponentially following excitation by a polarised laser pulse:

$$r(t) = r_0 \sum_j g_j e^{-\frac{t}{\psi_j}}. \tag{2.22}$$

where ψ_j are the separate rotational correlation times and g_j and are their fractional amplitudes. To determine the parameters of $r(t)$, equation 2.8 may be rearranged to model each decay separately:

$$I_{\parallel}(t) = \frac{1}{3} I(t)[1 + 2r(t)] \tag{2.23}$$

$$I_{\perp}(t) = \frac{1}{3} I(t)[1 - r(t)], \tag{2.24}$$

where:

$$I(t) = \sum_i \alpha_i e^{-\frac{t}{\tau_i}} \tag{2.25}$$

2.1.4 *Solving for Decay Parameters*

For analysis, fluorescence decays were described as $\boldsymbol{A}\boldsymbol{f}^*$, where $\boldsymbol{A} \in \mathbb{R}_+^{N\times M}$ is a matrix comprising the convolution of the Instrument Response Function (IRF) $\boldsymbol{h} = [h_1, h_2 \ldots, h_N]$ with the exponential decay functions of each lifetime component $\boldsymbol{\tau} = [\tau_{1,}\tau_2, \ldots, \tau_M]$ at time $\boldsymbol{t} = [t_{1,}t_2, \ldots, t_N]$:

$$\boldsymbol{A} = \begin{bmatrix} h_i * \begin{bmatrix} e^{-t_1/\tau_1} & \ldots & e^{-t_N/\tau_1} \end{bmatrix} \\ \vdots \quad \ddots \quad \vdots \\ h_i * \begin{bmatrix} e^{-t_1/\tau_M} & \ldots & e^{-t_N/\tau_M} \end{bmatrix} \end{bmatrix}^T, \tag{2.26}$$

and $\boldsymbol{f}^* \in \mathbb{R}_+^M$is a vector of lifetime components. The Poisson model was used to determine the probability of observing a particular set of photon counts $\boldsymbol{y} \in \mathbb{N}_+^N$ for a given vector $\boldsymbol{f}$. The expected value of the decay at time t_i is given as

$$\breve{}_{\mathrm{i}} := \mathrm{E}(y_i|\boldsymbol{A}_i) = \boldsymbol{A}_i\boldsymbol{f} + b, \tag{2.27}$$

where $b \in \mathbb{R}_+$ is the background photon count and the Poisson distribution's probability mass function is given by:

$$\begin{aligned} p(y_i|\boldsymbol{A}_i;\boldsymbol{f}) &= \frac{\lambda_i^{y_i}}{y_i!}e^{-\lambda_i} \\ &= \frac{(\boldsymbol{A}_i\boldsymbol{f}+b)^{y_i}e^{-\boldsymbol{A}_i\boldsymbol{f}+b}}{y_i!}. \end{aligned} \tag{2.28}$$

Thus the total probability of the dataset $\boldsymbol{y}$ is given by

$$p(\boldsymbol{y}|\boldsymbol{A};\boldsymbol{f}) = \prod_{i=1}^{N} \frac{(\boldsymbol{A}_i\boldsymbol{f}+b)^{y_i}e^{-\boldsymbol{A}_i\boldsymbol{f}+b}}{y_i!}. \tag{2.29}$$

This is simplified by the product rule for logarithms (the logarithm of a product is equal to a sum of logarithms):

$$\begin{aligned} -\log[p(\boldsymbol{y}|\boldsymbol{A};\boldsymbol{f})] &= -\log\left[\prod_{i=1}^{N} \frac{(\boldsymbol{A}_i\boldsymbol{f}+b)^{y_i}e^{-\boldsymbol{A}_i\boldsymbol{f}+b}}{y_i!}\right] \\ &= -\sum_{i=1}^{N}(y_i\log(\boldsymbol{A}_i\boldsymbol{f}+b) - \log(y_i!) - \boldsymbol{A}_i\boldsymbol{f}+b) \end{aligned} \tag{2.30}$$

We may ignore the the $\log(y_i!)$ term as it is a constant, so the problem reduces to minimising the function

$$F(\boldsymbol{f}) = \|\boldsymbol{A}\boldsymbol{f}+b\|_1 - \sum_{i=1}^{N} y_i\log(\boldsymbol{A}_i\boldsymbol{f}+b). \tag{2.31}$$

In addition, an $L1$-norm penalty term is included to encourage the generation of a sparse solution, $\boldsymbol{f}^*$as the solution to:

$$\begin{aligned} &\Phi(\boldsymbol{f}) = F(\boldsymbol{f}) + \omega\|\boldsymbol{f}\|_1 \qquad\qquad \boldsymbol{f}^* = \arg\min\Phi(\boldsymbol{f}), \\ &\quad \text{subject to } \boldsymbol{f} \geq 0. \end{aligned} \tag{2.32}$$

2.1.4.1 *Optimising the objective function*

Taylor's theorem states that the value of an infinitely differentiable function $f(x)$ at a point a is equal to

$$f(x) = \sum_{k=0}^{\infty} \frac{f^{(k)}(a)}{k!}(x-a)^k$$
$$= f(a) + f'(a)(x-a) + \frac{f''(a)}{2!}(x-a)^2 + \cdots \tag{2.33}$$

This can also be used to approximate multivariable functions:

$$f(\boldsymbol{x}) \approx f(\boldsymbol{a}) + (\boldsymbol{x}-\boldsymbol{a})^T \nabla f(\boldsymbol{a}) + \frac{1}{2}(\boldsymbol{x}-\boldsymbol{a})^T \nabla^2 f(\boldsymbol{a})(\boldsymbol{x}-\boldsymbol{a}) \tag{2.34}$$

Here $\nabla f(\boldsymbol{a})$ signifies the first derivative or the gradient of the function, and ∇^2 signifies the second derivative, also known as the Hessian. The gradient is a length M vector equal to

$$\nabla F(\boldsymbol{f}) = \boldsymbol{A^T}\mathbb{1} - \sum_{i=1}^{N} \frac{y_i}{\boldsymbol{A}_i \boldsymbol{f} + b}\boldsymbol{A}_i, \tag{2.35}$$

while the Hessian is approximated by scaled $M \times M$ identity vector $\alpha_k I$. Therefore for a given estimate $\boldsymbol{f}_k$, the next iterate can be given by minimising

$$F_k(\boldsymbol{f}) + \omega \left\| \boldsymbol{f} \right\|_1, \tag{2.36}$$

where

$$F^k(\boldsymbol{f}) = F(\boldsymbol{f}_k) + (\boldsymbol{f} - \boldsymbol{f}_k)^T \nabla F(\boldsymbol{f}^k) + \frac{\alpha_k}{2} \left\| \boldsymbol{f} - \boldsymbol{f}_k \right\|_2^2. \tag{2.37}$$

$F(\boldsymbol{f}^k)$ is constant, so

$$\Phi^k(\boldsymbol{f}) = \frac{(\boldsymbol{f}-\boldsymbol{f}_k)^T \nabla F(\boldsymbol{f}^k)}{\alpha_k} + \frac{1}{2}\|\boldsymbol{f}-\boldsymbol{f}_k\|_2^2 + \frac{\omega}{\alpha_k}\|\boldsymbol{f}\|_1 \tag{2.38}$$

The minimum is found by differentiating:

$$\begin{aligned} \frac{d}{d\boldsymbol{f}}\Phi_k(\boldsymbol{f}) = \frac{\nabla F(\boldsymbol{f}_k)}{\alpha_k} + \boldsymbol{f} - \boldsymbol{f}^k + \frac{\omega}{\alpha_k}\mathbb{1} = 0 \\ \boldsymbol{f} = \boldsymbol{f}_k - \frac{\nabla F(\boldsymbol{f}_k)}{\alpha_k} - \frac{\omega}{\alpha_k}\mathbb{1} \end{aligned} \tag{2.39}$$

$$\text{subject to} \boldsymbol{f} \geq \boldsymbol{0}$$

The Barzilai-Borwein method was used to approximate the Hessian matrix using $\boldsymbol{\delta}_k = \boldsymbol{f}_k - \boldsymbol{f}_{k-1}$:

$$\alpha_k = \frac{\left\|\sqrt{\boldsymbol{y}} \cdot (\boldsymbol{A}\boldsymbol{\delta}_k)/(\boldsymbol{A}\boldsymbol{f}_k + b)\right\|_2^2}{\|\boldsymbol{\delta}_k\|_2^2} \tag{2.40}$$

where $\sqrt{\cdot}$, $\cdot$, and $/$ act component-wise and is safeguarded in the range $10^{-30} \leq \alpha_k \leq 10^{30}$. The result was then subject to an acceptance criterion

$$\Phi(\boldsymbol{f}_{k+1}) \leq \max_{i=[k-L]_+,\ldots,k} \Phi(\boldsymbol{f}_i) - \frac{\sigma\alpha_k}{2}\left\|\boldsymbol{f}_{k+1}-\boldsymbol{f}_k\right\|_2^2 \tag{2.41}$$

for $L \in \mathbb{N}_+$ and $\sigma \in (0,1)$. Typical values used were $L = 10$ and $\sigma = 0.1$. Finally, a termination criterion was applied, being either a

maximum number of steps or where $\left\|f_{k+1} - f_k\right\|_2 / \left\|f_k\right\|_2 \leq$ tolPfor some small tolP. A typical value used was tolP $= 10^{-8}$.

2.1.4.2 *Analysis of anisotropy decays*

As per 2.23 and 2.24, the total fluorescence decay can be determined by $I(t) = I_{\parallel}(t) + 2I_{\perp}(t)$. To determine the anisotropy values, this sum was used to determine basic fluorescence lifetime components. The difference was used to determine anisotropy:

$$I_{\parallel}(t) - I_{\perp}(t) = I(t)r(t) \tag{2.42}$$

The determined lifetime distribution for the total emission was held constant and the same process described above was used to determine the distribution of anisotropy lifetimes. A custom program to carry out the analysis was written in Julia[1].

2.1.5 *Fluorescent Proteins*

Since its discovery and isolation from the jellyfish *Aequorea victoria* in 1962 (Shimomura, Johnson and Saiga, 1962), Green Fluorescence Protein (GFP) and its derivatives have become one of the most important tools to study protein behaviour. In 1994, it was shown GFP could be used as a marker for recombinantly expressed proteins (Chalfie et al., 1994) and fluorescent proteins have proven to be extremely effective at generating large quantities of tagged proteins in living cells while retaining their native function (Stadler et al., 2013). This eliminates the need to use exogenous fluorescent dyes and allows for very high protein specificity. Uses include intracellular tracking, including real-time

1 Available at: https://github.com/alexllew/Anisotropy-Analyser/blob/master/Anisotropy.jl

live-cell imagine and single molecule microscopy; the development of biosensors, typically using FRET, for a diverse array of uses such as detecting receptor activation, measuring membrane potentials, and as sensors for intracellular molecules, as well as more conventional imaging techniques to study intracellular localisation (Kremers et al., 2011). Over the years numerous mutants and derivatives with different properties have been developed. These have included variants with more practical excitation wavelengths and improved quantum yields such as eGFP (Cormack, Valdivia and Falkow, 1996), different colours, including blue, cyan (Heim and Tsien, 1996) and yellow (Griesbeck et al., 2001). Other examples include fluorescent proteins from *Anthozoa*, such as the tetrameric dsRed and its derivatives found in *Discosoma sp.*, and tagRFP from *Entacmaea quadricolor*.

As previously noted, for molecules with large values of ψ and/or low values of τ, $r \approx r_0$. This is because the fluorescence intensity decays to very low values before significant diffusional rotation has taken place. Consequently, time-resolved anisotropy data in such situations are of low resolution, making observations of small changes unlikely to exceed noise, especially if attempting to measure multiexponential anisotropy decay. One of the main drawbacks of GFP in its application to anisotropic techniques is its short fluorescence lifetime—around 2-2.5 ns. This is not only much shorter than the typical rotational correlation time for a large protein (>20 ns), but is also problematic for experiments in plants, which typically display autofluorescence due to native pigments with a lifetime of around the same magnitude (Schleifenbaum et al., 2010).

Lumazine Protein (LumP) is a 20 kDa fluorescent protein isolated from the marine bioluminescent bacterium *Photobacterium leiognathi*.

With an absorption maximum at 420 nm, it is yellow in colour and emits cyan fluorescence with a peak at 475 nm (O'Kane, Karle and Lee, 1985). It has an unusually long fluorescence lifetime of 14.8 ns (Lee, O'Kane and Visser, 1985), the longest of any known protein fluorophore, though more recent data has placed this value at 13.6 ns (Hoepker et al., 2015). The crystal structure has been solved, showing it contains two β-barrel domains with nearly identical folds. The N-terminal domain binds the chromophore 6,7-dimethyl-8-(1´-D-ribityl) lumazine (DMRL) by hydrogen bonds in a narrow cavity that are absent in the C-terminal domain. It also binds riboflavin and flavin mononucleotide but with lesser affinity (Sato et al., 2010). Riboflavin synthase is closely related to LumP and generates riboflavin from two DMRL molecules bound individually to each domain (Fischer and Bacher, 2008), suggesting LumP evolved from it, losing functionality in one of its domains.

LumP presents an ideal candidate to use to probe protein-protein interactions due to its long fluorescence lifetime. It has been used previously to develop highly efficient FRET probes, proving twice as efficient as the equivalent CFP probe. It was furthermore demonstrated to be simple to produce in large quantities in bacteria, sequestering DMRL from the cytoplasm (Hoepker et al., 2015). The presence of DMRL in all kingdoms of life as a result of its role in the biosynthesis of riboflavin (Fischer and Bacher, 2008) suggests it may further be a good candidate for probing anisotropy data *in planta*.

2.2 CONSTRUCTION AND VALIDATION OF A TIME-RESOLVED FLUORESCENT MICROSCOPE SYSTEM

In order to utilise these techniques to study proteins *in planta*, a system to make time-resolved fluorescence measurements of leaves was designed and constructed. A Zeiss Axiovert 135 inverted microscope (kindly donated by Prof. Phil Gates) was used as the basis for the system with a 100× oil immersion Ph3 objective lens (Zeiss). In order to coincide with the excitation spectrum of both LumP and GFP, an LDH-P-C-405B laser (Picoquant) was used for excitation at 405 nm, with a 70 ps FWHM pulse at 20 MHz.

The laser was mounted on two Ø200 mm stainless steel rods manufactured in-house and securely affixed to an optical table. Ø1" optical tubing (Thorlabs) was used to contain the laser beam, which was directed into the rear of the microscope through a Ø1" half-wave plate. A longpass dichroic mirror (Thorlabs), with a cut-off at 425 nm was used to direct the excitation beam upwards towards the sample. Fluorescence excitation above 425 nm was therefore able to pass back through the dichroic mirror and a Ø½" 480/10 nm filter before being directed towards the detector.

The emission beam passed out of the microscope through optical tubing into a 1" polarising beamsplitter cube (Thorlabs), which allowed transmission of vertically polarised light and reflection of horizontally polarised light by 90°. Light was finally passed through a polariser to clean up the emission and focussed onto the Id Quantique 100-50 single photon detector. Two different detectors were used to enable simultaneous recording of data. This removes problems associated with photobleaching, sample degradation, temperature variation,

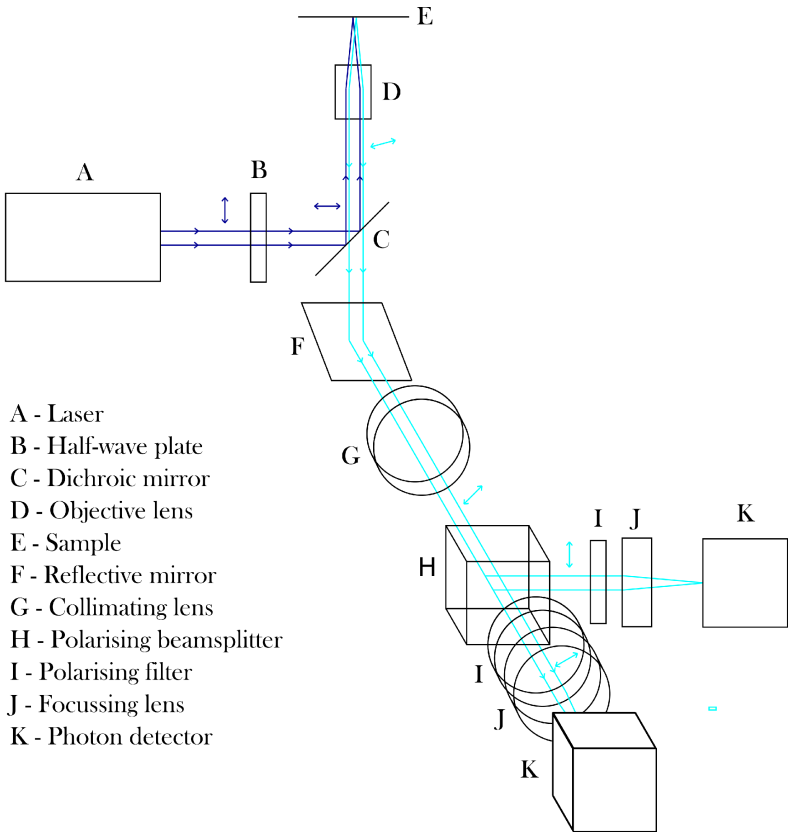

Figure 2.3: Schematic representation of the microscope setup.

changes in alignment and other factors that could influence results where measurements are made sequentially. Time-Correllated Single Photon Counting was carried out using an SPC-130 (Becker and Hickl) PC card and a PDL 800-B (Picoquant) laser controller, with the Spcm64 (Becker and Hickl) program being used to control experimental conditions and record the data. Data could then be converted to an ASCII file for analysis as described above. All components were firmly secured to the optical table to ensure minimum movement of components.

2.2.1 *Validation and Testing*

To ensure the setup was accurate and that measurements were valid, control substances were measured. Fluorescein is a fluorescent mo-

lecule with a very short rotational correlation time due to its small size. This means the expected fluorescence signal has equal parallel and perpendicular intensity. A dilute sample of fluorescein was measured for 30 s and the anisotropy calculated for each data point. As this should decay to zero very quickly, any deviation is due to differential photon detection due to factors like alignment, focussing and hardware differences. This difference may be captured as the G factor, which is a correction that can be applied to remove the error within the system. This is defined as:

$$r = \frac{I_{\parallel} - GI_{\perp}}{I_{\parallel} + 2GI_{\perp}}, \tag{2.43}$$

meaning tail-matching may be used to calculate the G-factor. Rearranging 2.43 gives:

$$G = \frac{1 + 2r}{1 - r} \tag{2.44}$$

There was a clearly higher intensity recorded in the vertical detector. Anisotropy was calculated between 6 and 10 ns, resulting in a value of 0.159 (see 2.4). To confirm this difference was due to bias in the system and that it can be corrected for (rather than an innate property of the fluorophore or conditions), the half-wave plate was used to rotate the excitation emission by 90°. This resulted in a measured anisotropy value of -0.140. The corresponding G-factors for these values are 1.57 and 0.63. As $\frac{1}{0.63}$ =1.58, these values are consistent with each other.

While measurements were consistent within any one recording session, measured G-factors were highly sensitive to small changes in

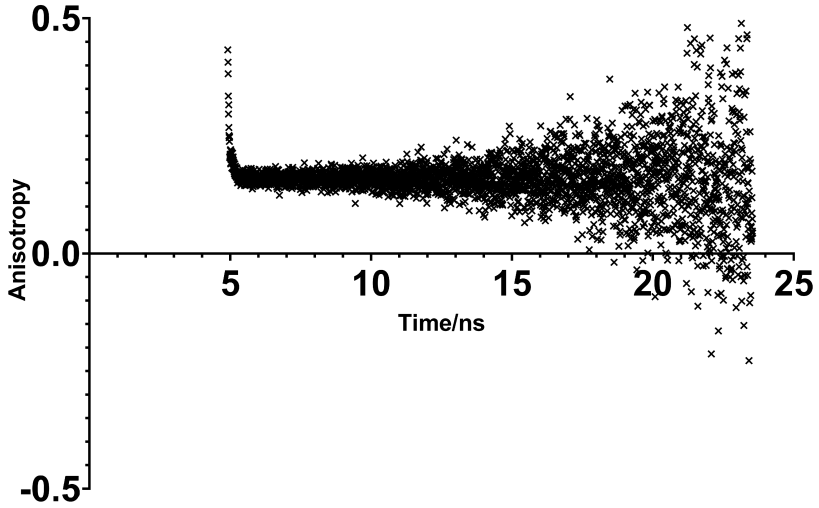

(a) Anisotropy decay of fluorescein, showing a rapid decay to a plateau at 0.159. $n = 3$

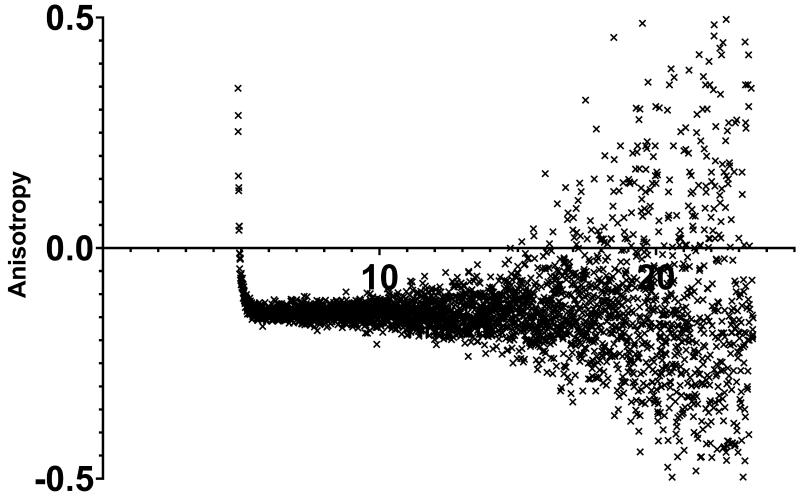

(b) Anisotropy decay of fluorescein with the excitation polarisation at 90° indicating a rapid decay to a plateau at -0.14

Figure 2.4

alignment and varied significantly from session to session. This may be due to small movements caused by thermal expansion, unintentional outside movement and by the shifting of components when changing fluorescence filters and other components. Consequently, it is necessary to determine an accurate G-factor by the described method before each recording session. This set up provides a method to investigate anisotropy measurements *in vivo* and *in vitro.*

3

IN VITRO RX1 EXPERIMENTS

3.1 INTRODUCTION

Rx1 is a plant NLR found in *Solanum tuberosum* ssp. *andigena* and confers extreme resistance to Potato Virus X in response to the detection of the viral Coat Protein (CP). A number of studies have probed the regulation and signalling of Rx1. Expressing soluble plant NLRs is challenging and previous experiments have used limited quantities of protein purified from plants or expression of a truncated protein (typically CC-NBARC) as inclusion bodies in *Escherichia coli* that must be refolded (Fenyk, Townsend et al., 2015).

Rx1 is a relatively large protein of around 107 kDa and contains three primary domain: the CC, the NBARC (subdivided into the NB, ARC1 and ARC2 domains) and the LRR (see 3.1). Rx1 is highly similar to Gpa2, a receptor that recognises potato cyst nematode *Globodera pallida.* In work by the Slootweg lab, domain-swapping experiments with these two proteins have found the ARC2 and LRR domains of Rx1 and Gpa2 are incompatible: when the LRR of Rx1 is combined with the ARC2 domain of Gpa2, the protein becomes constitutively active, while when the LRR of Gpa2 was combined with the ARC2 domain of Rx1, the protein becomes inactive. Furthermore, this change in activity is retained even when only the first 2-3 repeats of the LRR or an N-terminal fragment of the ARC2 domain is replaced, indicating

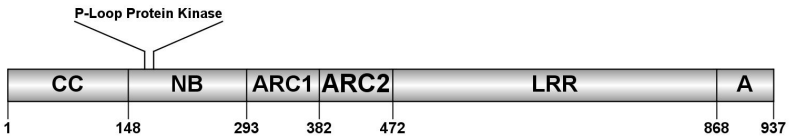

Figure 3.1: Domains of Rx1, showing the Coiled Coil (CC); Nucleotide Binding Domain; Apaf-1, R proteins and Ced-4 Domains (ARC1 and ARC2); the Leucine-Rich Repeat (LRR) and Acidic Tail (A)

the interface between these two regions is vital in modulating the behaviour of the protein. Normal activity is observed when both regions are replaced by fragments from the other protein, with the C-terminus of the LRR being responsible for elicitor specificity (E.J. Slootweg et al., 2013).

Rx1 and other plant NLR NB-ARC domains have significant similarity to the Cdc6/ORC proteins found in *Pyrobacumaerophilum* and *Aeropyrumpernix*—replication machinery found in eukaryotes and archaea with DNA-binding activity. Electrophoretic mobility shift assay data using refolded Rx1 CC-NBARC demonstrated DNA binding activity. A mutation in the P-loop (K176R), which abolishes nucleotide-binding activity, reduced DNA-binding affinity. FRET experiments indicated bound DNA was bent at an angle of 42° in both Wild-Type (WT) and K176R proteins; however, the addition of ATP increased this

angle only in the WT (Fenyk, Townsend et al., 2015). The use of a ssDNA-specific nuclease showed WT CC-NBARC also triggers DNA melting, but this is not found in the mutant (Fenyk, Townsend et al., 2015). No sequence specificity is observed, suggesting the need for cofactors to direct DNA-binding.

This change in behaviour on nucleotide-binding may be explained by conformation changes in the protein. This could be as a result of a new stable structure becoming stabilised or a shift in an equilibrium of various protein conformations. G-Protein Coupled Receptors (GPCRs) have been shown to possess significant structural flexibility that cannot be captured by crystallographic data and molecular dynamics simulations have demonstrated this variation is caused by the destabilisation of the native conformation by ligand binding, causing greater flexibility and increasing the probability that a given protein adopts its less stable active state (Preininger, Meiler and Hamm, 2013). Experiments to investigate conformational changes and ligand binding may allow a model for how ATP-induced activation occurs in Rx1 to be developed.

A number of proteins that interact with Rx1 have been identified. *Nb*DBCP, a bromodomain protein, and *Nb*Glk, a putative transcription factor, are Rx1 interactors initially indentified from a Yeast Two Hybrid screen. *Nb*DBCP overexpression supresses the immune response and appears to act as a negative regulator (Dixon, 2017). *Nb*Glk is a DNA binding protein that has been shown to interact with Rx1 *in vitro* and *in vivo*. This interaction is known to reduce its DNA-binding affinity and it is proposed that Rx1 acts as a negative regulator on the activity of *Nb*Glk (Townsend et al., 2018).

SGT1 and HSP90 are chaperone proteins known to interact with Rx1. SGT1 silencing reduces the immune response of Rx1 (E. Slootweg et al., 2010). NRC1 is a separate plant NLR that has been found to be a necessary component of immunity mediated not only by Rx1, but a number of other R proteins, indicating it may play a more general role in the plant immune response (Gabriëls et al., 2007).

The aim of this section of work was to test the hypothesis that LumP may be used as a long-lifetime tag to assist the study of Rx1 *in vitro*. Work was undertaken to validate the use of LumP for this purpose and to compare it effectiveness to GFP. The behaviour of Rx1-LumP was also tested, including its interaction with proteins that bind Rx1, its DNA-binding behaviour, phosphatase activity, as well as the effect of the T452A mutation.

3.2 DNA BINDING STOICHIOMETRY

The DNA binding stoichiometry of Rx1 was tested. Refolded Rx1 CC-NBARC was used for this experiment, as previously described (Fenyk, Townsend et al., 2015).

Previous unpublished work has indicated presence of both monomeric and multimeric forms of refolded Rx1 in solution—figure 3.2 shows the results of an analytical ultracentrifugation experiment, which separates macromolecules by mass, and indicates four distinct sizes are present in solution. Furthermore, the oligomerisation domains present in NLRs (Erzberger and Berger, 2006), together with previous data demonstrating oligomerisation of NLRs both before and after activation, suggests a potentially important role of higher-order structures in signalling (Gutierrez et al., 2010; Bernoux, Ve et al., 2011; J. Wang, Hu et al., 2019). Experiments were therefore conducted

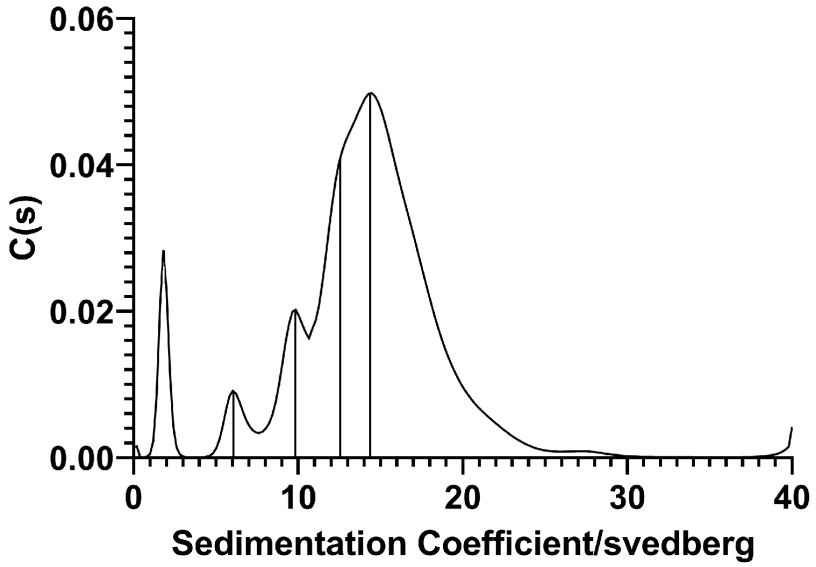

Figure 3.2: Results of ultracentrifugation experiment, showing 3 clear peaks and a shoulder, potentially indicating the presence of monomeric, dimeric, tetrameric and octomeric forms of Rx1 in solution. The sedimentation coefficient is the ratio of a particle's sedimentation velocity and the applied acceleration, measured in svedbergs (one svedberg is equal to 100 fs). C(s) is the sedimentation coefficient distribution or the weight-averaged relative concentration of molecules with a particular sedimentation coefficient.

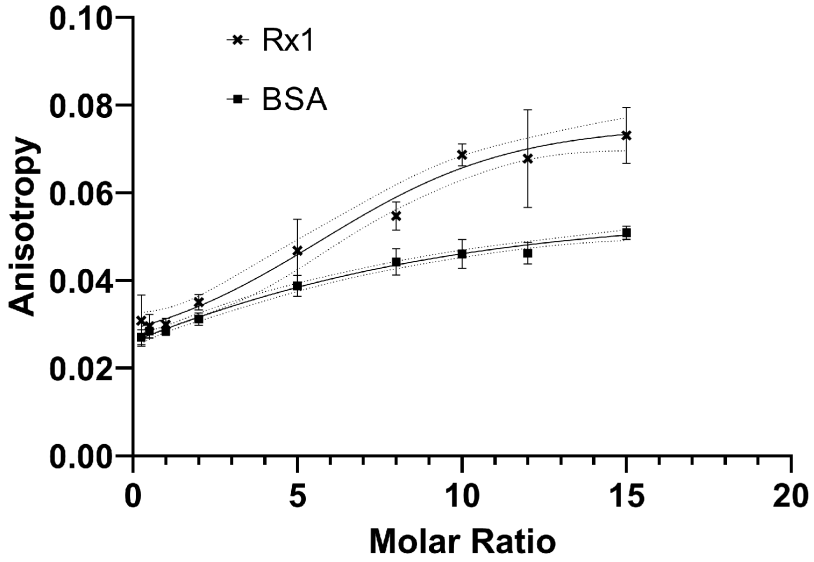

Figure 3.3: Steady-state anisotropy values for 100 μM fluorescein-labelled ssDNA oligonucleotide in the presence of different molar ratios of $Rx1_{1\text{-}489}$ and BSA, excited at 485/20 measured at 528/20 nm, with 95% confidence intervals. $n = 6 - 15$. Standard curve is sigmoidal four-parameter (4PL) least squares fit, with 95% confidence intervals.

to determine the binding stoichiometry of Rx1 for DNA to test the hypothesis that Rx1 forms higher-order structures *in vitro*.

The DNA binding properties of the truncated $Rx1_{1\text{-}489}$ CC-NBARC previously demonstrated (Fenyk, Townsend et al., 2015) were exploited to test the binding stoichiometry of Rx1 for DNA. A low concentration of fluorescently tagged ssDNA oligonucleotide was used to determine Rx1 DNA binding using steady-anisotropy with BSA as a control, as seen in figure 3.3. At low concentrations of protein, very low anisotropy values were found, consistent with freely rotating fluorophore in solution. Increasing concentrations of both Rx1 and BSA resulted in an increasing anisotropy value, indicating non-specific interactions with BSA or an increased viscosity induced by protein concentration. However, Rx1 increased anisotropy by a larger amount with the dif-

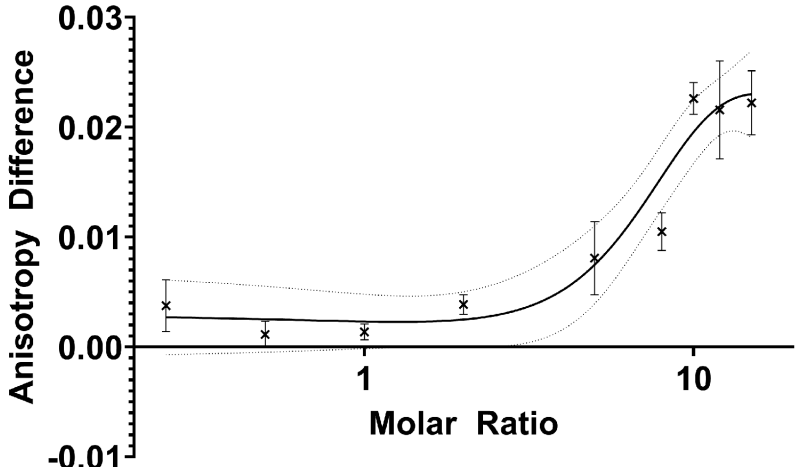

Figure 3.4: Difference in steady-state anisotropy of 100 μM fluorescein-labelled ssDNA oligonucleotide in the presence of different molar ratios of $Rx1_{1\text{-}489}$ and BSA on a logarithmic x-axis, with 95% confidence intervals. $n = 6 - 15$. Standard curve is the difference of the sigmoidal four-parameter (4PL) least squares fits, with 95% confidence intervals.

ference stabilising at around a 10-fold molar ratio, as seen in figure 3.4. As the protein was not 100% pure, this difference is consistent with an octomeric form; however when purifying by gel filtration, the retention time is consistent with a monomeric protein. It is therefore possible that higher order structures are triggered by DNA binding.

All experiments were conducted using 60 mM NaCl. Salt concentration is known to affect protein DNA-binding behaviour—in particular higher salt concentrations can disrupt protein-DNA electrostatic interactions and reduce binding affinity. Furthermore, specific interactions tend to be more robust to higher salt concentrations than non-specific interactions (Thompson and Woodbury, 2001). To ensure the response being observed was not dependent on the salt concentration, DNA binding was compared at different salt concentrations. This showed

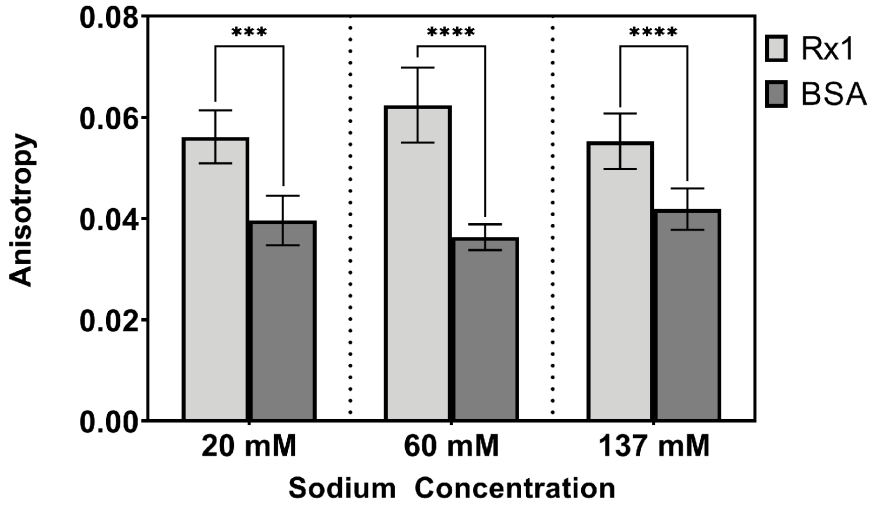

Figure 3.5: Anisotropy values for 100 μM fluorescein-labelled ssDNA oligonucleotide with a 5-fold molar excess of $Rx1_{1\text{-}489}$ and BSA at different salt concentrations, with 95% confidence intervals. *** indicates$p < 0.001$, **** indicates$p < 0.0001$. p-values determined by Welch's t-test. $n = 17$.

DNA binding was retained at both hypotonic (20 mM) and physiological (137 mM) sodium chloride, as seen in figure 3.5.

This demonstrates that DNA-binding behaviour is exhibited by refolded Rx1 under physiological conditions. Furthermore, this binding occurs with a stoichiometry of around 10:1, suggesting Rx1 does indeed form higher order structures *in vitro*. This may occur in response to DNA binding, as this is not observed for apoprotein in other experiments, and is consistent with the octomeric form observed in ultracentrifugation. This is supported by work discussed previously indicating the formation of multimeric structures in NLRs (Gutierrez et al., 2010; Bernoux, Ve et al., 2011; J. Wang, Hu et al., 2019).

3.3 LUMAZINE PROTEIN

As described in Chapter 2, Lumazime Protein (LumP) was identified as a potential tool to investigate oligomeric state, as well as other

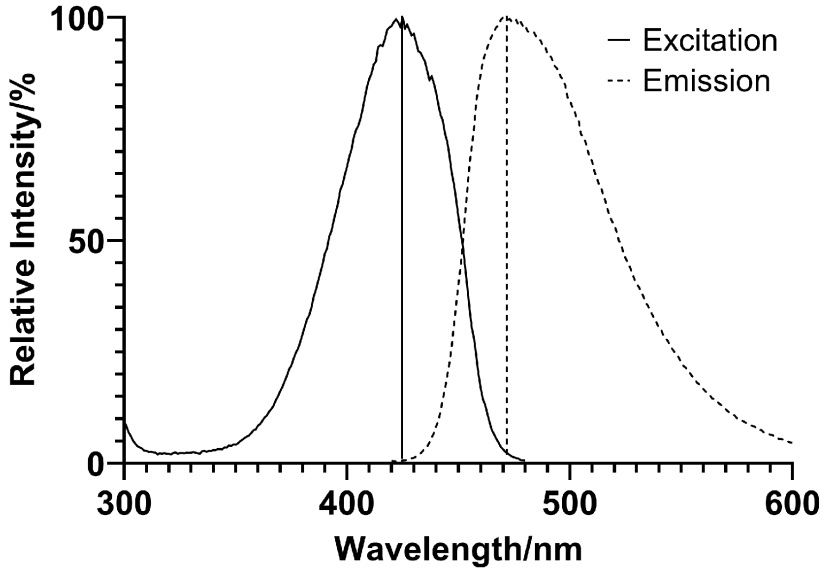

Figure 3.6: Excitation-emission spectrum of LumP. Relative intensity is the measured strength of fluorescence normalised to 100% measured at 500/9 nm for a given excitation wavelength (excitation) or the normalised intensity at a given wavelength with an excitation wavelength of 400/9 nm (emission). 100 measurements per datapoint.

interactions of Rx1. The properties of LumP were therefore explored experimentally.

3.3.1 *Expression of LumP*

Lumazine Protein (LumP) was expressed in *E. coli*. The protein was yellow in colour, and was observed to fluoresce cyan light under UV. A one-step purification of the His_6-tagged protein using Ni-NTA was sufficient to obtain large quantities of LumP at ~90% purity. The excitation-emission spectrum showed an absorption peak at 422 nm a fluorescence emission peak at 470 nm, in line with previously recorded data (Hoepker et al., 2015), as seen in 3.6.

3.3.2 *Time-Resolved Anisotropy Measurements of LumP*

TCSPC was used to make lifetime measurements of LumP. The protein was excited at 440 nm and the emission was detected using a band-pass filter at 480 nm. Two measurements were made parallel and perpendicular to the excitation polarisation to permit anisotropy analysis and the summed decays used to analyse the lifetime. The parallel lifetime peaked as expected at around three times the intensity of the perpendicular emission. The lifetime distribution was determined using the ℓ_1-norm penalised negative log-likelihood Poisson objective function previously described, using logarithmically scaling lifetimes from 0.25 ns to 100 ns with 100 subdivisions using a custom implementation in Julialang.

To test the hypothesis that LumP is a more effective tool than GFP for investigating protein hydrodynamics, high molecular weights were simulated using a mixture of water and glycerol to increase the viscosity. Three fluorescent lifetimes were observed at 0.31 ± 0.02, 2.83 ± 0.08 and 13.0 ± 0.02. The primary lifetime is somewhat below but consistent with the previously documented value of 13.6 ns (Hoepker et al., 2015). The observed fluorescence lifetimes were consistent at all measured viscosities, as seen in figure 3.7.

The algorithm was adapted to calculate anisotropy by first fitting the total intensity decay ($I_{\parallel} + 2I_{\perp}$) and then fitting the difference decay ($I_{\parallel} - I_{\perp}$) with fixed lifetime values to determine the anisotropy. As expected, a roughly linear increase in anisotropy was observed with increased viscosity, as seen in figure 3.8. The long fluorescence lifetimes allowed relatively accurate measurements to be made even at very long fluorescence lifetimes. Using the equation $\psi = \frac{\mu M}{RT}(\bar{v} + h)$

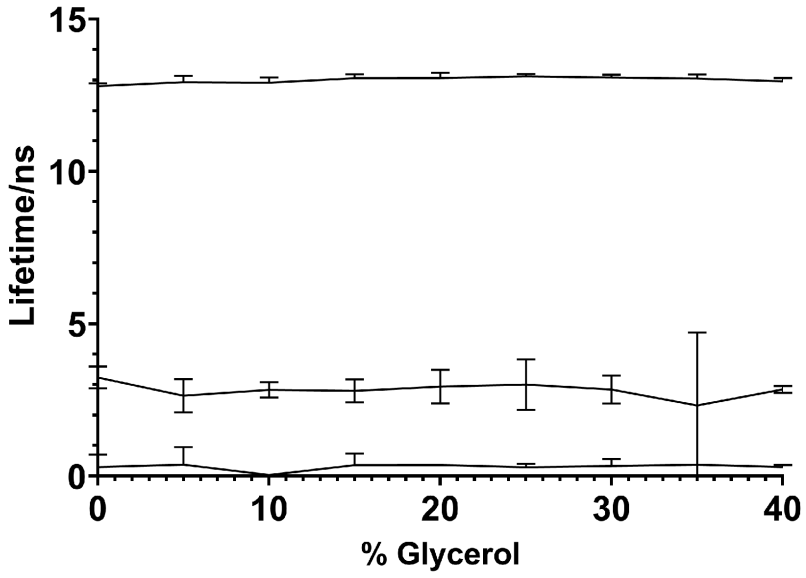

Figure 3.7: Separable lifetime components of LumP measured at different concentrations of glycerol, with 95% condidence intervals with 95% confidence intervals. $n = 3$.

it is possible to convert measured anisotropies to an estimated mass measurement. This resulted in an accurate estimate of the mass of LumP (20 kDa): measurements yielded mostly consistent measurements at all viscosities, indicating the method is accurate even at very long rotational correlation times. The slight decrease in the observed size at higher viscosities may be due to the stabilising effect of glycerol reducing the cross-section of the protein or due to a reduced hydration shell at higher concentrations.

This method was used to compare the utility of LumP compared to traditionally used GFP. While GFP also showed an increasing trend in rotational correlation times with increased viscosity, significantly greater errors were observed, while the trend failed to show the expected linear trend at higher glycerol concentrations as seen in figure 3.10. This is indicative of the limitations of using a fluorophore with a short fluorescence lifetime (measured at 2.71 ± 0.02) for measuring

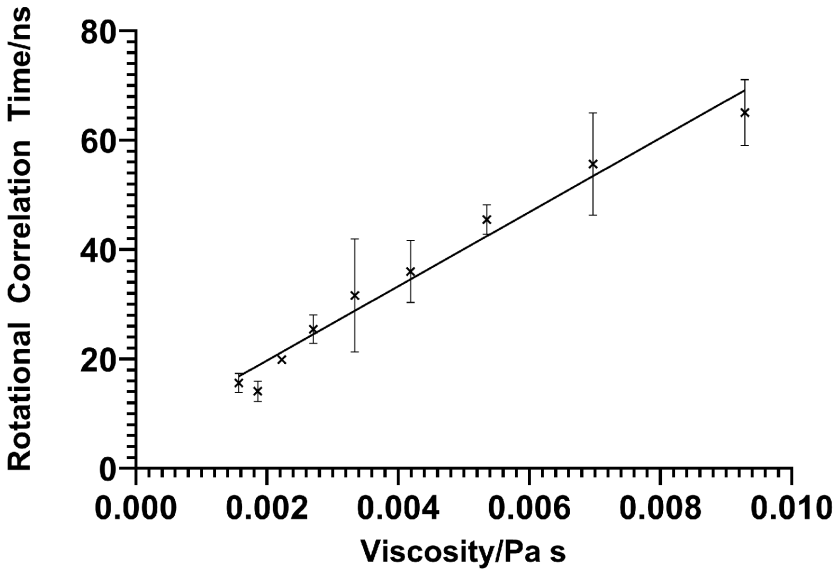

Figure 3.8: Time resolved LumP rotational correlation times, with 95% confidence intervals. $r = 0.91$. $n = 3$.

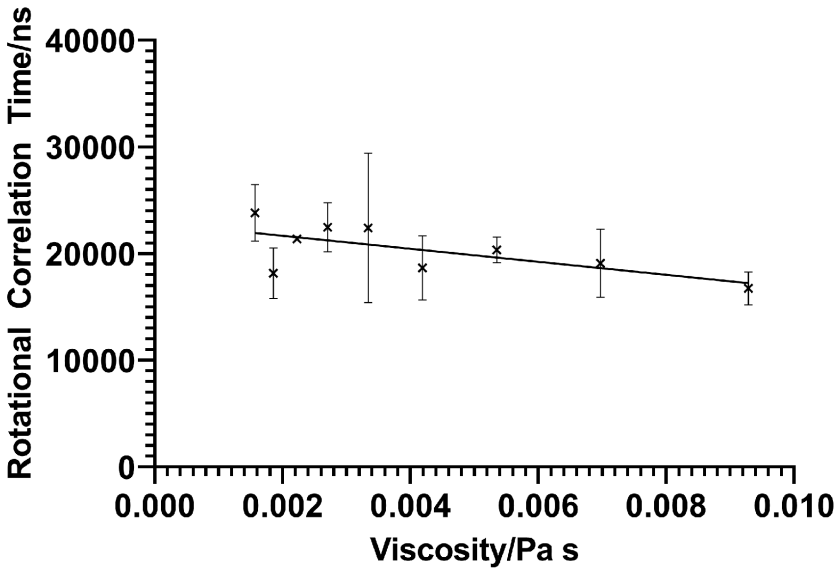

Figure 3.9: Estimation of LumP mass from rotational correlation time at different viscosities, with 95% confidence intervals. $r = 0.18$. $n = 3$

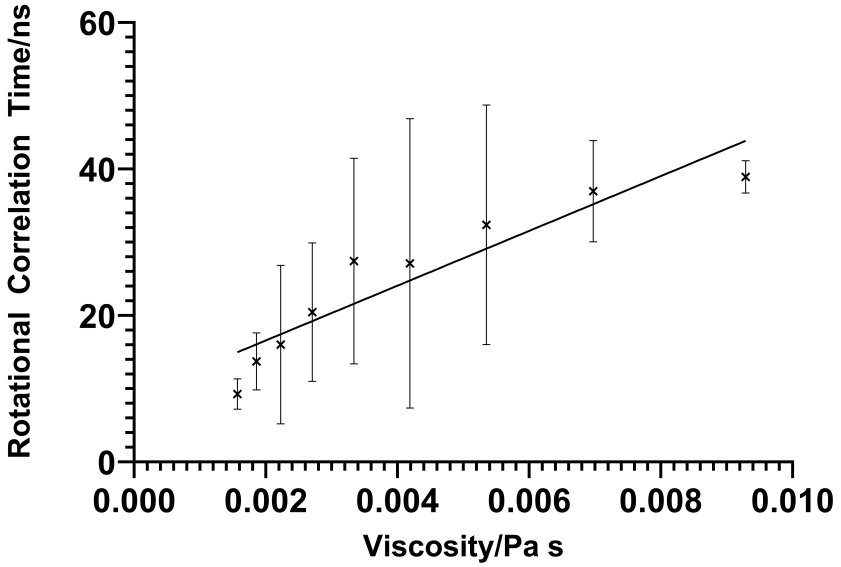

Figure 3.10: Time resolved GFP rotational correlation times, with 95% confidence intervals . $r = 0.76$ $n = 3$.

long rotational correlation times, especially when the expected changes are small. This illustrates the benefits of using LumP over GFP for such experiments.

3.4 CC-NBARC-LUMP

3.4.1 *Expression of $Rx1_{1\text{-}489}$-LumP*

In order to use LumP to study Rx1, the CC-NBARC truncation was cloned as an N-terminal fusion with LumP and recombinantly expressed. Surprisingly, small amounts (~0.2 mg/L culture) of soluble protein was produced, suggesting the LumP was acting as a solubilising factor. Ni-NTA purification resulted in highly impure protein. The protein was further purified on phenyl sepharose resin by hydrophobic interactions, eluting the protein in 5 mM NaCl. Following size-exclusion chromatography, acceptable purity was achieved (see figure 3.11); however, around 90% yield losses were observed, likely

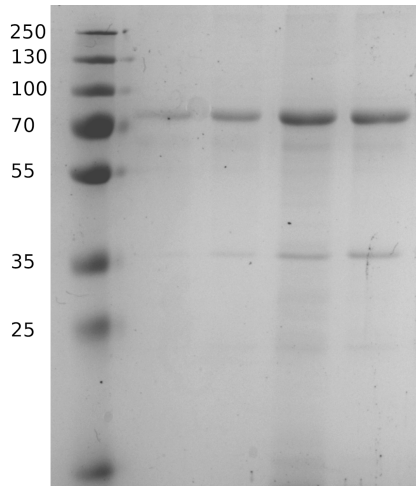

Figure 3.11: SDS-PAGE gel of elutions of $Rx1_{1\text{-}489}$-LumP used following purification by Ni-NTA and hydrophobic interactions chromatography, with band representing the protein at ~80 kDa

because of protein precipitation due to the relatively harsh conditions required. This result enabled experimentation to take place on a soluble protein expressed without refolding.

The emission-excitation spectrum showed an absorption peak at 405 nm and an emission peak at 457 nm as seen in figure 3.12. There are several factors that may cause blue-shifting of fluorescence spectra. For example, tryptophan residues in proteins can exhibit emission peaks in a range as wide as 308 nm to 355 nm, with free tryptophan emitting at 351 nm. Therefore, in the vast majority of proteins, blue-shifting is observed, with the greatest shifts observed from residues in highly depolarised environments (Vivian and Callis, 2001). This may suggest that the LumP moiety is somewhat buried within the CC-NBARC subunit, reducing the hydration of the lumazine ligand.

TCSPC was used to make lifetime measurements of the $Rx1_{1\text{-}489}$-LumP protein. The protein was excited at 440 nm and the emission collected using a band-pass filter at 480 nm.

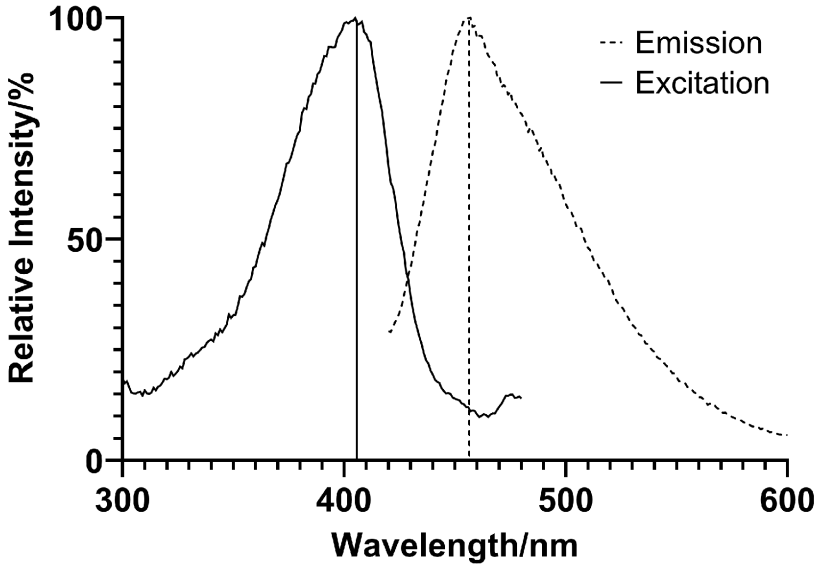

Figure 3.12: Excitation-emission spectrum of $Rx1_{1\text{-}489}$-LumP. Relative intensity is the measured strength of fluorescence normalised to 100% measured at 500/9 nm for a given excitation wavelength (excitation) or the normalised intensity at a given wavelength with an excitation wavelength of 400/9 nm (emission). 100 measurements per data point.

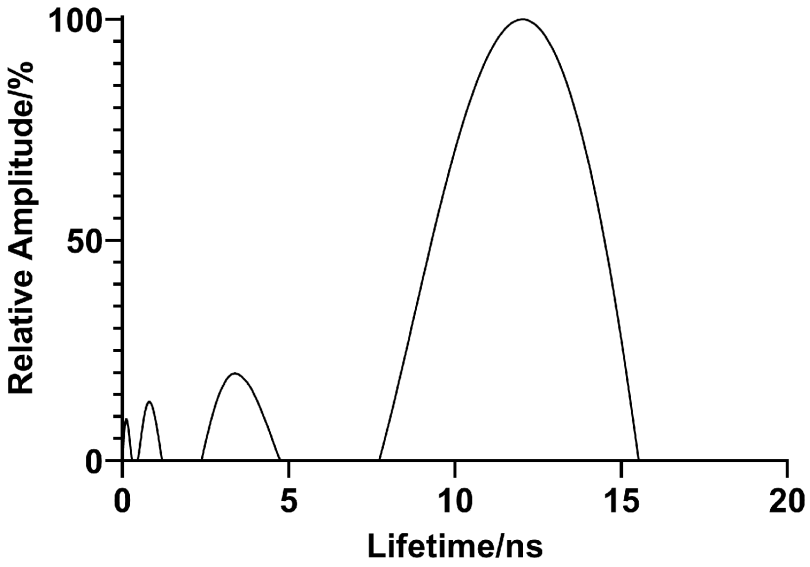

Figure 3.13: $Rx1_{1\text{-}489}$-LumP fluorescence lifetime distribution. Relative amplitude is the coefficient for each separable lifetime, normalised to 100%.

Using a lifetime range 0.01 ns to 40 ns with 1,000 subdivisions allowed for accurate and detailed lifetime analysis and revealed four lifetimes with a broad distribution. The primary lifetime was centred on 12.0 ns, somewhat shorter than the free LumP lifetime, and a secondary lifetime at 3.4 ns, as seen in figure 3.13. This may be due to energy transfer between molecules if the proteins interact. The shorter lifetimes had minimal contribution, as seen in figure 3.14. The anisotropy optimisation procedure produced a model with very close alignment to the data, as seen in figure 3.15.

3.4.2 *$Rx_{1\text{-}489}$-LumP Nucleotide Binding*

The NB-ARC domain of R proteins are predicted to activate upon binding of ATP (F.L.W. Takken and W.I.L. Tameling, 2009), and refolded $Rx1_{1\text{-}489}$ has been demonstrated to exhibit differing DNA-binding properties when bound to ATP (Fenyk, Townsend et al., 2015). Steady-

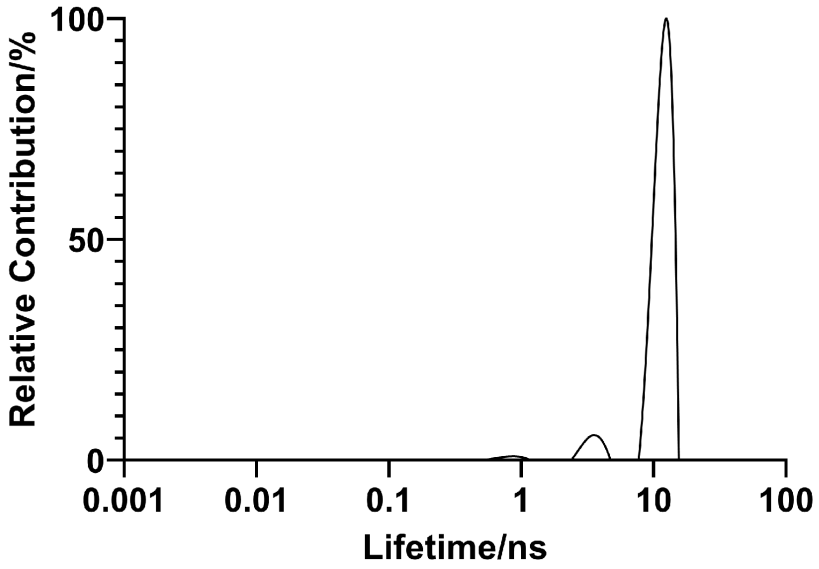

Figure 3.14: $Rx1_{1\text{-}489}$-LumP fluorescence lifetime yields. Relative contribution is the total number of photons contributed by each lifetime in the deconvolution

state anisotropy was therefore used to test the hypothesis that $Rx1_{1\text{-}489}$-LumP changes shape upon addition of ADP and ATP. As seen in figure 3.16, a small but insignificant increase in anisotropy was observed upon addition of ADP; a further and significant increase in size was observed upon addition of ATP, suggesting a conformational change may be taking place.

To investigate this potential phenomenon in more detail, time-resolved anisotropy measurements were made of $Rx1_{1\text{-}489}$- LumP on its own and with ADP and ATP to determine if a difference in rotational correlation can be determined and if nucleotide affects the lifetime distribution. As was found in the steady-state data, the ADP-bound protein exhibited a slightly larger but non-significantly larger rotational correlation time, while the ATP-bound protein was significantly larger than both. The FWHM of the peak was also slightly larger for the ATP-bound protein, suggesting it adopts a more flexible structure.

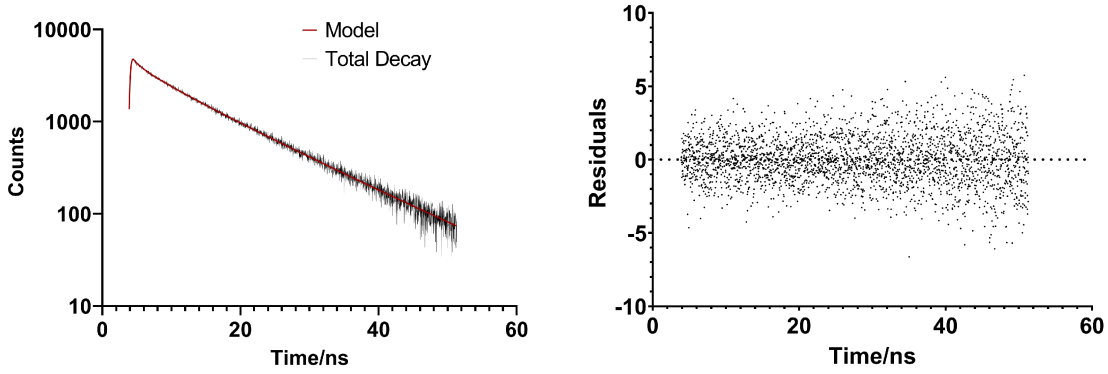

(a) $Rx1_{1\text{-}489}$-LumP fluorescence lifetime simulated decay vs measured data with residuals.

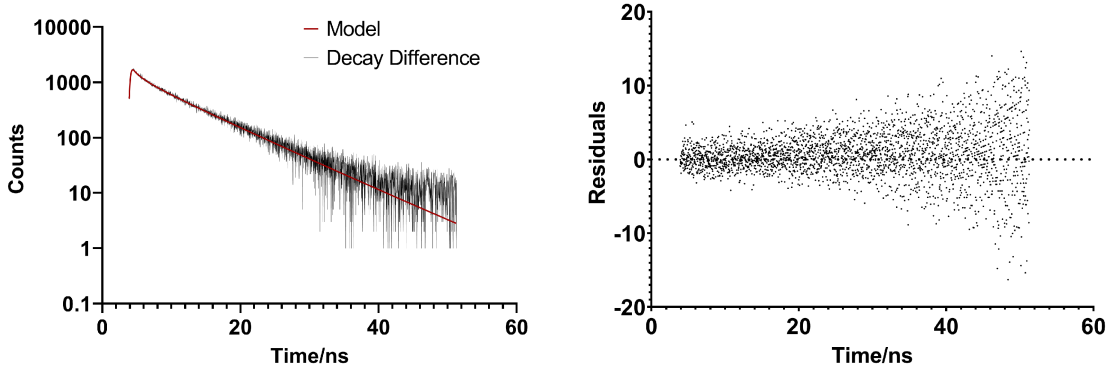

(b) $Rx1_{1\text{-}489}$-LumP parallel–perpendicular fluorescence lifetime difference simulated decay vs measured data with residuals.

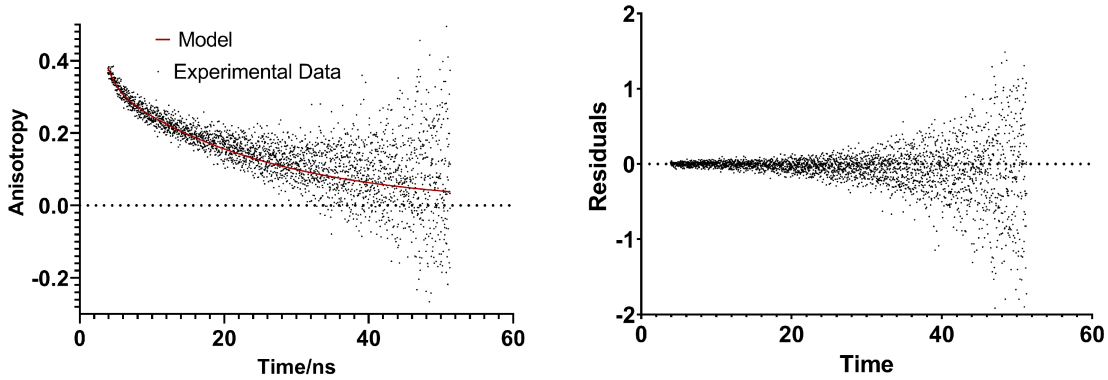

(c) $Rx1_{1\text{-}489}$-LumP anisotropy simulated decay vs measured data with residuals.

Figure 3.15

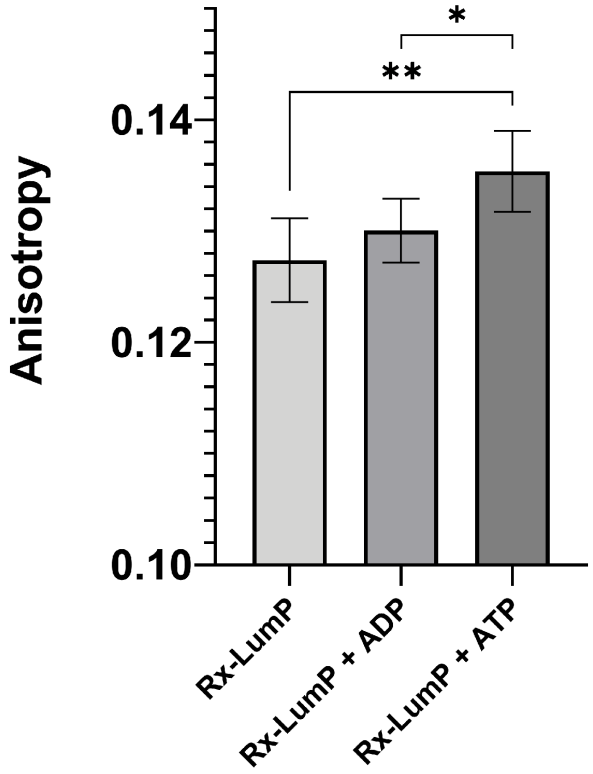

Figure 3.16: Steady-state anisotropy measurements of 1 μM $Rx1_{1\text{-}489}$-LumP upon addition of 5 μM ADP and ATP, with 95% confidence intervals. * indicates $p < 0.05$. ** indicates $p < 0.01$. $n = 9$.

	LIFETIME ONE		LIFETIME TWO		YIELD
	LIFETIME	FWHM	LIFETIME	FWHM	
Apoprotein	1.3 ± 0.04	0.08 ± 0.002	22.0 ± 0.4	2.0 ± 0.13	98.8 ± 0.01
ADP	1.4 ± 0.05	0.16 ± 0.009	22.7 ± 0.05	1.9 ± 0.11	98.8 ± 0.05
ATP	1.6 ± 0.18	0.21 ± 0.08	24.5 ± 0.5	2.5 ± 0.17	98.6 ±0.25

Table 3.1: Rx-LumP Time-Resolved Anisotropy with Nucleotide. 95% confidence intervals shown. $n = 3$

As the concentrations used were lower than for LumP due to the reduced stability of the protein *in vitro* and limited quantities, a longer acquisition time was necessary. Temperature affects anisotropy both by affecting the rotational energy of molecules and the viscosity of the medium. Consequently while previous experiments were conducted using a cooled cuvette and protein taken directly off ice, these experiments were conducted at room temperature. On the assumptions made above adjusted to room temperature 22 ns indicates a protein approximately of size 64 kDa, while the larger 24.5 ns suggests 72 kDa. This compares to the true size of the construct of 76 kDa. While this is not completely accurate, it confirms the protein is a monomer in solution and furthermore that the fluorescence does not derive from cleaved LumP in solution. It does, however, indicate the limitation of this technique for making absolute quantitative statements about size, as there are many variables and assumptions in the calculation. The data are summarised in table 3.1.

These data are consistent with the hypothesis that ATP binding causes the release of the LRR from the CC domain, adopting a more open structure, as well as previous data demonstrating that nucleotide binding is important for the activation of Rx1, such as melting DNA upon ATP binding (Fenyk, Townsend et al., 2015) and losing activity

in vivo when the P-loop in the NB domain is mutated (E. Slootweg et al., 2010). The importance of protein conformational flexibility has been established for some time, but traditional methods of probing protein structure such X-ray crystallography suffer from representing a snapshot in time rather than the diversity of protein structure (Huber, 1979).

More recent evidence has shown the importance of protein conformational flexibility in drug design: the traditional approach of maximising the enthalpic contribution to stabilising an active or inactive state in the target can have some unintended effects, especially if the transition state is also stabilised. This can result in the protein adopting a greater number of configurations meaning that despite enthalpic optimising, entropic effects take over, causing the protein to be less likely to adopt the desired conformation. In particular, it was demonstrated that many small-molecule interactors with HSP90 do not exhibit significant enthalpic stabilisation, but cause a switch to a more flexible, entropically favoured, conformation (Amaral et al., 2017). Indeed, it has previously been shown that AMPPCP (an ATP analogue) activates the helical lid form of HSP90 by enhancing its conformational flexibility, while ADP maintains the protein in its inactive state by increasing conformational rigidity. If ATP triggers similar behaviour in Rx1 and actively promotes structural flexibility, as suggested by the larger anisotropy lifetime distribution, this may allow Rx1 to adopt enthalpically unfavourable conformations in its active state, while ensuring that in the absence of nucleotide the protein is safely locked in its inactive state. Indeed, G-protein– coupled receptors have demonstrated this behaviour *in silico*. Upon ligand binding, the extracellular domains of the protein are stabilised, while

the intracellular domains exhibit increased flexibility that is necessary to recruit the G protein, whereupon the receptor is fully stabilised. This mechanism appears to rely on an unfavourable conformation becoming more likely upon ligand binding due to the increased 'search space' resulting from greater flexibility (Preininger, Meiler and Hamm, 2013).

Further work will be required to determine if this is a robust observation as the difference is relatively small. If this hypothesis is correct the P-loop K176R mutant should have the same rotational correlation time as the apoprotein, while the constitutively active D460V mutant may have a large apparent size even in the absence of nucleotide.

3.4.3 Nb*Glk and* Nb*DBCP Binding*

*Nb*Glk and *Nb*DBCP are known interactors with Rx1 (Dixon, 2017; Townsend et al., 2018). Steady-state anisotropy measurements were used to test the hypothesis that $Rx1_{1\text{-}489}$-LumP binds these proteins. Equimolar additions of protein were made 30 minutes before measurement. BSA was used as a control, with an increase in anisotropy observed upon its addition, suggesting non-specific interactions or increased sample viscosity. *Nb*DBCP showed no significant difference from the BSA control; however addition of *Nb*Glk showed a significant increase in anisotropy suggesting a binding interaction, as seen in figure 3.17.

To act as a control for this potential binding, the Rx1 Coiled Coil (CC) was expressed with an N-terminal Glutathione S-Transferase (GST) and purified using immobilised glutathione agarose resin. Previous work has demonstrated an interaction between GST-CC and *Nb*Glk (Townsend et al., 2018). To investigate whether *Nb*Glk can facilitate an

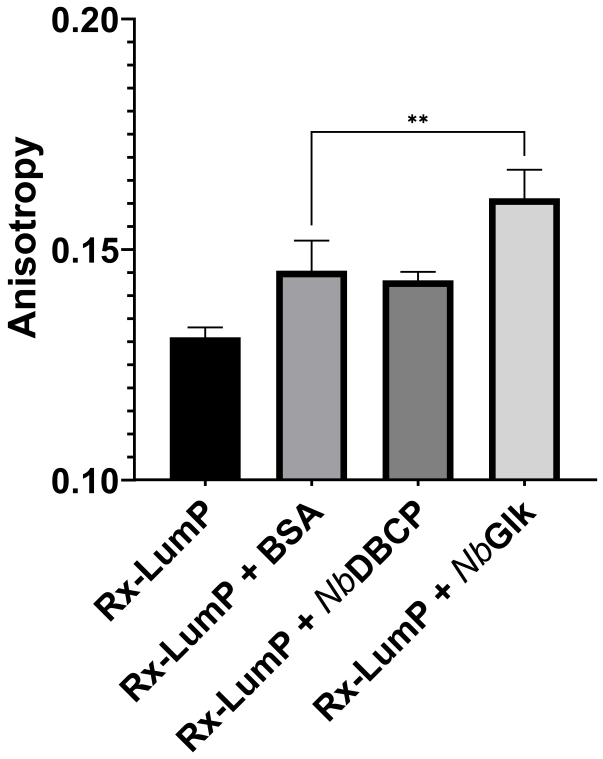

Figure 3.17: Steady-state anisotropy measurements of 1 μM $Rx1_{1\text{-}489}$-LumP upon addition of 1 μM BSA, *Nb*$DBCP_{1\text{-}475}$ and *Nb*$Glk_{183\text{-}402}$, with 95% confidence intervals. ** indicates $p < 0.01$. $n = 9$.

interaction between Rx1 and *Nb*DBCP, gel filtration experiments were conducted. Gel filtration is a form of size-exclusion chromatography that uses column containing a bed of porous beads. As the sample flows through the column, smaller molecules diffuse further into these pore, allowing separation by size; hence a larger size is expected to cause a lower retention volume. The experiment was conducted on two columns of different sizes. Addition of *Nb*Glk and *Nb*DBCP caused an increase in the intensity of the lead protein peak as expected, as measured by UV absorbance. Both experiments demonstrated a clear shift for GST-CC in the presence of *Nb*Glk, as indicated in 3.18. No shift was observed in the presence of *Nb*DBCP, corroborating the previously observed results for CC-NBARC-LumP. Surprisingly, both experiments also showed no shift in the presence of both NbDBCP and *Nb*Glk, indicating that *Nb*DBCP may either be inhibiting the binding of *Nb*Glk to Rx1 either by sequestering of *Nb*Glk or by disrupting its interaction at the binding site in a manner not picked up by the gel filtration. These data corroborate the *Nb*Glk binding identified for Rx-LumP, but further indicate that adding *Nb*DBCP and *Nb*Glk together may abolish this interaction.

3.4.4 *DNA Binding*

Previous unpublished homology modelling had identified a number of residues within Rx1 that may be involved in DNA binding. An initial screen using refolded protein had suggested the T452A mutant was deficient in DNA binding based on $n = 3$ repeats at one protein concentration. Therefore, single point mutagenesis was used to make the T452A mutant of $Rx1_{1\text{-}489}$-LumP to test the hypothesis that this mutation affects the DNA binding affinity of soluble Rxl. The

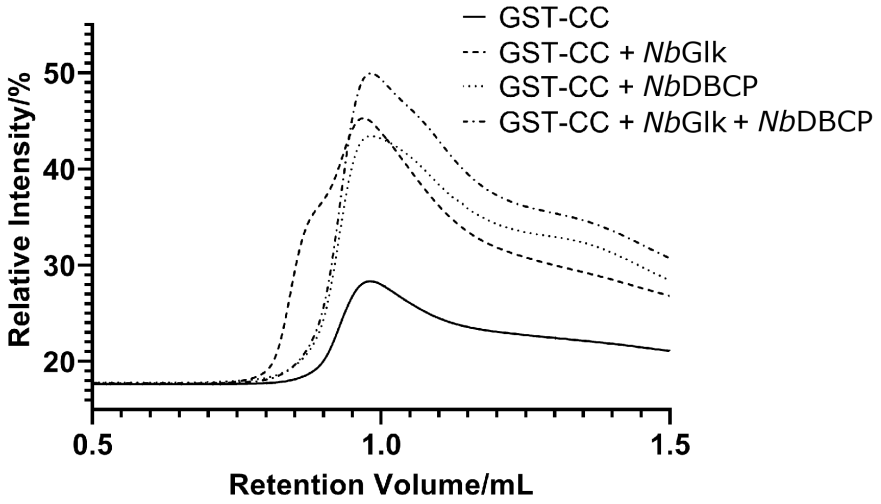

(a) Gel filtration of GST-$Rx_{1\text{-}144}$ with *Nb*$Glk_{83\text{-}402}$ and *Nb*$DBCP_{1\text{-}475}$ using a Superdex 75 PC 3.2/30 column at 0.1 mL/min. A shoulder at a lower retention volume was observed for *Nb*Glk only.

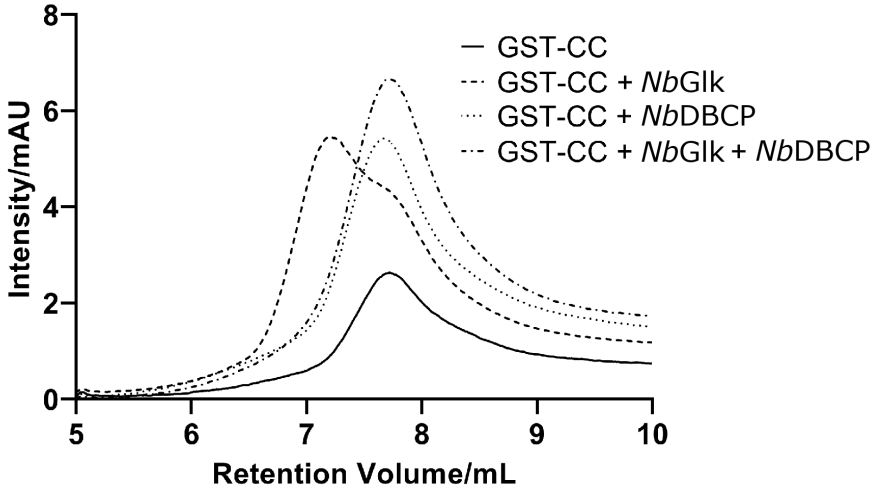

(b) Gel filtration of GST-Rx1-144 with *Nb*$Glk_{83\text{-}402}$ and *Nb*$DBCP_{1\text{-}475}$ using a Superdex 75 10/300 GL column at 0.5 mL/min. A peak at lower retention volume was observed for *Nb*Glk only.

Figure 3.18

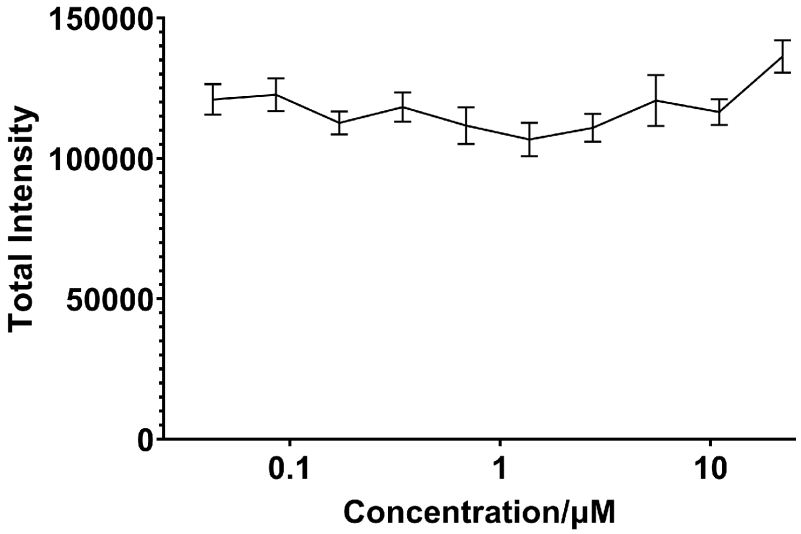

Figure 3.19: Total fluorescence emission ($I_{\parallel} + 2I_{\perp}$) from 10 nM fluorescein-labelled oligonucleotide at different concentrations of $Rx1_{1\text{-}489}$-LumP, with 95% confidence intervals. WT and T452A data combined, $n = 6$.

experiment was conducted as previously using refolded Rx1; however a lower concentration of 10 nM oligonucleotide was used. The wavelengths used do not coincide significantly with the excitation spectrum of LumP and no significant fluorescence from LumP was observed at the excitation intensity used at any concentration, as seen in figure 3.19, demonstrating the additional fluorophore was not interfering with the experiment. No significant change in anisotropy was found for BSA.

DNA binding was observed for both wild type and mutant and no difference was observed in binding affinity, as seen in figure 3.20. Unusual behaviour was also noted at higher protein concentrations, with anisotropy decreasing. This may be due to protein aggregation causing dissociation of DNA or behaviour related to the formation of higher order structures. This suggests that the previously identified difference was either an artefact as a result of testing a large number

of mutants with low replicate numbers, or that the effect is only seen in refolded protein.

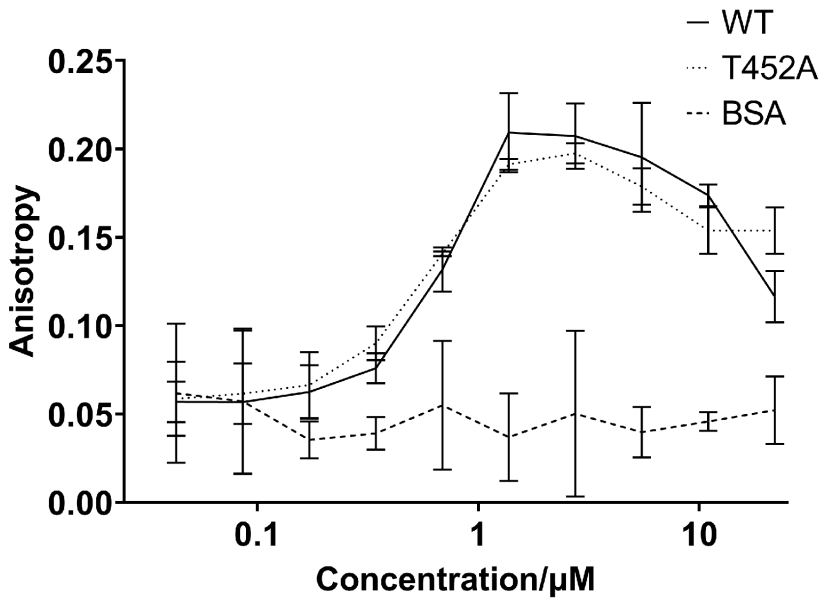

Figure 3.20: Difference in anisotropy of 10 nM fluorescein-labelled ssDNA oligonucleotide in the presence of different concentrations of $Rx1_{1\text{-}489}$-LumP WT and T452A and BSA on a logarithmic x-axis, excited at 485/20 measured at 528/20 nm,with 95% confidence intervals. $n = 3$.

3.4.5 *Twin-Strep Tag*

To improve the purity and yield of the $Rx1_{1\text{-}489}$-LumP protein, an N-terminal twin-strep tag was cloned into the construct and dual purification using StrepTactin XT resin followed by Ni-NTA purification was able to both enhance yield (recovery of around 0.4 mg/L culture), reduce losses and improve purity (see 3.21).

However, when this protein was tested for activity, it failed to replicate the previously observed DNA-binding behaviour observed. As

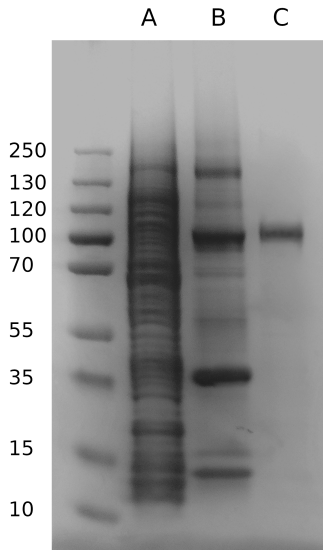

Figure 3.21: SDS-PAGE gel of Twin-Strep–$Rx1_{1\text{-}489}$–LumP–His_6. Lane A contains the cell lysate, lane B contains the protein sample after twin-strep purification and lane C contains the protein after dual purification.

an alternative approach to diagnose the issue, native PAGE was used to determine if a shift could be observed in the mass of fluorescently labelled oligonucleotide. While Native PAGE was able to show that the protein was soluble and running as a monomer, no shift or reduction in the oligonucleotide band was observed, as seen in figure 3.22. This indicates the process of Twin-Strep purification or the tag itself may be affecting its activity.

3.4.6 *Phosphatase Assay of $Rx1_{1\text{-}489}$-LumP*

While phosphatase activity has previously been observed in various R proteins (Fenyk, San et al., 2012), it has never been observed in Rx1, despite containing a canonical phosphatase domain. To test the hypothesis that soluble Rx1 exhibits enzymatic activity not seen in the refolded protein, an assay was conducted using para-nitrophenylphosphate (pNPP). This colourless compound is used as a marker for phosphatase

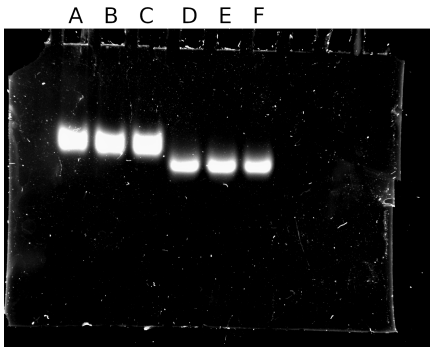

(a) Native PAGE of Twin-Strep–$Rx1_{1\text{-}489}$–LumP (A-C) and LumP (D-F) visualised under UV.

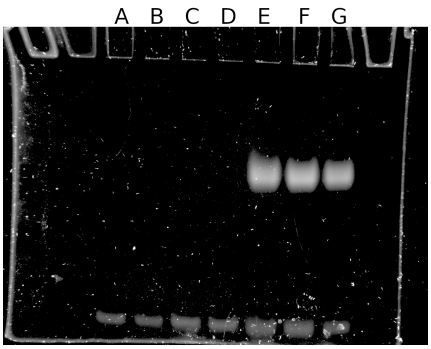

(b) Native PAGE of fluoroscein-labelled oligonucleotide (A), BSA with oligonucleotide (B-D) and Twin-Strep–$Rx1_{1\text{-}489}$–LumP with oligonucleotide (E-G).

Figure 3.22

activity: when the phosphate group is cleaved, para-nitrophenol is liberated, which is yellow in colour, absorbing at 405 nm. 2 mM pNPP was incubated with 1 μM protein at 37 °C for 60 min. Very low but measurable level of phosphatase activity was observed, as seen in figure 3.23. This indicates that expressing soluble Rx1 by using LumP as a solubilising factor may allow it to retain some activity that is lost in the denaturation and refolding process. It is therefore possible that some previous *in vitro* data does not reflect the native behaviour of Rx1 and using the LumP fusion may allow some previously unknown activity (or activity identified *in vivo*, but not replicated *in vitro*) to be characterised.

3.5 CONCLUSION

Experiments using refolded protein indicated the formation of higher-order molecular structures, which have large apparent masses and long rotational correlation times. The properties of LumP were investigated to determine its suitability for use in accurate time-resolved anisotropy experiments to measure such long rotational correlation

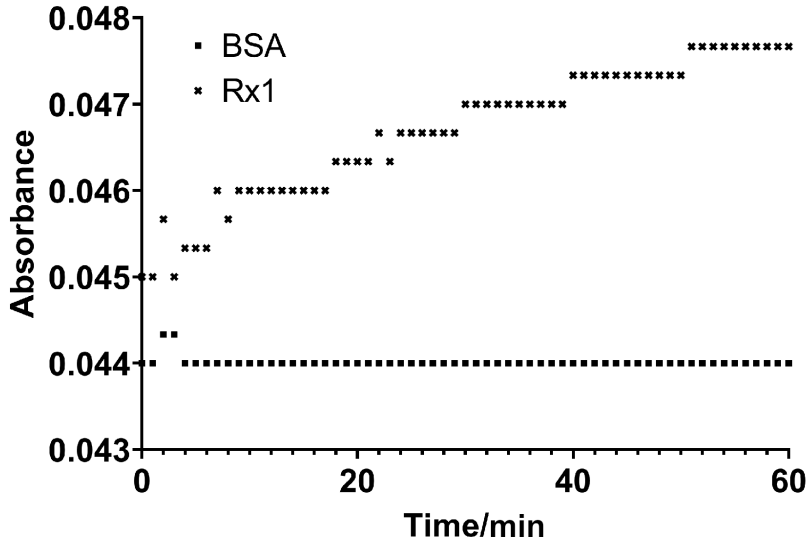

Figure 3.23: Phosphatase assay using pNPP and $Rx1_{1\text{-}489}$-LumP. Absorbance is at 405/20 nm.

times. It was demonstrated that the long fluorescence lifetime of LumP conferred a much greater degree of accuracy than GFP for such measurements, especially for larger or more rotationally hindered molecules. An Rx1-LumP construct was made, which unexpectedly permitted the expression of soluble Rx1. The fluorescence behaviour of this protein was characterised, showing it shared the long-lifetime primary lifetime of LumP, but additionally exhibited more complex fluorescent properties, with several minor additional, shorter lifetimes. A sophisticated method of analysing this data was developed, utilising compressive sensing to generate a lifetime distribution for both fluorescence and rotation, which was able to deconvolute the data with excellent correlation to the data as indicated by residual analysis.

The LumP fusion enabled investigation into structural protein changes. Both steady-state and time-resolved anisotropy experiments revealed a conformational change upon binding of ATP, with an increase in hydrodynamic radius. Furthermore, the size distribution

for the ATP-bound protein was found to be broader than for the ADP-bound or the apoprotein. The LumP fusion also allowed for investigation of protein interactors, and confirmed previous work that demonstrated *Nb*Glk binding. Furthermore, gel filtration with the GST fusion, replicated this *Nb*Glk-binding activity and demonstrated that *Nb*DBCP was able to abolish this binding. Finally, the LumP fusion may possess activity not found in refolded Rx1, as phosphatase activity was demonstrated, which is not found in the refolded protein.

LumP was therefore used to study protein hydrodynamics, protein-protein interactions, as well as potentially restore activity lost in the process of refolding and therefore represents a highly useful tool for studying Rx1 and protein activity more broadly.

4

IN VIVO RX1 EXPERIMENTS

4.1 INTRODUCTION

The expression of Rx1 in *Nicotiana benthamiana* may trigger one of two responses. Coexpression of PVX with Rx1 results in a drastic reduction in viral load compared to virus expressed alone, as monitored by a fluorescently-labelled virus construct (Peart et al., 2002). Expression of a virulent form of the coat protein has the more severe effect of cell death as part of the hyper-sensitive response (Bendahmane, Kanyuka and Baulcombe, 1999). A variety of proteins have been identified that are important in plant immune signalling (detailed below). Some are required for resistance to a broad range of threats, while others are specific to the Rx1-mediated response to PVX. Identifying these proteins, and in particular interactors with Rx1, and their functions is vital in elucidating the signalling processes that occur in immunity. Rx1 alone lacks a number of features that would be necessary to confer resistance alone, suggesting a larger complex must be required. In particular, the lack of any DNA-binding specificity and an apparent absence of interaction between the viral coat protein and Rx1 (as indicated by coimmunoprecipitation experiments and a yeast two hybrid screen conducted by the Cann group for Dixon, 2017) suggests there must at minimum be a guard-type protein interactor and a transcription factor to direct specific DNA transcription. Many

other functions such as positive and negative regulators of immunity, intracellular localisation regulators, chromatin remodellers, regulators of other signalling pathways such as phosphorylation, and structural proteins may also be necessary for properly regulated immune function. It is therefore essential to determine whether and how such a complex may form *in vivo* by finding interactors and characterising their function.

4.1.1 *Nucleocytoplasmic Partitioning*

The CC domain of Rx1 interacts with RanGAP2 *in vivo* (W.I.L. Tameling and Baulcombe, 2007). RanGAP proteins are important regulators of nucleocytoplasmic trafficking (Meier, 2007). Nuclear localisation appears to be an important factor in Rx1 function *in planta*: the CC domain, expressed separately, is localised in the nucleus, bound to immobile elements; the LRR domain is found in the cytoplasm; and the NB-ARC domain may be found in both compartments. This nucleocytoplasmic distribution may be an important factor in the control of Rx1 activity in the cell, as despite the lack of a canonical nuclear localisation sequence, the protein is found in both the nucleus and the cytoplasm under normal conditions. Furthermore, the inclusion of either a nuclear localisation or a nuclear export sequence resulted in a significant reduction in activity (E. Slootweg et al., 2010).

RanGAP2 acts as a regulator of nucleoplasmic partitioning of Rx1 independently of GAP activity by sequestering Rx1 in the cytoplasm. Silencing of one or both RanGAP proteins results in localisation to the nucleus and a concomitant reduction in activity, as does coexpression with RanGAP2 fused to the SV40 NLS. On the other hand, overexpression of RanGAP2 causes Rx1 localisation to the cytoplasm,

but enhances activity. This may be due to a stabilising effect on Rx1 causing an overall increase in Rx1 levels in the cell (W.I. Tameling, Nooijen et al., 2010). This is supported by the fact that silencing of SGT1, which causes a similar cytoplasmic localisation, does not cause accumulation of Rx1 and reduces activity (E. Slootweg et al., 2010).

This suggests the LRR acts as an autoinhibitor by causing export of the NBARC domain from the nucleus. This is consistent with the constitutional activity of truncated CC-NBARC, with the NBARC domain being sufficient for initiating HR and the CC domain not. Furthermore, a mutation in the P-loop of the NB domain abolishes activity and excludes Rx1 from the cytoplasm in an LRR-dependent manner (E. Slootweg et al., 2010). This is consistent with findings that P-loop mutations disrupt the interaction between the CC (which locates to the nucleus and does not trigger HR) and the NBARC-LRR (which locates to the cytoplasm), but not the CC-NBARC (which is sufficient to cause HR) and the LRR (which abolishes this activity). Nonetheless, other systems have been demonstrated to exhibit HR in the presence of only the CC or TIR domain, suggesting there may exist different signalling mechanisms (Swiderski, Birker and J.D.G. Jones, 2009).

4.1.2 Nb*Glk*

*Nb*Glk is a known interactor of Rx1, identified through a yeast two hybrid screen and is known to interact with Rx1 *in vitro* and *in vivo* (Dixon, 2017). It has been shown to possess both weak non-specific DNA-binding activity and strong affinity for specific consensus sequences, suggesting it may act as a transcription factor to target Rx1 binding. *Nb*Glk overexpression is known to be sufficient to confer ex-

treme resistance to PVX but does not trigger cell death in response to CP. Neither Rx1 nor *Nb*Glk are found to bind DNA *in planta* when expressed alone; however, when coexpressed, Rx1 is found to bind DNA in a manner that may be enhanced by *Nb*Glk's non-specific DNA binding behaviour. When coexpresssed alongside CP or PVX, this complex changes to allow *Nb*Glk to bind its consensus sequence and trigger an immune response. This is consistent with overexpression of *Nb*Glk being sufficient to induce resistance, but not HR, suggesting that a large enough pool of *Nb*Glk is able to bind its consensus sequence in the absence of the targeting by Rx1 to the genome (Townsend et al., 2018).

4.1.3 Nb*DBCP*

*Nb*DBCP has been identified as a potential interactor with Rx1 through a yeast two-hybrid screen (Dixon, 2017). Current evidence is mixed as to whether these two proteins interact directly; however, both Rx1 and CP inhibit *Nb*DBCP DNA binding *in planta*. Furthermore, *Nb*DBCP suppressed Rx1- and *Nb*Glk- conferred resistance to PVX, while silencing enhanced resistance. Overexpression of *Nb*DBCP with a mutation to a putative acetyl lysine binding site however resulted in resistance to PVX. As a bromodomain protein, *Nb*DBCP may bind histones and therefore natively suppress the immune response by upregulating or downregulating genes through chromatin remodelling. Rx1 may bind *Nb*DBCP to reverse this suppression to enhance resistance (Dixon, 2017).

4.1.4 *NRC1*

NRC1 is a CC-NB-LRR protein that has been found to be required for HR by a variety of proteins, including Cf-9, LeEix, Pto, Mi and Rx1, as well as Cf-4–induced resistance to *C. fulvum* (Gabriëls et al., 2007). Silencing of a variety of proteins involved in HR along with a constitutively active mutant of NRC 1 demonstrated that NRC1 requires RAR1 and SGT1 to be functional and acts upstream of a MAP kinase pathway but downstream of EDS1, which is required for Cf-4 function (Gabriëls et al., 2007).

4.1.5 *Yeast Two-Hybrid Screen*

To facilitate the identification of unknown Rx1 interactors, a yeast two hybrid screen previously identified a number of putative Rx1 binding proteins (Dixon, 2017). Ten proteins were selected for testing from this screen, summarised in table, with information from the NCBI on predicted domains, with the LOC numbers from *N. sylvestris.*

PROTEIN	DOMAINS OF INTEREST
APRR/APRR2 LOC104222218/ LOC104232658	REC: Homodimeric signal receiver domain found in both prokaryotes and eukaryotes. Phosphorylation by histidine kinases transmits intracellular signals from a variety of proteins, including the Arabidopsis ethylene receptor ETR1.
	myb-like DNA-binding domain, SHAQKYF class: a DNA-binding domain found mainly in plant proteins.

	*Nb*Glk-like region.
D-3- phosphoglycerate dehydrogenase LOC101246616a	Phosphoglycerate dehydrogenase (PGDH): catalyses the synthesis of L-serine from D-3-phosphoglycerate.
	Helix-Turn-Helix: DNA-binding domain found in several plant transcription factors. May contain an effector-binding site at the C-terminus and a DNA-binding site at the N-terminus.
	ACT: Found adjacent to PGDH domains that form serine-binding sites. ACT domains can interact, creating an asymmetric binding site.
Chromodomain-helicase DNA-binding 1 LOC104213245	DEXDc: Involved in ATP-dependent DNA unwinding.
	HELICc: Found in a variety of helicase proteins.
	CHROMO: Chromatin organisation modifier domain. Involved in the functional organisation of the eukaryotic nucleus and may bind methylated histones as well as RNA.

PM23 LOC104221989	TMF_TATA_bd: CC region of TATA element modulatory factor 1 proteins. These bind to the TATA motif in RNA polymerase II promoters and inhibit their expression.
HBP-1b(c38)–like LOC104244616	bZIP_HBP1b-like: Basic leucine zipper domain found in mostly uncharacterised transcription factors. Dimerisation of these domains permits DNA-binding form with various effects on transcription.
	DOG1: Controls seed dormancy.
	CAF-1_p150-like region: Chromatic assembly factor 1 complex p150 subunit. Inserts acetylated histones H3/H4 into chromatin.
TCP4 LOC104241617	TCP: Involved in a number of developmental processes. Contain a DNA-binding domain.
LOC104230625	Homeodomain: DNA binding domain involved in developmental regulation in eukaryotes.
	Polo Kinase Kinase: Ser/Thre kinase involved in mitosis.

	DDT: Interacts with nucleosomal linker DNA and ISWI proteins, acting as a spacer between adjacent nucleosomes.
	HARE-HTH: May have a chromatin function such as distinguishing hmC-modified DNA.
	WHIM1/2/3: Cooperates with the DDT domain to distinguish methylated DNA.
LOL1 LOC104236337	LSD1: Zinc finger domain. Negatively regulates cell-death in response to a superoxide-dependent signal.
Ethylene-Insensitive 3–Like 5 LOC104211924	EIN3: Ethylene insensitive 3 proteins are plant DNA-binding proteins that respond to ethylene-mediated cell growth inhibition and senescence.

4.2 VIRUS-INDUCED GENE SILENCING

Viral-Induced Gene Silencing (VIGS) is a technique used to reduce or knock out the expression of genes in plants that was used to determine whether the genes identified in the Y2H screen played a role in immune signalling. Two 300 bp sequences complementary to two different parts of each gene were designed (sequences listed in chapter 5) and cloned into TRV2, a plasmid derived from the Tobacco Rattle Virus with virulence genes removed. This was coinfiltrated with

TRV1 into 2-week old *N. benthamiana* plants, using a silencing construct for phytoene desaturase (PDS) as a positive control for silencing, which results in leaf bleaching, as seen in 4.1 (Velásquez, Chakravarthy and Martin, 2009).

Figure 4.1: PDS-silenced plant indicating successful gene silencing, with bleached leaves identified by *

After 3 weeks, GFP-labelled PVX was infiltrated into leaves with and without Rx1. After three days, viral load was measured by GFP fluorescence. The effect of the silencing on Rx1-mediated resistance was measured by comparing the relative effect of Rx1 in the silenced plants to unsilenced plants.

GFP silencing constructs were used as a negative control, with differences measured on this basis. These exhibited around a 10% reduction in Rx1-conferred PVX immunity compared to the unsilenced control, possibly due to the stress incurred by the expression of silencing genes.A great deal of variability in viral load was found between replicates, which made it difficult to determine if silencing had an effect. However, five silencing constructs were tested with the two sequences.

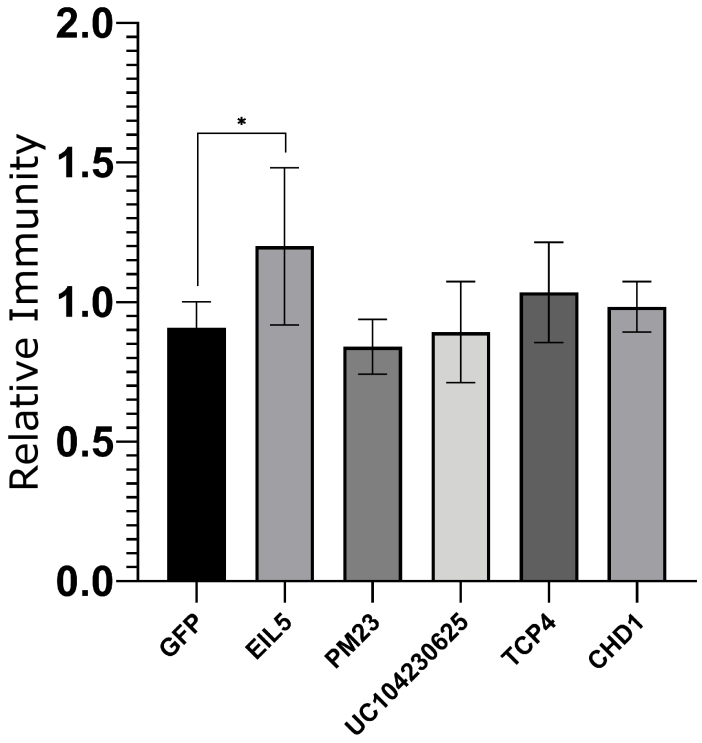

Figure 4.2: Relative Rx1-induced immunity to PVX for gene-silenced plants, determined as the proportional reduction in PVX-GFP fluorescence induced by Rx1 in silenced plants relative to unsilenced wild-type plants/. Excitation at 485/20, emission measured at 528/20 nm. * indicates $p < 0.05$. $n = 24 - 42$.

No significant effect was found for any of the tested constructs, except for EIL5, as seen in 4.2. EIL5 is therefore a new preliminary Rx1 interactor, verified by Y2H and function.

In PTI and ETI, the ethylene biosynthesis pathway is triggered by a number of mechanisms, including G-protein molecular switches, MAPK cascades, Ca^{2+} signalling leading to the activation of 1-aminocyclopropane-1-carboxylate synthase (ACC), which makes the biosynthetic precursor to ethylene, and ROS such as H_2O_2 and nitric oxide, which trigger the transcription of genes involved in ethylene bioysnthesis (Vidhyasekaran, 2015). Ethylene production is also a known target for suppression by pathogen effectors.

The precise role of ethylene in plant immunity is unclear. Evidence from ethylene-responsive transcription factor mutants such as *ein3/eil1* in *Arabidopsis* has indicated that ethylene signalling is effective in resistance against necrotrophic pathogens such as fungi, but negatively impacts bacterial immunity (Glazebrook, 2005). There is a great degree of cross-talk between the ethylene, Salicylic Acid (SA) and jasmonic acid signalling pathways (Pieterse et al., 2012) — Salicylic acid Induction Deficient 2 is a key target of EIN3 and EIL1, meaning there is an accumulation of SA in plants deficient in these proteins, with a corresponding enhancement of bacterial resistance (Chen et al., 2009). More recent evidence using *acc* mutants, has suggested that ethylene in fact has a positive impact on bacterial resistance and the previously identified negative effect is due to the other interactions of the mutated proteins (Guan et al., 2015). These VIGS data suggest EIL5 silencing enhances Rx1-conferred resistance. This suggests EIL5 may play a similar role in viral resistance to that which related protein EIL1 plays in bacterial resistance.

Due to the large number of replicates needed to acquire good data and the lengthy nature of the experiment, there was insufficient time to complete this work. Further work should investigate the remainder of the silencing constructs and conduct more repeats on the EIL5 construct to improve statistical significance. Furthermore, *acc* mutants or ACC-silenced plants could be used to verify whether this difference is due to a negative effect of ethylene activity itself on viral resistance or other signalling activity controlled by EIL5, such as interaction with the SA pathway. The reason for the direct interaction between EIL5 and Rx1 should also be investigated. For example, it may be that Rx1 inhibits EIL5 activity when activated in order to enhance its resistance.

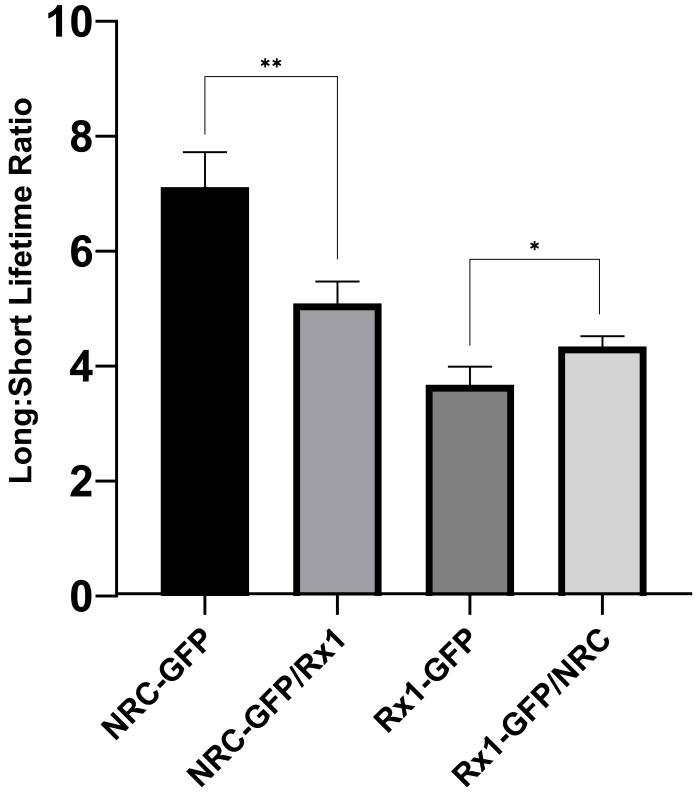

Figure 4.3: Ratio of long:short lifetime yields in GFP-tagged NRC and Rx1 constructs *in vivo*. * indicates $p < 0.05$, ** indicates $p < 0.01$. $n = 3$

This might be tested by measuring its effect on EIL5 DNA-binding activity *in vitro* and *in vivo*.

4.3 NRC1-RX1 INTERACTION *in vivo*

As NRC1 is known to be required for Rx1-induced HR, an experiment was designed to investigate whether NRC1 interacts with Rx1. In particular, two hypotheses were tested: first, that NRC1 brings Rx1 to DNA in the absence of CP and second that NRC1 is brought to DNA by Rx1 in the presence of coat protein. This work was carried out using a method previously described using the DNA-binding dye LDS-751. The absorption peak of LDS is at 543 nm, which overlaps with the

emission spectrum of GFP. This allows energy transfer from GFP to take place by FRET when in close proximity, indicated by a drop in the fluorescence lifetime. Time-resolved measurements allow the short FRET-associated lifetime and the longer free protein lifetime to be measured, with the relative yields being used to determine the relative degree of DNA-binding activity. It is predicted that DNA binding by a GFP-tagged protein should exhibit a larger contribution by this shorter lifetime than free protein (Townsend et al., 2018). GFP-NRC1 was coexpressed in *N. benthamiana* with Rx1 as well as NRC1 with the avirulent PVX coat protein CP106 and GFP-Rx. Leaves were then stained by the DNA-binding dye LDS-751 and fixed in formaldehyde.

As seen in 4.3, experiments showed that coexpression of Rx1 with NRC-GFP decreased the long:short lifetime ratio, which is indicative of FRET occurring against LDS. This suggests Rx1 is promoting the localisation of NRC1 to DNA, either by triggering binding by NRC1 directly, or by associating with NRC1 and subsequently binding to DNA itself. The reverse experiment shows a smaller effect, with an apparent increase in the long:short lifetime contributions upon coexpression of NRC1 with Rx1-GFP. This suggests NRC1 may be promoting Rx1 disassociation from DNA.

Further work will be required to determine the exact role of NRC1; however, these experiments together suggest that NRC1 binds Rx1 *in vivo*. Furthermore, it suggests that NRC1 does not bind DNA on its own, despite being an NLR, and is dependent on Rx1 to be brought towards chromatin. The data is also consistent with a cytoplasmically localised protein, which may explain why Rx1-GFP appears somewhat less bound to DNA when coexpressed with NRC1, as it may be sequestered in the cytoplasm.

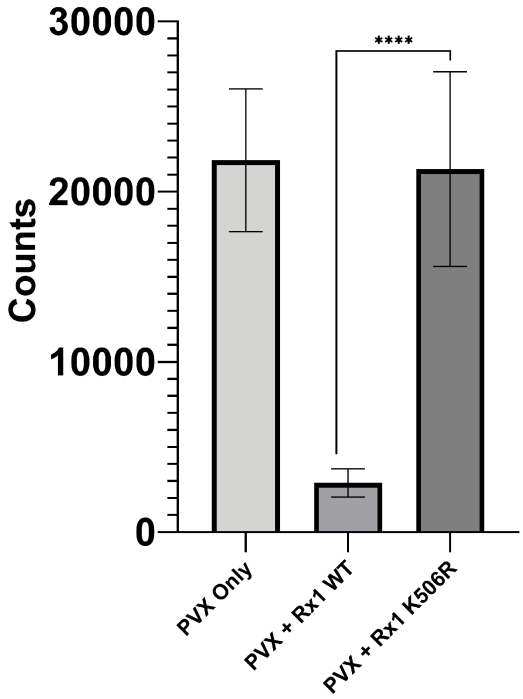

Figure 4.4: Comparison of the fluorescence of PVX in the presence of Rx1 WT and Rx1 K506R. Excitation at 485/20, emission measured at 528/20 nm. **** indicates $p < 0.0001$. $n = 16$.

4.4 K506R RX1 MUTATION

Protein-protein interactions can be both non-covalent, as with the interactors discussed so far, and covalent, as with ubiquitination. Small Ubiquitin-like MOdifiers (SUMOs) are small proteins that are known to covalently bind lysine residues of protein substrates and induce functional changes, playing an essential role in a variety of biological processes including gene expression, DNA repair and cell signalling (Geiss-Friedlander and Melchior, 2007). For example, the SUMO-1 modification of RanGAP1,which is involved in the plant immune response, directs it from the cytoplasm to the nuclear pore complex (Matunis, Coutavas and Blobel, 1996). Furthermore, SUMOylation has been shown to play a role in mediating signalling, suppressing

both ethylene production and HR during PTI in response to LeEix in Tomato (Hanania et al., 1999), causing the degradation of NPR1, a key protein involved in SA-mediated resistance (Saleh et al., 2015), and is suppressed in response to PTI-induced nitric oxide signalling (Skelly et al., 2019). SUMO-binding sites can also be predicted computationally (Ren et al., 2009). *in silico* modelling work with Dr. Ari Sadanandom (Durham University) revealed the K506 and K787 residues within the LRR of Rx1 are potential SUMO binding sites. A K506R Rx1 mutation was used to determine if this affects activity. Hypersensitive response was also tested by coinfiltrating the WT and mutant with CP106, an avirulent allele of the PVX coat protein that triggers HR when expressed with Rx1, and CP105, a virulent allele of the coat protein, which is not recognised by Rx1 and is not expected to induce HR.

While Rx1 WT resulted in a reduction in viral load of around 90%, PVX resistance was abolished for the K506R construct, as seen in 4.4. HR was also mostly abolished, as seen in 4.5, although a slight yellowing was visible in the presence of K506R and CP106. This may be for a variety of reasons. As SUMOylation can cause differential nucleocytoplasmic partitioning, the Rx1 mutant may be sequestered in either the cystoplasm or the nucleus, abolishing activity. SUMOylation has also been shown to block ubiquitin-associated protein degradation (Ramachandran et al., 2015), so the mutant protein's relative abundance may be sufficiently reduced in the cell to abolish PVX resistance. SUMOylation can also mask binding sites or recruit proteins, so this mutation may permit a negative regulator to bind the protein and

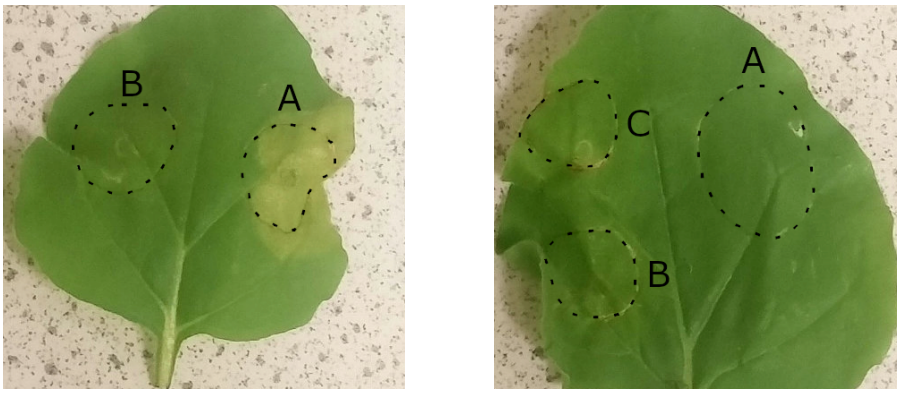

Figure 4.5: Dotted lines indicate extent of each region of infiltration *Left*. A. Rx1 WT + CP106. B. Rx1 WT + CP105. *Right*. A. Rx1 K506R. B. Rx1 K506R + CP105. C. Rx1 + CP106. Representative sample after 2 days.

reduce its activity or sequester it. Finally SUMOylation may confer a conformational change that activates the protein.

To test these hypotheses, a number of approaches will be necessary—a GFP-labelled K506R mutant would allow nucleocytoplasmic activity to be monitored by both confocal microscopy and DNA-binding activity. The conjugation of an immunogenetic tag, such as haemagglutinin, would allow for Western blotting to determine whether protein degradation is taking place. The final hypothesis is the most difficult to test, particularly as the mutation is located in the LRR, so cannot be tested *in vitro*. The approach most likely to succeed would be to screen a number of potential interactors from the Y2H screen *in vivo* to determine whether silencing one of them can restore activity in the mutant.

4.5 EXPRESSION OF RX1-LUMP AND LUMP *in planta*

As was demonstrated in chapter 3, LumP is a protein fluorophore that may provide a way to acquire detailed information about protein hydrodynamics and interactions by time-resolved fluorescence

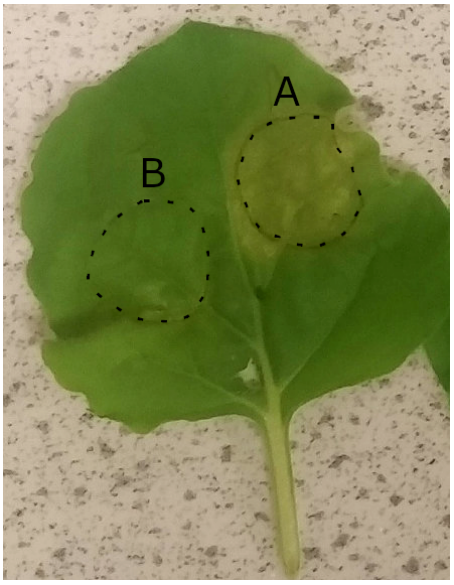

Figure 4.6: Dotted lines indicate extent of each infiltration A. Rx1-LumP + CP106. B. Rx1-LumP + CP105. Representative sample after 2 days.

anisotropy, and a microscope was built (described in chapter 2) to study these interactions *in planta*. Coexpression with *in vivo* binding partners, such as PVX CP, *Nb*DBCP, *Nb*Glk and NRC1 could therefore allow investigation into how these proteins affect the mobility of Rx1 in the cell, and whether binding behaviour was simply a two-way interaction or if a larger complex arose, as seen for ZAR1 (J. Wang, J. Wang et al., 2019), or if the protein is bound to static elements in the cell. GFP would not be a suitable fluorophore for this purpose as it is not accurate enough to distinguish between the sizes of large complexes.

To establish whether LumP could be used as a tool to study Rx1, a full-length Rx1-LumP fusion construct was cloned and infiltrated into *N. benthamiana*. To test whether the protein was being functionally expressed it is necessary to determine whether it is able to recognise its effector substrate *in vivo* and trigger HR. Rx1-LumP was therefore coinfiltrated with CP106 and CP105. HR was observed after 2 days

when coexpressed with the avirulent coat protein only as seen in 4.6. This suggests that the Rx1 portion of the protein fusion is being expressed and is functional. However, fluorescent microscopy and steady state fluorescence readings revealed there was no observable fluorescence above background that could be identified either by its characteristic spectrum, an overall increase in fluorescence levels or from a long lifetime contribution (data not shown). This may be due to an inactive LumP domain or because of cleavage *in vivo* that left only the Rx1 intact.

To determine whether this phenomenon was due to an active Rx1 domain but an inactive LumP domain, a plant LumP construct was cloned and infiltrated alongside GFP as a positive control to determine whether it was possible to express free LumP in plants at all. A number of additives were used in combination, including 5-azacytidine, ascorbic acid, tween-20, acetosyringone and the p19 plasmid, which have been shown to significantly improve expression (Zhao et al., 2017) in order to enhance any low levels of expression that may be occurring. LumP and GFP expression were measured by fluorescence on days 2, 3 and 4. While statistically significant fluorescence above background was observed for LumP on day 2, the difference was too small to be usable and no significant difference was measured on the remaining days. GFP was clearly expressed over the same timeframe (although day 4 was not significant due to highly variable data), as seen in 4.7.

This is quite a surprising result. LumP expresses very readily in bacteria and is highly soluble. In *E. coli* , overexpression of LumP causes the sequestration and overproduction of 6, 7-DM-8-RL (Hoepker et al., 2015). As the immediate precursor to riboflavin, including in plants, there does not seem to be an immediately obvious reason

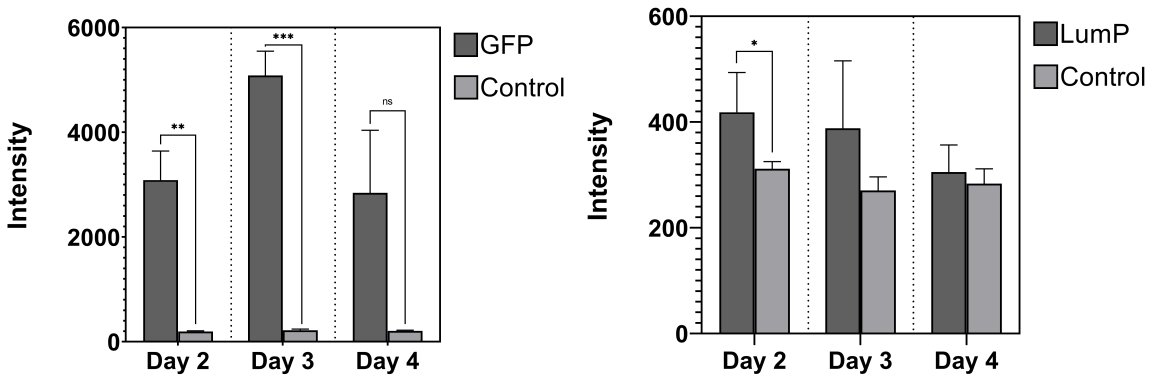

(a)

Figure 4.7: Leaf fluorescence after various timepoints for transiently expressed fluorescent proteins compared to uninfiltrated leaves, intensity measured out of 100,000 using 100% gain,with standard error bars. *Left*. GFP fluorescence in leaves after 2, 3 and 4 days. Excitation at 480 nm, emission at 510 nm. *Right*. LumP fluorescence in leaves after 2, 3 and 4 days. Excitation at 420 nm, emission at 470 nm. * indicates $p < 0.05$, ** indicates $p < 0.01$, *** indicates $p < 0.001$ $n = 3$.

why this cofactor would not be accessible to LumP *in planta*. Lumazine synthase is localised post-translationally to the chloroplast, where it is cleaved into its mature form. This may mean that 6, 7-DM-8-RL is only found in significant quantities in the chloroplast, where is it quickly converted to riboflavin, while LumP is found in the cytoplasm. Furthermore, while recombinant lumazine synthase expresses in *E. coli* at up to 30% of total protein, native levels in spinach are <0.02% of total chloroplast protein, and a much smaller of total cell protein (Jordan et al., 1999).

This may mean there is not a sufficient level of the cofactor in the cell for the functional fluorescent protein to be synthesised. One way to circumvent this may be to coexpress recombinant 'mature' lumazine synthase to increase the concentration of DMRL in the cell and in particular to synthesise it outside of the chloroplast so it may be

sequestered by LumP. A simple way to test whether this is an appropriate strategy might be to clone a LumP construct with a chloroplast localisation sequence. If this results in measurable fluorescence, the clear reason for the lack of fluorescence found in both LumP and Rx-LumP constructs is the absence of cofactor in the cytoplasm. This therefore may still be a viable strategy to study protein interactions *in vivo*, but some modifications may yet need to be made.

4.6 CONCLUSION

Several aspects of Rx1 behaviour *in vivo* were investigated. Finding Rx1 interactors is critical to discerning its function in the cell — regulation of its activity, substrate detection, DNA-binding, and signal transduction are all likely to involve one or multiple accessory proteins, and several have been previously described. VIGS was used to screen potential interactors from a yeast two-hybrid screen and one, EIL5, which is likely to be involved in ethylene-mediated signalling, was identified. This may provide a clue as to a different mechanism (other than transcriptional changes induced by DNA binding) by which Rx1, and potentially other NLRs, is able to trigger an immune response. NRC1, another protein known to be involved in Rx1-conferred immunity, was also found to locate towards DNA in the presence of Rx1 and Rx1 DNA-binding was reduced in the presence of NRC1. This is indicative of a direct interaction between the two, which should be further investigated using previously described methods *in vitro* and *in vivo*. The role of another protein, SUMO, which is known to affect the activity of numerous proteins by covalent binding and plays an important role in the plan immune system, was also studied. A putative SUMO binding site, K506, was mutated and it was found that

this activity abolishes the HR in response to PVX coat protein. This suggests that SUMOylation may play a more direct role in R-protein activity than previously known. Finally, it was investigated whether LumP could be used as a tool to study protein-protein interactions and the hydrodynamic behaviour of LumP *in vivo*. While Rx1 retained functionality when transiently expressed as a fusion with *in planta*, LumP was not functional either as a fusion or when expressed as a free protein. This may make this a less useful tool for *in vivo* experiments than it has proven to be *in vitro*. However, some modifications to restore LumP activity as described may still enable the protein-protein interactions described here and elsewhere to be measured in greater detail than previously possible.

5

CONCLUSION

5.1 A MODEL FOR RX1 SIGNALLING

Plant immune response signalling involves a complex network of proteins working in tandem to create a finely balanced network to control responses to external threats. This thesis has built on previous work to elucidate the processes involved in detection, control and transduction of Rx1-mediated extreme resistance to PVX. A schematic of a model supported by the evidence uncovered in this work and by other authors is shown in 3.1.

As seen in (A), Rx1 is held in an inactive state by the interactions between the N-terminal region of the LRR and the ARC1 and NB domains (E.J. Slootweg et al., 2013). While ADP is shown bound to this form, it is likely not directly responsible for maintaining this inactive state as the P-loop mutant of Rx1, K176R, which is deficient in nucleotide-binding, exhibits similar behaviour to the ADP-bound wild type (Fenyk, Townsend et al., 2015). Also shown is a network of chaperone proteins, SGT1, HSP90 and RAR1, which are necessary in several NLRs, including Rx1 for proper folding and function (Kadota, Shirasu and Guerois, 2010). Furthermore, SGT1 and RAR1 interact with the SCF and COP9, which regulate protein degradation by ubiquitination (Catlett and Kaplan, 2006). It was shown in this thesis that a mutation in proposed SUMO-binding site, K506, was sufficient to abolish Rx1

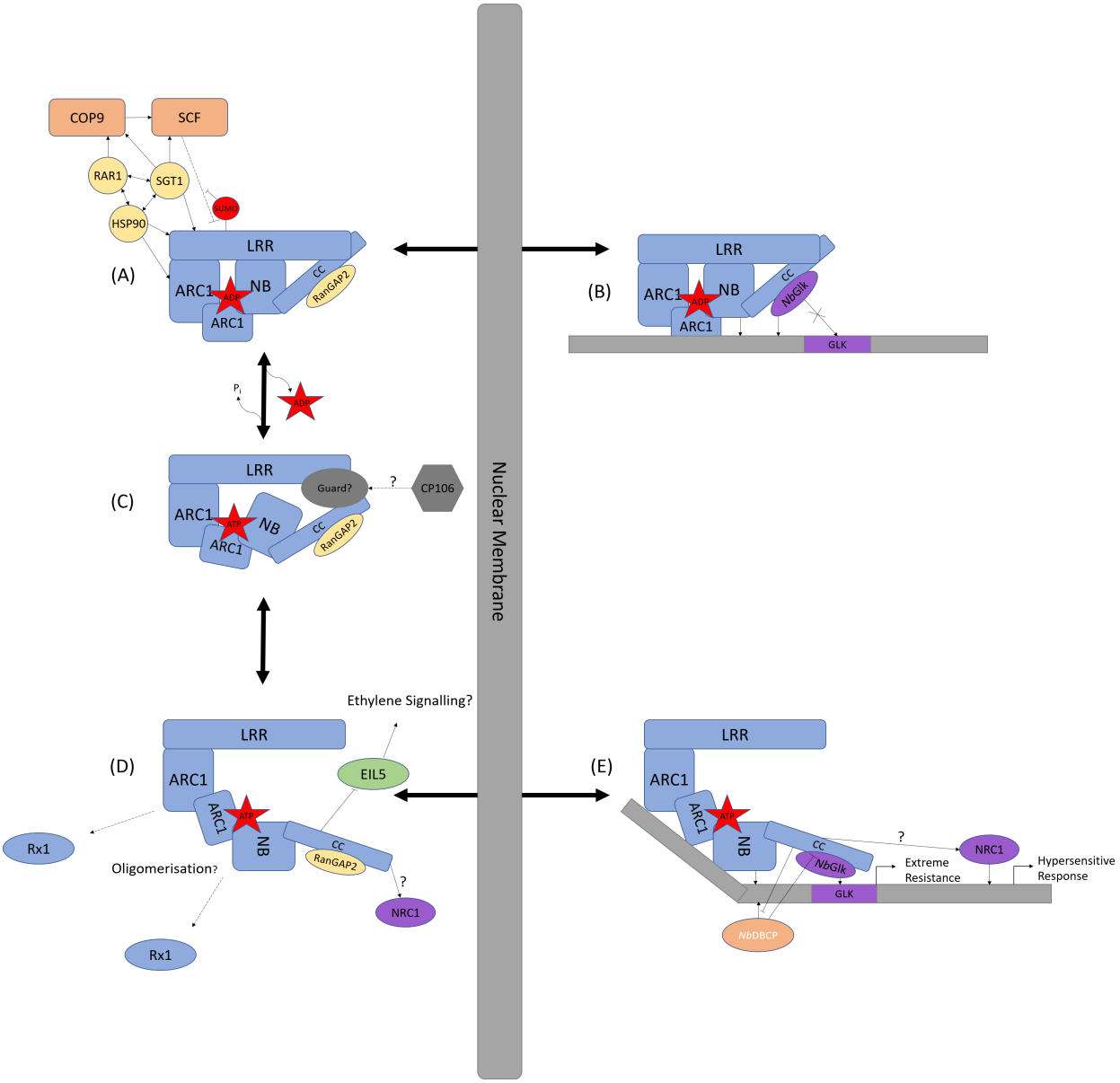

Figure 5.1: (A) Inactive ADP-bound Rx1 in the cytoplasm, (B) Inactive ADP-bound Rx1 in the nucleus, (C) Transition state ATP-bound Rx1 with CP/guard (D) Active ATP-bound Rx1 in cytoplasm (D) Active ATP-bound Rx1 in nucleus.

activity. This may mean that the degradation of Rx1 is controlled by SUMOylation at this residue, protecting it from ubiquitination by the SGT1-localised SCF. This seemingly contradictory behaviour may be necessary to maintain appropriate levels of Rx1 in the cell, so as to prevent too strong or too weak an immune response being mounted. Rx1 is also shown binding RanGAP2. This appears to play a dual role in regulating Rx1 activity. It is known that a nucleocytoplasmic distribution of Rx1 is necessary for proper function; however, when RanGAP2 is silenced, the protein accumulates in the nucleus and activity is suppressed (E. Slootweg et al., 2010). Therefore, RanGAP2 appears to sequester Rx1 in the cytoplasm, allowing it to bind PVX CP. RanGAP2 also appears to play a role in stabilising the structure of Rx1, as overexpression causes an accumulation of Rx1 in the cell (W.I. Tameling, Nooijen et al., 2010).

In (B), Rx1 is shown binding to DNA. However, while Rx1 binds DNA in a sequence-independent way *in vitro*, this behaviour is not replicated *in planta* when expressed alone. Similar behaviour is seen for its interactor *Nb*Glk. However, when the two are coexpressed *in vivo*, DNA binding is observed, suggesting the two behave cooperatively to bind DNA together (Townsend et al., 2018). This is consistent with evidence collected for this thesis that Rx1 and *Nb*Glk interact *in vitro*.

In (C), Rx1 is activated by the avirulent PVX coat protein CP106. It is not currently known whether this is a direct interaction or whether an intermediary guard or decoy protein is required for activation. This triggers the exchange of ADP for ATP. Previous work has suggested that Rx1 does not possess any innate ATPase activity (Fenyk, Townsend et al., 2015), suggesting that a return to the inactive state would require exchange of ATP for ADP. However, using the soluble protein

produced when expressing $Rx_{1\text{-}489}$-LumP in *E. coli*, I showed that a low level of phosphatase activity could be observed. This indicates that a more conventional hydrolysis reaction may be responsible for returning Rx1 to its inactive state.

In (D), ATP binding promotes a more open confirmation as a result of disrupting intradomain interactions (E.J. Slootweg et al., 2013). This model is supported by the time-resolved anisotropy data collected for this thesis, which showed the ATP-bound protein had a larger hydrodynamic radius. Furthermore, rather than being a simple conformational change to the active state, it may be that instead the active state is promoted by an increase in the conformational flexibility of the protein (perhaps by stabilising a transition state), resulting in an equilibrium of active and inactive protein, as a broader distribution of rotational correlation times was observed for the ATP-bound species. This is contrary to previous findings for other R proteins in which ATP was found to stabilise the active form, while ADP-bound protein existed in an active-inactive equilibrium (Bernoux, Burdett et al., 2016).

It was also shown that silencing of EIL5, a putative Rx1 interactor from a Y2H screen, enhanced Rx1-mediated resistance to PVX. EIL5-induced ethylene signalling may play a similar role in suppressing viral immunity to that played by related protein EIL1 in bacterial immunity (Chen et al., 2009). There may be two possible explanations for its interaction with Rx1. It may be that Rx1 inhibits EIL5 activity and thus prevents downstream signalling (as shown in 3.1), or it may be that EIL5 directly inhibits Rx1.

Also shown in (D) is a possible oligomerisation event for Rx1. This is supported by previous unpublished ultracentrifugation data, and by DNA-binding stoichiometry data collected for this thesis showing a

possible 8- to 10-mer. This would be similar to behaviour seen for other NLRs such as ZAR1 (J. Wang, Hu et al., 2019), but is not consistent with some other evidence, such as gel filtration and anisotropy experiments. It may be that this behaviour is triggered upon DNA binding or only under certain conditions, or it may be an artefact from the use of refolded Rx1.

*Nb*Glk is known to bind DNA consensus sequences *in vitro*. Furthermore, expression of high *Nb*Glk is sufficient to confer extreme resistance to PVX (but not HR) in an Rx1-independent matter, suggesting it is capable of triggering the gene expression necessary to invoke resistance. At native levels, however, it is proposed on the basis of the interactions previously demonstrated (Townsend et al., 2018) that DNA binding *in vivo* is dependent upon Rx1. In particular, as shown in (E), the active form of Rx1 is thought to be required to trigger this response, as specificity for its consensus sequences is inhibited by the inactive form of Rx1 *in vitro* (Townsend et al., 2018). In this model, it is the combination of the non-specific DNA-binding behaviour of both proteins cooperating to allow DNA binding with a conformational change to allow *Nb*Glk to bind specific sites that leads to the proper gene expression for extreme resistance. However, as *Nb*Glk is not sufficient, even when overexpressed, to trigger HR in response to CP106, it is likely there is another transcription factor responsible for this activity.

It is proposed from *in vivo* DNA binding data collected for this thesis that Rx1 binds NRC1 in the cytoplasm and translocates it to the nucleus in a CP-dependent way. This is due to NRC1 being observed to bind DNA in the presence of CP106 in an Rx1-dependent manner, while conversely inhibiting the binding of Rx1 to DNA, suggesting

it may be sequestering it in the cytoplasm. As NRC1 is known to be required for HR in a number of different R proteins (Gabriëls et al., 2007), it is proposed that NRC1 the missing link here for HR-related signalling. However, it is not known whether NRC1 is responsible for signalling directly or whether it recruits an *Nb*Glk-like protein for this purpose.

Also shown in (E) is the DNA bending/melting behaviour demonstrated in Fenyk, Townsend et al., 2015. While this activity is not necessary for *Nb*Glk activity, it may play a role in enhancing expression either by *Nb*Glk or by other nearby transcription factors. Further work is required to determine what role, if any, this plays.

Finally, an interaction between *Nb*DBCP and Rx1 is shown. While an interaction was indicated by Y2H and gel filtration previously, I was not able to replicate a direct interaction *in vitro* in this thesis. Instead, *Nb*DBCP appeared to abolish the interaction between Rx1 and *Nb*Glk. This is consistent with evidence that *Nb*DBCP inhibits Rx1-mediated resistance. Also shown is a reduction in the DNA-binding behaviour of *Nb*DBCP by Rx1 demonstrated previously (Sukarta et al., 2020).

5.2 FURTHER WORK

A great deal of questions have been raised by this work and below is proposed further work that may help further elucidate the functions of Rx1, as well as the viability of LumP as a tool to explore protein hydrodynamics.

5.2.1 *LumP Experiments*

While LumP has shown clear viability as a tool to study proteins *in vitro*, it was not possible to observe LumP fluorescence in plants. This

may be because its cofactor, DMRL, is produced only in low quantities and only in the chloroplast. There are a number of experiments that could be tried.

1) Western blotting to test for expression of LumP would enable us to rule out the possibility that the protein itself is not being expressed or is being degraded *in planta*.

2) LumP could be expressed with a chloroplast localisation sequence. While this would not be a viable strategy to study non-chloroplastic proteins, if LumP fluorescence is observed it would tell us that the problem is with cofactor binding.

3) Mature lumazine synthase could be overexpressed alongside LumP to elevate DMRL levels in the cytoplasm and enable binding to LumP. Expression levels would need to be carefully modulated to ensure that native biochemical pathways were not disrupted and background levels of DMRL fluorescence were not too high, while also ensuring that enough was present for LumP to bind.

in vitro time-resolved anisotropy data enabled more detailed information about Rx1 conformational changes to be garnered. To further enhance this data collection, a more robust laser system could be constructed.

4) No imaging capability was possible with the system as constructed. The use of a DCS-120 FLIM system (Beckr and Hickl) would allow for simultaneous detection of two fully parallel confocal channels, with in-built scanning function. This would enable the collection of time-resolved anisotropy images, allowing us to discern differences in protein behaviour in different subcellular compartments.

5) A two-photon excitation system combined with a Z-stacking function would enable the collection of 3-dimensional data, without

the risk of photo-toxicity to the sample in addition to reducing background fluorescence and light scattering within tissues.

5.2.2 *Rx1 Experiments*

A number of further experiments are proposed to advance the work conducted in this thesis.

1) Anisotropy data for Rx1-LumP with and without DNA would be able to determine if it is DNA binding that is responsible for the oligomerisation observed in the refolded Rx1 DNA-binding stoichiometry experiments.

2) Additional repeats for the time-resolved anisotropy experiments with ADP- and ATP-bound Rx1-LumP should be conducted, ideally with a higher concentration of protein to confirm the observed difference.

3) To confirm the difference in size and flexibility observed is due to nucleotide binding, the experiment should be repeated with the K176R P-loop mutant, which is deficient in this activity. Results similar to the apoprotein are expected for each experiment.

4) The constitutively active D460V should also be tested, with results similar to the ATP-bound WT expected for each experiment.

5) Further attempts should be made to replicate previous data that showed a direct interaction between *Nb*DBCP and Rx1.

6) The phosphatase activity observed for Rx1-LumP should be independently verified by using radioactively labelled ATP and silica TLC to measure any hydrolysis.

7) The remainder of the putative Rx1 interactor VIGS constructs should be tested for their effects on Rx1-mediated immunity.

8) *acc* mutants or ACC-silenced plants could be used to determine if EIL5 signalling with relation to Rx1 is dependent on or independent of ethylene signalling.

9) The EIL5-Rx1 interaction should be confirmed by independent means, such as by *in vitro* gel filtration, fluorescence anisotropy, or coimmunoprecipitation.

10) The effect of nucleotide and CP on any such interaction could be explored.

11) The signalling and activity of EIL5 should be investigated.

12) Experiments should be conducted to confirm the interaction of Rx1 and NRC1.

13) A GFP-labelled K506R mutant would allow its effect on nucleo-cytoplasmic partitioning to be tested.

14) Western blotting combined with RT-PCR or Northern blotting would allow any degradation of the K506R mutant to be detected, while confirming the gene is being expressed normally.

6

MATERIALS AND METHODS

Unless otherwise stated, all chemicals were purchased from Sigma-Aldrich.

6.1 RECIPES AND STOCKS

6.1.1 *Buffers*

BUFFER	COMPONENTS
TAE	40 mM Tris base
	20 mM acetic acid
TE	10 mM Tris-HCl, pH 8.0
	1 mM EDTA
Inoue	10 mM PIPES, pH 6.7
	250 mM KCl
	55 mm $MnCl_2$
	15 mM Ca Cl_2
10× SLiCE buffer	500 mM Tris-HCl, pH 7.5
	100 mM $MgCl_2$
	10 mM ATP
	10 mM DTT

6× DNA Loading Dye	20 mM Tris-HCl, pH 8.0 60 mM EDTA 0.48% m/v SDS 0.12% m/v Orange G 0.03% m/v Bromophenol Blue 15 % m/v Ficoll-400
SDS-PAGE Running Buffer	30.3 g L^{-1} Tris base 144 g L^{-1} Glycine 10 g L^{-1} SDS
4× SDS-PAGE Sample Buffer	250 mM Tris-HCl, pH 6.8 40% glycerol 8% SDS 20% β-mercaptoethanol 0.2% m/v bromophenol blue
10% SDS-PAGE Resolving Gel	3.8 mL Milli-Q H_2O 3.4 mL 30% acrylamide/bis-acrylamide (37.5:1) 2.6 mL 1.5 M Tris-HCl, pH 8.8 50 µL 20 % SDS 100 µL 10% ammonium persulphate (APS) 4 µL TEMED

SDS-PAGE Stacking Gel	2.55 mL Milli-Q H_2O 1.7 mL 30% acrylamide/bis-acrylamide (37.5:1) 650 µL 1 M Tris-HCl, pH 6.8 25 µL 20 % SDS 50 µL 10% APS 5 µL TEMED
Protein Storage Buffer	50 mM Tris-HCl, pH 7.5 160 mM NaCl 1 mM EDTA 1 mM DTT
Ni-NTA Buffer	50 mM NaH_2PO_4, pH 8.0 500 mM NaCl
Strep-Tactin Buffer	100 mM Tris-HCl, pH 8.0 150 mM NaCl 1 mM EDTA 1 mM DTT
Glutathione Buffer	125 mM Tris-HCl, pH 7.4 150 mM NaCl 1 mM DTT 1 mM EDTA
Agrobacterium Preparation Buffer	10 mM MES, pH 5.6 10 mM $MgCl_2$

Agrobacterium Infiltration Buffer	10 mM MES, pH 5.6 10 mM $MgCl_2$ 560 mM ascorbic acid 150 mM μM acetosyringone 20 μM 5-azacytidine 0.03 % Tween-20
High Salt Inclusion Body Wash Buffer	100 mM Tris-HCl, pH 7.5 1.5 M NaCl 5 mM EDTA 5 mM DTT 2% Triton X-100
Low Salt Inclusion Body Wash Buffer	100 mM Tris-HCl, pH 7.5 150 mM NaCl 1 mM DTT 1 mM EDTA
Inclusion Body Solubilisation Buffer	100 mM Tris-HCl pH 7.5 20 mM NaCl 2 mM $MgCl_2$ 2 mM DTT 8 M Urea

Inclusion Body Refolding Buffer	50 mM Tris-HCl pH 8.5
	9.6 mM NaCl
	0.4 mM KCl
	2 mM $MgCl_2$
	2 mM $CaCl_2$
	0.5 M arginine
	0.4 M sucrose
	0.75 M guanidine-HCl
	1 mM GSSG
	0.1 mM GSH

6.1.2 *Antibiotic Stocks*

Antibiotic stocks were generally prepared as 1000× stock concentrations and stored as 1 mL aliquots at -20 °C.

Table 6.2: Antibiotic stock preparation

ANTIBIOTIC	SOLVENT	STOCK CONCENTRATION / µG ML^{-1}
Ampicillin	ddH_2O	100
Chloramphenicol	100% EtOH	25
Gentamicin	ddH_2O	10
Kanamycin	ddH_2O	50
Rifampicin	100% MeOH[a]	50[b]
Spectinomycin	ddH_2O	50
Tetracycline	70% EtOH	10

[a] Add 10 mM NaOH dropwise to aid solubility
[b] 500×

6.1.3 *Media*

In general, media components were added to 500 mL ddH_2O or to the desired volume in appropriate glassware. Media was autoclaved for 15 min at 121 °C and stored at 4 °C .

6.1.3.1 *Lysogeny Broth*

Lysogeny Broth (LB), also known as Luria-Bertani broth, was used for routine molecular biology applications

Table 6.3: LB Components

COMPONENT	CONCENTRATION / G L^{-1}
Casein Digest (Peptone)	10
Sodium Chloride	10
Yeast Extract	5

6.1.3.2 *Super Optimal Broth*

Super Optimal Broth (SOB), also known as Hanahan's broth, was used for the preparation of competent cells

Table 6.4: SOB Components

COMPONENT	CONCENTRATION / G L^{-1}
Casein Digest (Peptone)	20
Yeast Extract	5
Magnesium Sulphate	2.4 (10 mM)
Sodium Chloride	0.584 (10 mM)
Potassium Chloride	0.186 (2.5 mM)

6.1.3.3 *Yeast Extract Broth*

Yeast Extract Broth (YEB) was used for the growth of *Agrobacterium tumefaciens*.

Table 6.5: YEB Components

COMPONENT	CONCENTRATION / G L^{-1}
Casein Digest (Peptone)	5
Beef Extract	5
Yeast Extract	1
Sucrose	5
Magnesium Sulphate	0.3

6.1.3.4 *LB Agar*

LB Agar was used for the preparation of agar plates for the propagations of bacterial lines and cloning purposes.

Table 6.6: LB agar components

COMPONENT	CONCENTRATION / G L^{-1}
Casein Digest (Peptone)	10
Sodium Chloride	10
Yeast Extract	12
Agar	5

6.1.3.5 *Agar Plates*

Agar plates for molecular biology were prepared in a laminar flow hood. 25 mL molten LB agar was added to a 25 mL 92 × 16 mm triple vented petri dish (Sarstedt) along with an appropriate volume of any necessary antibiotic stock (6.1.2). Agar was allowed to cool to room

temperature and plates used immediately or stored upside down at 4 °C.

6.2 DNA PROTOCOLS

6.2.1 *Miniprep of supercoiled DNA*

5 mL of sterile LB (6.1.3.1) was transferred to a sterile 14 mL polypropylene culture tube (Starlab) using a sterile serological pipette (Starlab). An appropriate volume of antibiotic stock (6.1.2) was added to the media. A single colony of *E. coli* (typically DH5α, Mach1 T1 or Top10) on an agar plate containing the desired plasmid, derived from a glycerol stock (6.2.10) or transformation (6.2.2), was transferred to the culture tube using a sterile polystyrene loop (Starlab). The culture was incubated overnight at 37 °C with shaking at 180 RPM.

In the morning, the culture was centrifuged at 4 000×g for 10 min. Buffers and columns from the Monarch Plasmid Miniprep Kit (New England Biolabs). The supernatant was discarded and resuspended in 200 µL of buffer B1 and transferred to a 1.5 mL centrifuge tube (Sarstedt). 200 µL buffer B2 was added to the resuspension and mixed by repeated inversion. 400 µL buffer B3 was added, mixed by repeated inversion and incubated for 2 min. The mixture was centrifuged at 21 000×g for 10 min. The supernatant was carefully transferred to a silica-based DNA-binding column in a collection tube. The column was centrifuged at 16 000×g for 30s and the flow-through discarded. 200 µL wash buffer 1 was added and the column centrifuged at 16 000×g for 30 s. 400 µL wash buffer 2 was added and the column centrifuged at 16 000×g for 30s. The supernatant was discarded and the column centrifuged at 21 000×g. The column was transferred to a

1.5 mL centrifuge tube and 50 µL Milli-Q water was added. The tube was centrifuged at 16 000×g for 1 min. The DNA concentration of the eluate was measured using a NanoDrop (Fisher Scientific).

6.2.2 *Transformation of* E. coli

100 µL competent *E. coli* (6.2.3) was thawed on ice. 1 µL supercoiled plasmid DNA (6.2.1) or 5 µL of a DNA cloning sample (6.2.4) was added to the cells and incubated for 30 min on ice. The cells were heat shocked in a 42 °C water bath for 45 s then returned to ice for 2 min. 1 mL warm SOC (SOB (6.1.3.2) with 20 mM glucose) was added and the culture incubated at 37 °C for 90 min. 50 µL (plasmid transformation) or 1 mL (cloning transformations) culture was spread on an agar plate containing the appropriate antibiotic (6.1.2) using a sterile L-shaped spreader. Plates were sealed using Parafilm (Bemis) and stored upside down overnight at 37 °C. Successful transformants were identified and used immediately or the plates were stored at 4 °C for up to a month.

6.2.3 *Preparation of competent* E. coli

A single colony of *E. coli*, (freshly transformed (6.2.2) with a desired plasmid if required) was transferred to an sterile 250 mL conical flask containing 25 mL LB (6.1.3.1) using a sterile polystyrene loop (Starlab). This starter culture was grown at 37 °C, shaking at 200 RPM, until exponential phase, as determined by OD_{600} reading at 0.4-1.0 (6-8 hours). Three sterile 1 L flasks containing SOB (6.1.3.2) were inoculated by 10 mL, 1 mL and 100 µL of starter culture and incubated overnight at 18 °C , shaking at 150 RPM.

When the OD_{600} measured 0.55 in one of the flasks, the cells were divided among five 50 mL falcon tubes and centrifuged at 2 500×g for

10 min at 4 °C. The supernatant was discarded and residual medium removed with a vacuum aspirator. The cells were gently resuspended in 80 mL sterile ice-cold Inoue buffer (6.1.1). The cells were centrifuged at 2 500×g for 10 min at 4 °C. The supernatant was discarded and residual medium removed with a vacuum aspirator. The cells were resuspended in 20 mL ice-cold Inoue buffer and 1.5 mL dimethyl sulphoxide (DMSO) was added. Cells were incubated on ice for 10 min. Cells were pipetted into 100 µL aliquots in sterile chilled 1.5 mL microcentrifuge tubes (Sarstedt) and snap-frozen in liquid N_2 and stored at -80 °C.

6.2.4 *DNA Cloning*

6.2.4.1 *Conventional Ligation Cloning*

Suitable restriction sites were identified on a target plasmid. DNA oligonucleotide primers were designed with a suitable 5′ restriction site in frame with a sequence identical to the 5′-end of the target cloning sequence on the sense primer and with reverse complementarity to the 3′-end of the target cloning sequence on the antisense primer. The complementary sequences were designed to have a melting temperature (T_m) of around 55 °C, as determined by the New England Biolabs T_m calculator (New England Biolabs, 2011), or 15 nucleotides in length, whichever was longer. Primers were ordered from Eurofins, resuspended in Milli-Q water to a final concentration of 100 µM and stored at -20 °C.

A high-fidelity Polymerase Chain Reaction (PCR) was conducted on the template plasmid using these primers (6.2.7.1). The PCR product was resolved on, and purified from, a DNA agarose gel (6.2.9). The PCR fragment was initially blunt-ligated into pJet1.2 (6.2.9).

Colonies were tested for successful insertion by colony PCR (6.2.7.2) and two positive clones were grown overnight for miniprep, as well as the target plasmid (6.2.1). Miniprepped samples were digested using the appropriate restriction enzymes (6.2.6). Vector and inserts were purified by gel extraction (6.2.9) and the inserts ligated with the vector (6.2.5). Colonies were tested for successful insertion by colony PCR (6.2.7.2) and a positive clone for each PCR insert was grown overnight for preparation of glycerol stocks (6.2.10) and miniprep (6.2.1). Samples of miniprepped plasmid were sent for DNA sequencing (DBS Genomics) to confirm successful cloning.

6.2.4.2 *Blunt Ligation in pJet1.2*

Reagents from the CloneJET PCR Cloning Kit (New England Biolabs) were used to clone blunt PCR products into pJet1.2. The ligation reaction was assembled as in table 6.7.

Table 6.7: Components of pJet1.2 blunt cloning

COMPONENT	VOLUME/μL^{-1}
Milli-Q H_2O	3
2× Reaction buffer	5
pJet1.2/blunt (50 ng μL^{-1})	0.5
PCR Product (150 nM)	1
T4 DNA Ligase	0.5

The ligation reaction was incubated at room temperature for 30 minutes and transformed (6.2.2) into Mach1 T1 (Invitrogen).[1]

1 Enhanced W-type *E. coli* derivative. Genotype: *str. W ΔrecA1398 endA1 fhuA Φ80Δ(lac)M15 Δ(lac)X74 hsdR(rK–mK+)*

6.2.4.3 *Site-directed mutagenesis*

Site-directed mutagenesis was used to introduce single-point mutations or insert sequences into plasmids. Phosphorylated primers (Eurofins) were designed in a similar fashion to that described in 6.2.4.1, with the reverse primer abutting the forward primer at the site of the intended mutation, with the insert appended to the 5′-end of the forward primer. In this way the whole plasmid was replicated by high-fidelity PCR (6.2.7.1). DpnI, which degrades methylated DNA was added to the completed PCR reaction and allowed to incubate at 37 °C for 3 hr. The plasmid was isolated and purified by agarose gel electrophoresis (6.2.9) and ligated overnight (6.2.5). Ligations were transformed, checked, grown, miniprepped and sent for sequencing as in (6.2.4.1).

6.2.4.4 *Gateway Cloning*

Gateway is a method developed by Invitrogen that was used to clone inserts easily into a number target vectors containing specific flanking sequences based on the bacteriophage lambda site-specific recombination system. PCR primers were designed in a similar fashion to that described in (6.2.4.1), with *att*B flanking sequences replacing restriction sites:

$$\overset{attB1}{att\text{B1} : 5' - \overbrace{\mathbf{GGGG\ ACA\ AGT\ TTG\ TAC\ AAA\ AAA\ GCA\ GGC\ T}}\text{TC}\ldots}$$

$$\overset{Shine-Dalgarno}{\ldots\overbrace{\text{GAA GGA GAT AGA}}}\ \overset{Kozak}{\overbrace{\text{ACC}}}\ \overset{Start}{\overbrace{\underline{\text{ATG}}}} - 3'$$

$$\overset{attB2}{att\text{B2} : 5' - \overbrace{\mathbf{GGGG\ AC\ CAC\ TTT\ GTA\ CAA\ AGC\ TGG\ GT}}\text{T}}\ \overset{Stop}{\overbrace{\text{TTA}}} - 3'$$

These primers were used to clone the insert of interest (6.2.7.1) for insertion into pDONR plasmids containing *att*P flanking regions. The reactions was set up in a 250 µL PCR tube as in table 6.8.

Table 6.8: BP Gateway cloning components

COMPONENT	VOLUME/µL^{-1}
TE buffer[a]	to 5
PCR Product	[b]
Donor Vector (75 ng µL^{-1})	1
BP Clonase II	1

[a] 6.1.1
[b] 15 ng kbase^{-1}

Samples were incubated at 25 °C overnight then 0.5 µL Proteinase K was added. Samples were incubated for 10 min at 37 °C and transformed, checked, grown and miniprepped as in (6.2.1). Successfully cloned donor vectors were used to shuttle the insert into desired expression vectors. Reactions were set up in a 250 µL PCR tube as in table 6.9.

Table 6.9: LR Gateway cloning components

COMPONENT	VOLUME/µL^{-1}
TE buffer[a]	2
Donor Vector (75 ng µL^{-1})	1
Destination Vector (75 ng µL^{-1})	1
LR Clonase II	1

[a] 6.1.1

Samples were incubated at 25 °C overnight then 0.5 µL Proteinase K was added. Samples were incubated for 10 min at 37 °C and transformed, checked, grown and miniprepped as in 6.2.4.1.

6.2.4.5 *SLiCE Cloning*

Seamless Ligation Cloning Extract (SLiCE) cloning was used to clone more challenging constructs without convenient restriction sites. Primers for the site of interest were chosen with flanking sequences of around 20 bp matching the desired site of entry in the target vector. This method allows for a gene or gene section too be inserted anywhere in a plasmid without introducing any extraneous base pairs, as well as removing any undesired parts of the target plasmid. The target sequence was amplified by PCR (6.2.7.1) and reactions were set up as in table 6.10.

To prepare the SLiCE extract, a glycerol stock 6.2.10 of DH5α was streaked out on an agar plate 6.1.3.5 and incubated at 37 °C overnight. A single colony was used to inoculate 25 mL SOB 6.1.3.2 in a 50 mL falcon tube and incubated at 37 °C overnight. The culture was diluted in SOB to an OD_{600} of 0.03. The culture was incubated at 37 °C with shaking at 200 RPM until the OD_{600} reached 5.0. L-(+)-arabinose was added to a final concentration of 0.2% and the culture was shaken for a further 2 hours at 37 °C. 25 mL of the the culture was transferred to a 50 mL falcon tube and centrifuged at 5 000×g for 20 min at 4 °C. The cells were resuspended inn ice-cold Milli-Q water and centrifuged at 5,000×g for 20 min at 4 °C.

The cells were then resuspended in 1.2 mL 50 mM Tris-HCl, pH 8.0, 3% (w/v) Triton X-100 and incubated for 10 min at room temperature. The cells were centrifuged at 20 000×g for 2 min at 4 °C. The supernatant was removed and an equal volume of 80% (v/v) glycerol was added. The lysate was snap-frozen in liquid nitrogen and stored at -80 °C.

Table 6.10: Components of SLiCE reaction

COMPONENT	VOLUME/μL^{-1}
Milli-Q H_2O	to 10
Target Vector (100 ng μL^{-1})	1
Insert	[a]
10× SLiCE buffer[b]	1
DH5α SLiCE extract	1

[a]Insert added to 3:1 molar ratio with vector
[b](6.1.1)

The reaction was incubated at 37 °C for 1 hour and checked, grown and miniprepped as in 6.2.4.1.

6.2.5 *DNA Ligation*

Ligations were assembled in order as in table 6.11.

Table 6.11: Components of ligation

COMPONENT	VOLUME/μL^{-1}
Milli-Q H_2O	to 10
10× Ligation buffer[a]	1
ATP (10 mM)	1
Vector (100 ng μL^{-1})	1
Insert	[b]
T4 DNA ligase[a]	1

[a]New England Biolabs
[b]Insert added in 3:1 molar ratio with vector if required

Ligations were incubated at 16 °C overnight and transformed (6.2.2) into Mach1 T1.

Table 6.12: Cloned plasmids and oligonucleotides

PLASMID NAME	GENE/INSERT	ORGANISM	OLIGONUCLEOTIDES	DESCRIPTION
pYL156	VIGS sequences × 19	*N. benthamiana*	N/A	pYL156 was a gift from Erik Slootweg, Wageningen University. Digested with HindIII/NcoI and HindIII/XhoI and the 9000 bp and 2400 bp fragments purified. pEX-A2 containing VIGS sequences ordered from Eurofins, digested with NcoI/XhoI and 300 bp fragment purified. Fragments combined in 3-way ligation.
pEarleyGate201	Rx1 FL K506A Rx1 FL K787A	*S. tuberosum*	N/A	pENTR207 containing desired sequence was a gift from Erik Slootweg, Wageningen University. Gateway cloned with pEarleyGate201

pEarleyGate201	LumP (C-terminal of Gateway region)	*Photobacterium leiognathi*	Sense: GGCCTAGATGTTTAGAGGTATTGTT CAAGGTC Antisense: GGCACTAGTCTACCATTCATTAA AATTTCAACGTT	130_pSKB3-LUMP-P.leioghnati was a gift from Gerard Marriott (Addgene plasmid # 65894 ; http://n2t.net/addgene:65894 ; RRID:Addgene_65894). Sequence cloned into pJet1.2 then into pEarleyGate with AvrII/SpeI
pEarleyGate201-LumP	Rx1 FL	*S. tuberosum*	Sense: GGGGACAAGTTTGTACAAAAAAGCA GGCTGGATGGCTTATGCTGCTGTTACTTCCC Antisense: GGGGACCACTTTGTACAAGAAAGC TGGGTGCACATTATTGCGGCAAGAAGCAACTTC	Sequence gateway cloned into pDONR207, then pEarleyGate201.
pSKB3-LUMP	His_6-Rx1 (CCNBARC) (N-terminal of LumP)	*S. tuberosum*	Sense: ACTTTAAGAAGGAGATATACCATGG CACATCATCATCATCATCAATGGCTTATGCT GCTGTTA Antisense: TTGAACAATACCTCTAAACATA TTGCACATGAATTTTGATCAC	SLiCE cloning

pET28b (Rx FL)	LumP (C-terminal of Rx FL with linker sequence)	*P. leiognathi*	Sense: CTTCTTGCCGCAATAATGTGCTGGAA GTTCTGTTCCAGGGGCCATGGGCAGCAGCC Antisense: TGTGGTGGTGGTGGTGCTCGAG CCATTCATTTAAAATTTCAACGTTC	SLiCE cloning
pBin35S	LumP	*P. leiognathi*	Sense: CCATGGCAATGTTTAGAGGTATTGT TCAA Antisense: GGTACCATTCATTTAAAATTT CAACGTTC	Sequence cloned into pJet1.2, then into pRAP35S with NcoI/KpnI, then into pBin35S with AscI/PacI

pSKB3-His6-CCNBARC-LumP	HRV3C cleavage site	Rhinovirus	1 Sense: CTTGGTAGTCATTGATGACATTTGG ACTACAGAAGCTTGGG 1 Antisense: CCCAAGCTTCTGTAGTCCAAATG TCATCAATGACTACCAAG 2 Sense: TATGTCGGATCTGGAAGTTCTGTTC CAGGGGCCCCTGCA 2 Antisense: TATGCAGGGGCCCCTGGAACAG AACTTCCAGATCCGACA	Site-directed mutagenesis to remove NdeI site in Rx1. Plasmid digested with NdeI and ligated with annealed insert.
pSKB3-His6-CCNBARC-HRV3C-LumP	T452A mutation	N/A	Sense: CAATTTTAGTTTTCGTGGAGCAATAG AAAGTTGTGGAATG Antisense: CATTCCACAACTTTCTATTGCTCC ACGAAAACTAAAATTG	Site-directed mutagenesis

pSKB3-His_6-CCNBARC-HRV3C-LumP	Twin-Strep	N/A	Sense: TGGTGGATCGGGAGGTTCGGCGTG GTCTCATCCACAATTTGAAAAGTAGGCGG CCGCAC Antisense: CCTCCGGAACCTCCACCTTTCTCG AACTGCGGGTGGCTCCAACCGGTCCATTC ATTTAAAATTTCAACGTT	Site-directed mutagenesis

pSKB3 LumP	Twin-Strep, HRV3C, Rx1 (CCNBARC) (C-terminal of LumP)	Rhinovirus, *S. tuberosum*	1 Sense: TTAATTAAGCGGCCGCACTC 1 Antisense: CCATTCATTTAAAATTTCAACG TTC 2 Sense: TAAGCTGGAAGTTCTGTTCCAGGG GCCCGC 2 Antisense: GGCCGCGGGCCCCTGGAACAGA ACTTCCAGTTAAT 3 Sense: GCGGCCGCAATGGCTTATGCTGCTG 3 Antisense: GCCCTCGAGTGCACATGAATTT TGATCACTC 4 Sense: CCATGGCATGGAGCCACCCGC 4 Antisense: CATATGTGCCGACTTTTCAAATT GTGGATGAG 5 Sense: CCATGGCATGGAGCCACCCGC 5 Antisense: CATATGTGCCGACTTTTCAAAT TGTGGATGAG	LumP stop codon mutated to PacI site. Plasmid digested with PacI/NotI and ligated with annealed HRV3C insert. Rx1 (CCNBARC) sequence cloned into pJet1.2 then into pSKB3 with NotI/XhoI. Twin-Strep sequence cloned into pJet1.2 and cloned into pSKB3 with NcoI/NdeI.

pSKB3 His_6-CCNBARC–HRV_3C–LumP–Twin-Strep	Rx1 (CCNBARC, Synthetic)	N/A	Sense: CCATGGCACATCATCATCATCATCATGCAATGGCGTATGCGGCGG Antisense: CATATGAACGTTACGGCTCTCGCTAT	Plasmid of optimised synthetic Rx1 WT, T452A, D460V and K176R ordered from GenscriptSequence cloned into pJet1.2 then into pSKB3 with NcoI/NdeI
pSKB3 Twin-Strep–LumP-HRV_3C-CCNBARC-His_6	Rx1 (CCNBARC, Synthetic)	N/A	Sense: GCGGCCGCAATGGCGTATGCGGCGG Antisense: CTCGAGCTAAACGTTACGGCTCTCGCTAT	Sequence cloned into pJet1.2 then into pSKB3 with NotI/XhoI

6.2.6 *Restriction Digestion*

Restriction digestion was used to prepare linear DNA samples with compatible ends for ligation. Digests were assembled in order as in table 6.13.

Table 6.13: Components of restriction digest

COMPONENT	VOLUME/μL^{-1}
Milli-Q H_2O	17
5× Restriction buffer[a]	10
Plasmid (100 ng μL^{-1})	20
Restriction enzyme 1[b]	1
Restriction enzyme 2[b]	1
Alkaline phosphatase[c]	1

[a]Buffers selected using the NEB-cloner double digest website (New England Biolabs, 2014)
[b]New England Biolabs
[c]Used for vector only

6.2.7 *Polymerase Chain Reaction*

6.2.7.1 *High-fidelity Polymerase Chain Reaction*

A PCR reaction was assembled in a 250 µL PCR tube (Sarstedt) in order as in table 6.14.

The samples was placed in a thermal cycler, which was run using the program detailed in table 6.15.

6.2.7.2 *Colony PCR*

Table 6.14: Components of high-fidelity PCR

COMPONENT	VOLUME/μL^{-1}
Milli-Q H_2O	30.5
5× HF buffer[a]	10
dNTPs (2.5 mM)	5
DMSO	2.5
Template plasmid (1 ng μL^{-1})	1
Sense primer (100 μM)	0.25
Antisense primer (100 μM)	0.25
Phusion Hot Start II DNA Polymerase (2 U μL^{-1})[a]	0.5

[a]Fisher Scientific

Colony PCR was routinely used to test colonies for successful cloning, as well as for general PCR applications where high fidelity was not required. Usually a screen of 14 or 28 colonies was conducted so as to be convenient for gel electrophoresis with 15-well combs. The PCR reaction was assembled in a 250 µL PCR tube (Sarstedt) in order as table 6.16.

The sample was placed in a thermal cycler which was run using the program detailed in table 6.17.

PCR reactions were visualised by gel electrophoresis (6.2.9) without loading dye to identify positive clones.

6.2.8 *Agarose Gel DNA electrophoresis*

Agarose gel electrophoresis was used routinely to analyse DNA fragments. The percentage agarose used varied depending on the size of

Table 6.15: High-fidelity PCR program

	TEMPERATURE/°C	TIME/S
	98	30
35×	98	10
	T_m	30
	72	20/kbase
	72	600
	10	∞

the fragment to be resolved; however 1.2% was a typical concentration. Therefore typically 1.2 g was added to 100 mL TAE (6.1.1), which was microwaved for 2 min 30 s. Ethidium bromide was added to a final concentration of 0.5 µg/mL and the molten agaroseTAE was poured into a 15 × 10 cm gel tray, affixed in a gel caster (Bio-Rad) with a suitably sized gel comb, and allowed to cool for 20 min. The gel was placed into a Sub-Cell GT Cell (Bio-Rad), connected to a Power-Pac Basic Power Supply (Bio-Rad). The gel tank was filled with TAE to cover the gel.

A ⅕ volume of 6× loading dye (6.1.1) was mixed to the DNA sample, which was added to an appropriate well, alongside 5 µL of GeneRuler 1 kb Plus DNA Ladder (Fisher Scientific). The gel was run for 45-60 min at 120 V and visualised on a UV transilluminator.

6.2.9 *Agarose Gel DNA extractions*

DNA purification of plasmid restriction digests or PCR products from agarose gels (6.2.8) was routinely used in cloning protocols. The

Table 6.16: Components of colony PCR

COMPONENT	VOLUME/μL^{-1}
Milli-Q H_2O	11.75
2× Master Mix[a]	12.5
DMSO	1.25
Template[b]	-
Sense primer (100 μM)	0.25
Antisense primer (100 μM)	0.25

[a]OneTaq Quick-Load 2× Master Mix with Sandard Buffer (New England Biolabs)
[b]A sterile pipette tip was used to transfer a small quantity of the colony into the PCR reaction

relevant DNA band was excised using a scalpel and transferred to a 1.5 mL microcentrifuge tube. Buffers and columns from Monarch DNA Gel Extraction Kit (New England Biolabs) were used for purification. Four volumes of gel dissolving buffer were added, and the sample incubated at 55 ºC for 10 min. The dissolved sample was added to a silica-based DNA-binding column in a collection tube, which was centrifuged at 15 000×g for 30 s. The flow-through was discarded and 500 µL DNA wash buffer was added to the column and centrifuged at 15 000×g for 30 s. The flow-through was discarded and the wash step and centrifugation repeated. The flow through was discarded and the column centrifuged at 21 000×g for 1 min 30 s. 10 µL Milli-Q H_2O was added to the column, which was incubated for 2 min. The column was transferred to a 1.5 mL centrifuge tube and the DNA eluted by centrifugation at 21 000×g for 1 min. The concentration of the DNA sample was measured using a NanoDrop (Fisher Scientific).

Table 6.17: Colony PCR program

	TEMPERATURE/°C	TIME/S
	98	120
30×	98	20
	T_m	30
	72	20/kbase
	72	600
	10	∞

6.2.10 *Glycerol Stocks*

Glycerol stocks were used for long-term storage of bacterial strains and plasmids. 5 mL of sterile LB (6.1.3.1) was transferred to a sterile 14 mL polypropylene culture tube (Starlab) using a sterile serological pipette (Starlab). An appropriate volume of antibiotic stock (6.1.2) was added to the media. A single colony of the desired *E. coli* strain on an agar plate (6.1.3.5) containing any desired plasmid was transferred to the culture tube using a sterile polystyrene loop (Starlab). The culture was incubated at 37 °C overnight with shaking at 180 RPM. 0.5 mL of the culture was added to a cryogenic tube (Fisher Scientific) and mixed with 0.5 mL 80% glycerol. Glycerol stocks were snap-frozen in liquid nitrogen and stored at -80 °C.

Growth of bacteria stored in a glycerol stock was carried out by streaking out a small amount of the stock on an agar plate (6.1.3.5) using a sterile polystyrene loop (Starlab). Using a second sterile loop, the stock on the plate was streaked out further to reduce the bacterial density and again with a third loop. Plates were sealed using Parafilm (Bemis) and stored upside down at 37 °C overnight.

6.3 PROTEIN EXPRESSION

Protein expression was generally conducted using ER2566 (New England Biolabs)[2] . The expression plasmid was transformed and a single colony was transferred into 100 mL fresh LB (6.1.3.1) in a 500 mL conical flask. The culture was incubated overnight at 37 °C. 12 L terrific broth was prepared and in the morning 5 mL of start culture was used to inoculate each flask. The flasks were incubated with shaking at 37 °C with shaking at 200 RPM. When the OD_{600} reached 0.6, IPTG (Melford) was added to a final concentration of 1 mM. The cultures were incubated overnight at 18 °C with shaking at 150 RPM. In the morning the cells were transferred to six 1 L centrifuge bottles (Becker & Coulter) and centrifuged at 4 000×g for 20 min. The supernatant was discarded and the second batch of 6 L was centrifuged in the same bottles. The supernatant was discarded and the cells resuspended in PBS and centrifuged at 4 000×g for 20 min. The cell pellets were either used for purification or snap frozen in liquid nitrogen and stored at -80 °C.

6.3.1 *Cell Lysis*

The cells were resuspended in the appropriate lysis buffer (see purification sections below) and lysed by sonication, keeping the cells on ice. Where a higher yield was needed, a French press was used following sonication. The lysate was centrifuged at 50 000×g for 50 min. The

2 Enhanced BL21 *E. coli* derivative, also known as T7 Express. Genotype: *F- λ- fhuA2 [lon] ompT lacZ::T7p07 gal sulA11 Δ(mcrC-mrr)114::IS10 R(mcr-73::miniTn10–TetS)2 R(zgb-210::Tn10–TetS) endA1 [dcm]*

supernatant was removed and applied to the desired column or resin using a peristaltic pump.

6.3.2 *Purification*

Most proteins were purified at 4 °C using pre-packed columns (GE Healthcare, Cube Biotech) on an ÄKTA pure according to the column's specifications or using free resin (recycled industrial resin stored inhouse) and a peristaltic pump. After elution from the column, the protein was typically dialysed at 4 °C for 2 hours or overnight into an appropriate storage buffer, or a suitable buffer for further purification. Glycerol was added to a final concentration of 15% (v/v) and the protein was snap-frozen in liquid nitrogen for storage in aliquots at -80 °C. Protease inhibitors were used in all buffers.

6.3.2.1 *Ni-NTA Purification*

His_6-tagged proteins were purified using Ni-NTA resin. Cells were lysed in Ni-NTA buffer (6.1.1) with 10-25 mM imidazole and 0.1% Triton-X. The column was washed with at least 10 column volumes of Ni-NTA buffer with 25 mM imidazole or until no further protein washed off the column. A further 5 column volumes of a high salt wash of 1-1.5 M NaCl was used for DNA-binding proteins at this stage. The protein was eluted in Ni-NTA buffer with 250 mM imidazole .

To regenerate the column, the following buffers were passed through the column in sequence using a peristaltic pump:

1. 10 column volumes (cv) ddH_2O
2. 10 cv 100 mM EDTA
3. 10 cv ddH_2O
4. 10 cv 0.5 M NaOH, 2 M NaCl
5. 10 cv ddH_2O
6. 10 cv mM $NiSO_4$
7. 5 cv ddH_2O
8. 5 cv 100 mM ethanoic acid, 150 mM NaCl, incubate 15 min
9. 10 cv ddH_2O
10. 5 cv 20 mM Tris-HCl, pH 8.0
11. 10 cv ddH_2O
12. 10 cv 20% (v/v) EtOH

The column was stored at 4 ºC.

6.3.2.2 *Strep-Tactin XT Purification*

Twin-strep proteins were purified using Strep-Tactin XT resin. Cells were lysed in Strep-Tactin buffer. The column was washed with at least 10 cv buffer or until no further protein was washed off. A further 5 column volumes of a high salt wash of 1-1.5 M NaCl was used for DNA-binding proteins at this stage. The protein was eluted in Strep-Tactin buffer with 50 mM biotin.

Resin was washed with:

1. 10 cv 10 mM NaOH (fresh)
2. 10 cv 100 mM Tris-HCl, pH 8.0, 150 mM NaCl, 1 mM EDTA

The column was stored at 4 °C.

6.3.2.3 *Glutathione Purification*

GST-tagged proteins were purified using agarose-glutathione resin. Cells were lysed in Glutathione Buffer (6.1.1) with 1 mg/mL lysozyme and 1% Triton X-100. The column was washed with at least 10 cv buffer or until no further protein was washed off. A further 5 column volumes of a high salt wash of 1-1.5 M NaCl was used for DNA-binding proteins at this stage. The protein was eluted in Glutathione Buffer with 0.1% Triton-X and 50 mM GSH.

The resin was washed with:

1. 10 cv 125 mM Tris-HCl, pH 7.4, 150 mM NaCl, 1 mM DTT
2. 10 cv ddH_2O
3. 2 cv 0.1 M NaOH
4. 10 cv ddH_2O
5. 10 cv 125 mM Tris-HCl, pH 7.4, 150 mM NaCl, 1 mM DTT
6. 2 cv 70% EtOH
7. 10 cv ddH_2O
8. 10 cv 125 mM Tris-HCl, pH 7.4, 150 mM NaCl, 1 mM DTT

The column was stored at 4 °C.

6.3.2.4 *Hydrophobic Interactions Purification*

Rx1 proteins were typically further purified using phenyl sepharose resin. The protein was dialysed into 20 mM Tris-HCl, 1 M ammonium sulphate, 1 mM EDTA, 1 mM DTT. The protein was eluted with a descending concentration gradient of ammonium sulphate until the concentration reached zero.

6.3.2.5 *Gel Filtration*

Gel filtration was routinely used as polishing step in protein purification. The protein was concentrated to a volume < 5 mL and applied to an equilibrated HiLoad Superdex 200 prep grade gel filtration column. 1.5 cv of the desired storage buffer was run thorough the column at 0.5 mL min^{-1} and 1 mL fraction were collected. SDS-PAGE (6.3.5) was used to determine the fractions containing the desired protein, which was concentrated from those fractions.

Gel filtration was also used for protein binding experiments. For this purpose a Superdex 75 PC 3.2/30 and a Superdex 75 10/300 GL were used. Equimolar amounts of protein at 1 μM were used for these experiments, using 25 mM Tris-HCl, 60 mM NaCl, 1 mM EDTA, 1 mM DTT.

6.3.3 *Protein Concentration*

Proteins were typically concentrated following purification for use in experiments, or for further purification steps. Protein was added to Pierce Protein Concentrators with a 5 kD molecular weight cutoff (Thermo Scientific) and centrifuged at 5 000×g until the protein

reached the desired volume. For some proteins such as LumP and GFP, ammonium sulphate precipitation was used. Solid ammonium sulphate was added to 50% saturation. The protein solution was stirred vigorously overnight at 4 °C. The precipitate was centrifuged at 4 000×g for 20 min. The precipitate was resuspended in 20 mM Tris-HCl, pH 8.0 and the solubilised protein dialysed into the buffer of choice.

6.3.4 *Protein Refolding*

After lysis (6.3.1), Rx1 was refolded from inclusion bodies following lysis by resuspending the pellets in high salt wash buffer (6.1.1). The pellet was sonicated to fully resuspend, centrifuged at 50 000×g for 30 min and the supernatant discarded. This process was repeated 5-7 times until the supernatant was free of protein. The pellet was then resuspended in low salt wash buffer (6.1.1) and the sonication and centrifugation process repeated. This was repeated 3-5 times until the supernatant was free of protein. The pellet was then resuspended in solubilisation buffer (6.1.1) and allowed to incubate with rolling at 4 °C overnight. The resolubilised protein was centrifuged at 50 000×g for 1 hour, and the supernatant applied to free Ni-NTA resin. The protocol was completed as previously described (6.3.2.1), with the addition of 8 M urea. The purified protein was then dialysed into refolding buffer at 4 °C for 3 hours or overnight.

6.3.5 *SDS-PAGE*

SDS-PAGE was used to visualise proteins to determine their molecular weight and purity. 1.5 mm Mini-Protean glass plates were assembled in the casting rack (Bio-Rad). SDS-PAGE resolving gel (6.1.1, acrylamide and H_2O volumes changed according to desired

percentage) was pipetted between the plates to 2 cm below the top. 1 mL 100% propan-2-ol was pipetted on top. After 15 min, the propan2-ol was removed and the top washed with ddH2O. The remaining space was filled with stacking gel (6.1.1) and a comb of the proper size added. After 15 min, the gel was transferred to a Mini-PROTEAN tank (Bio-Rad), which was filled with running buffer (6.1.1). 4× SDS-PAGE sample buffer was added to each sample, with an appropriate volume being added to each well. 5 µL PageRuler Prestained Plus protein ladder (Thermo Scientific) was added to the outside lane and the gel tank connected to Power-Pac Basic Power Supply (Bio-Rad). The gel was run at 180 V for around 45 min or until the dye front approach the bottom of the gel. The gel was removed from the gel and incubated with Instant Blue (Expedeon) for 15 min-overnight. The gel was washed in in ddH_2O. Protein appeared as blue bands.

6.4 PLATE READER EXPERIMENTS

Steady state emission, anisotropy, spectrum and absorbance experiments were conducting using a Synergy H4 Plate Reader and Gen5 software.

6.4.1 *DNA Binding Experiments*

For refolded Rx1, 1 µM fluorescein-labelled 30 bp oligonucleotide was used, with Rx1 ranging from 250 nm to 15 µM in 10 mM Tris-HCl, 100 mM NaCl, 15% glycerol. 20 µL samples were incubated for 10 min in black 384-well Fluotrac plates (Greiner). Experiments were autoscaled in intensity by the instrument, using 485/20 nm excitation filter and a 528/20 nm emission filter. For the salt binding experiment, 1 µM oligonucleotide was used with 5 µM Rx1. For $Rx1_{1\text{-}489}$-LumP

DNA binding, 10 nM olignucleotide was used in 50 mM HEPES 60 mM NaCl 1 mM TCEP 1 mM EDTA, with protein concentration varying from 43 nM to 22 μM.

6.4.2 *Spectral Data*

50 μL 1 μM LumP and $Rx1_{1\text{-}489}$-LumP in 50 mM Tris-HCl, 150 mM Nacl, 1 mM EDTA, 1 mM DTT were used to acquire spectra in black 96-well fluotrac plates (Greiner). The proteins were excited at 400 nm, with emission intensity measured in 1 nm intervals from 420 to 600 nm. The excitation spectrum was collected by measuring emission at 500 nm and exciting in 1 nm intervals from 300 nm to 480 nm.

6.4.3 Nb*Glk and* Nb*DBCP Binding*

1 μM $Rx1_{1\text{-}489}$-LumP with 5 μM *Nb*Glk and *Nb*DBCP was used for steady-state anisotropy binding experiments in 25 mM Tris-HCl, 60 mM NaCl, 1 mM EDTA, 1 mM DTT.

6.5 *n. benthamiana* EXPERIMENTS

6.5.1 *Transformation of* Agrobacterium tumefaciens

A. tumefaciens was used to introduce a T-plasmid containing a desired gene into *N. benthamiana.* 100 μL electrocompetent *A. tumefaciens* GV3101 was thawed on ice. The desired plasmid was miniprepped (6.2.1) and 1 μL was transferred to the thawed cells. The sample was transferred to an electroporator and pulse with 16.7 kV/cm with a 6 ms time constant. Cells were transferred to a 15 mL falcon tube and 2 mL SOC (SOB (6.1.3.2) with 20 mM glucose) was added. Cells were incubated with shaking at 28 °C for 3-4 hours. Cells were then

spread on YEB (6.1.3.3) agar plates (6.1.3.5) containing rifampicin, gentamicin and the antibiotic of the desired plasmid (6.1.2) using a sterile L-shaped spreader. Plates were sealed using Parafilm (Bemis) and grown for 48 hours at 30 °C. Successful transformants were identified and used immediately or the plates were stored at 4 °C for up to a month.

6.5.2 *Preparation of Electrocompetent* Agrobacterium

A. tumefaciens from a glycerol stock (6.2.10) was spread on a YEB (6.1.3.3) agar plate (6.1.3.5), sealed with Parafilm (Bemis) and grown for 48 hours at 30 °C. A single colony was transferred using a sterile plastic loop (Starlab) to 5 mL YEB containing gentamicin and rifampicin (6.1.2). Cells were incubated with shaking at 28 °C for 8 hours. Three 1 L conical flasks containing 125 mL YEB, gentamicin and rifampicin were inoculated with 10 µL, 100 µL and 1 mL starter culture and incubated with shaking at 28 °C overnight. Cells were harvested at an OD_{600} of 1.0 (this typically took 30-40 hours). When one flask was sufficiently grown, cells were transferred to 50 mL falcon tubes and centrifuged at 4000×g for 20 min at 4 °C. The supernatant was discarded and cells were resuspended in a total of 60 mL ice-cold Milli-Q H_2O. Centrifugation was repeated cells were resuspended in 30 mL ice-cold Milli-Q H_2O. Centrifugation was repeated and cells were resuspended in 15 mL ice-cold Milli-Q H_2O. Centrifugation was repeated and cells were resuspended in 7.5 mL ice-cold Milli-Q H_2O. Centrifugation was repeated and cells were resuspended in 1.25 mL ice-cold 10% glycerol. Cells were dispensed in to 100 µL aliquots and flash-frozen in liquid nitrogen. Cells were used immediately or stored at -80 °C

6.5.3 *Transient Protein Expression*

Transgenic leaf material was obtained by infiltrating *N. benthamiana* with *A. tumefaciens* containing a T-plasmid with the desired gene. 5 mL YEB (6.1.3.3) with rifampicin, gentamicin and the desired antibiotic (6.1.2) was inoculated from a glycerol stock (6.2.10) or agar plate (6.1.3.5). Cells were grown for 36-48 hours until significant growth was visible. Cells were centrifuged at 4000×g for 20 min and resuspended in 5 mL preparation buffer (6.1.1). This was repeated 2-3 times. Cells were resuspended in fresh infiltration buffer (6.1.1) to a final OD_{600} of 0.4. Cells were incubated with shaking at room temperature for 3 hours. Cells were transferred to a plastic syringe (Starlab) and leaves of 4-week-old plants were infiltrated from the underside. Plants were grown at 26 ºC with 16-hour days. Leaves were harvested after 2-4 days. To improve expression, plants were often coinfiltrated with a p19-containing strain at an OD_{600} of 0.1, which suppresses post-transcriptional gene silencing Voinnet et al., 2003.

6.5.4 *DNA Binding Experiments*

For *in vivo* DNA-binding experiments, *N. benthamiana* leaves were infiltrated with NRC1 (pGWB401, untagged or pGWB552, GFP-tagged), Rx (pBin35S, untagged or GFP-tagged) and p19. After growth for 3 days, leaves were infiltrated with 0.5% LDS and fixed by incubating in 4% methanal at room temperature overnight. Leaves were quenched in 125 mM glycine for 1 hr and stored at 4 °C in PBS before use.

6.5.5 *PVX Abundance*

N. benthamiana leaves were infiltrated with *Agrobacterium* containing a GFP-tagged PVX construct in a T-plasmid (pGR208), either alone, or with. Leaves were grown for 3 days. 5 mL discs were made using a PCR tube and placed carefully onto 100 μL ddH_2O in a black 96-well plate. PVX abundance was measured by fluorescence with excitation at 485/9 nm and emission at 509/9 nm.

6.5.6 *Hypersensitive Response*

N. benthamiana leaves were coinfiltrated with *Agrobacterium* with a T-plasmid encoding the either the avirulent (CP106) or virulent (CP105) coat protein (pBin35S) alongside the NLR for testing. HR was observed after 2 days by discolouration of the leaves.

6.5.7 *VIGS*

2-week old plants were coinfiltrated with *Agrobacterium* with a T-plasmid encoding pTRV1 and pTRV2 (pYL156) containing a 300 bp sequence complementary to a portion of the gene targeted for silencing. Plants were allowed to grow for 3 weeks at 22 °C with 12-hour days, or until the positive control PDS-silencing plants had a number of white leaves. Plants were then used for subsequent experiments.

BIBLIOGRAPHY

Abramovitch, R.B., Anderson, J.C. and Martin, G.B., 2006. Bacterial elicitation and evasion of plant innate immunity. *Nature Reviews Molecular Cell Biology* [Online], 7(8), pp.601–611. Available from: https://doi.org/10.1038/nrm1984.

Aguilar, J., Zupan, J., Cameron, T.A. and Zambryski, P.C., 2010. Agrobacterium type IV secretion system and its substrates form helical arrays around the circumference of virulence -induced cells. *Proceedings of the National Academy of Sciences* [Online], 107(8) (), February, pp.3758–3763. Available from: https://doi.org/10.1073/pnas.0914940107.

Ahuja, I., Kissen, R. and Bones, A.M., 2012. Phytoalexins in defense against pathogens. *Trends in Plant Science* [Online], 17(2), pp.73–90. Available from: https://doi.org/10.1016/j.tplants.2011.11.002.

Amaral, M., Kokh, D.B., Bomke, J., Wegener, A., Buchstaller, H.P., Eggenweiler, H.M., Matias, P., Sirrenberg, C., Wade, R.C. and Frech, M., 2017. Protein conformational flexibility modulates kinetics and thermodynamics of drug binding. *Nature Communications* [Online], 8(1). Available from: https://doi.org/10.1038/s41467-017-02258-w.

Apel, K. and Hirt, H., 2004. Reactive Oxygen Species: Metabolism, Oxidative Stress, and Signal Transduction. *Annual Review of Plant*

Biology [Online], 55(1), pp.373–399. Available from: https://doi.org/10.1146/annurev.arplant.55.031903.141701.

Asai, T., Tena, G., Plotnikova, J., Willmann, M.R., Chiu, W.-L., Gomez-Gomez, L., Boller, T., Ausubel, F.M. and Sheen, J., 2002. MAP kinase signalling cascade in Arabidopsis innate immunity. *Nature* [Online], 415(6875), pp.977–983. Available from: https://doi.org/10.1038/415977a.

Asurmendi, S., Berg, R.H., Koo, J.C. and Beachy, R.N., 2004. Coat protein regulates formation of replication complexes during tobacco mosaic virus infection. *Proceedings of the National Academy of Sciences of the United States of America* [Online], 101(5), pp.1415–1420. Available from: https://doi.org/10.1073/pnas.0307778101.

Bahar, O., Mordukhovich, G., Luu, D.D., Schwessinger, B., Daudi, A., Jehle, A.K., Felix, G. and Ronald, P.C., 2016. Bacterial Outer Membrane Vesicles Induce Plant Immune Responses. *Molecular Plant-Microbe Interactions* [Online], 29(5), pp.374–384. Available from: https://doi.org/10.1094/MPMI-12-15-0270-R.

Baureithel, K., Felix, G. and Boller, T., 1994. Specific, high affinity binding of chitin fragments to tomato cells and membranes. Competitive inhibition of binding by derivatives of chitooligosaccharides and a Nod factor of Rhizobium. *The Journal of biological chemistry* [Online], 269(27), pp.17931–8. Available from: http://www.ncbi.nlm.nih.gov/pubmed/8027050.

Beijerinck, M., 1898. Ueber ein Contagium vivurn fluidum als Ursaehe der Fleekenkrankheit der Tabaksblätter. *Verhandelingen der Koninklijke Akademie van Wetenschappen te Amsterdam* [Online], 6(5), pp.3–

21. Available from: http://www.dwc.knaw.nl/DL/publications/PU00011860.pdf.

Bendahmane, A., Kanyuka, K. and Baulcombe, D.C., 1999. The Rx gene from potato controls separate virus resistance and cell death responses. *The Plant cell* [Online], 11(5), pp.781–92. Available from: https://doi.org/10.1105/tpc.11.5.781.

Benschop, J.J., Mohammed, S., O'Flaherty, M., Heck, A.J.R., Slijper, M. and Menke, F.L.H., 2007. Quantitative phosphoproteomics of early elicitor signaling in Arabidopsis. *Molecular & cellular proteomics : MCP* [Online], 6(7), pp.1198–214. Available from: https://doi.org/10.1074/mcp.M600429-MCP200.

Bernoux, M., Burdett, H., Williams, S.J., Zhang, X., Chen, C., Newell, K., Lawrence, G.J., Kobe, B., Ellis, J.G., Anderson, P.A. and Dodds, P.N., 2016. Comparative Analysis of the Flax Immune Receptors L6 and L7 Suggests an Equilibrium-Based Switch Activation Model. *The Plant Cell* [Online], 28(1) (), January, pp.146–159. Available from: https://doi.org/10.1105/tpc.15.00303.

Bernoux, M., Ve, T., Williams, S., Warren, C., Hatters, D., Valkov, E., Zhang, X., Ellis, J.G., Kobe, B. and Dodds, P.N., 2011. Structural and Functional Analysis of a Plant Resistance Protein TIR Domain Reveals Interfaces for Self-Association, Signaling, and Autoregulation. *Cell Host & Microbe* [Online], 9(3), pp.200–211. Available from: https://doi.org/10.1016/j.chom.2011.02.009.

Boller, T. and Felix, G., 2009. A renaissance of elicitors: perception of microbe-associated molecular patterns and danger signals by pattern-recognition receptors. *Annual review of plant biology* [Online],

60, pp.379–406. Available from: https://doi.org/10.1146/annurev.arplant.57.032905.105346.

Burkholder, W.H., 1948. Bacteria as Plant Pathogens. *Annual Review of Microbiology* [Online], 2(1), pp.389–412. Available from: https://doi.org/10.1146/annurev.mi.02.100148.002133.

Büschges, R., Hollricher, K., Panstruga, R., Simons, G., Wolter, M., Frijters, A., Van Daelen, R., Van der Lee, T., Diergaarde, P., Groenendijk, J., Töpsch, S., Vos, P., Salamini, F. and Schulze-Lefert, P., 1997. The barley Mlo gene: A novel control element of plant pathogen resistance. *Cell* [Online], 88(5), pp.695–705. Available from: https://doi.org/10.1016/S0092-8674(00)81912-1.

Caplan, J.L., Mamillapalli, P., Burch-Smith, T.M., Czymmek, K. and Dinesh-Kumar, S.P., 2008. Chloroplastic Protein NRIP1 Mediates InnateÂ Immune Receptor Recognition of a Viral Effector. *Cell* [Online], 132(3), pp.449–462. Available from: https://doi.org/10.1016/j.cell.2007.12.031.

Casey, L.W., Lavrencic, P., Bentham, A.R., Cesari, S., Ericsson, D.J., Croll, T., Turk, D., Anderson, P.A., Mark, A.E., Dodds, P.N., Mobli, M., Kobe, B. and Williams, S.J., 2016. The CC domain structure from the wheat stem rust resistance protein Sr33 challenges paradigms for dimerization in plant NLR proteins. *Proceedings of the National Academy of Sciences of the United States of America* [Online], 113(45), pp.12856–12861. Available from: https://doi.org/10.1073/pnas.1609922113.

Catanzariti, A.M., Lim, G.T. and Jones, D.A., 2015. The tomato I-3 gene: A novel gene for resistance to Fusarium wilt disease. *New*

Phytologist [Online], 207(1), pp.106–118. Available from: https://doi.org/10.1111/nph.13348.

Catlett, M.G. and Kaplan, K.B., 2006. Sgt1p is a unique co-chaperone that acts as a client adaptor to link Hsp90 to Skp1p. *Journal of Biological Chemistry* [Online], 281(44), pp.33739–33748. Available from: https://doi.org/10.1074/jbc.M603847200.

Cesari, S., Moore, J., Chen, C., Webb, D., Periyannan, S., Mago, R., Bernoux, M., Lagudah, E.S. and Dodds, P.N., 2016. Cytosolic activation of cell death and stem rust resistance by cereal MLA-family CC-NLR proteins. *Proceedings of the National Academy of Sciences of the United States of America* [Online], 113(36), pp.10204–10209. Available from: https://doi.org/10.1073/pnas.1605483113.

Chalfie, M., Tu, Y., Euskirchen, G., Ward, W.W. and Prasher, D.C., 1994. Green fluorescent protein as a marker for gene expression. *Science* [Online], 263(5148), pp.802–805. Available from: https://doi.org/10.1126/science.8303295.

Chan, S.L., Mukasa, T., Santelli, E., Low, L.Y. and Pascual, J., 2010. The crystal structure of a TIR domain from Arabidopsis thaliana reveals a conserved helical region unique to plants. *Protein Science* [Online], 19(1), pp.155–161. Available from: https://doi.org/10.1002/pro.275.

Chang, J.H., Urbach, J.M., Law, T.F., Arnold, L.W., Hu, A., Gombar, S., Grant, S.R., Ausubel, F.M. and Dangl, J.L., 2005. A high-throughput, near-saturating screen for type III effector genes from Pseudomonas syringae. *Proceedings of the National Academy of Sciences of the United*

States of America [Online], 102(7), pp.2549–2554. Available from: https://doi.org/10.1073/pnas.0409660102.

Chen, H., Xue, L., Chintamanani, S., Germain, H., Lin, H., Cui, H., Cai, R., Zuo, J., Tang, X., Li, X., Guo, H. and Zhou, J.M., 2009. ETHYLENE INSENSITIVE3 and ETHYLENE INSENSITIVE3-LIKE1 repress SALICYLIC ACID INDUCTION DEFICIENT2 expression to negatively regulate plant innate immunity in Arabidopsis. *Plant Cell* [Online], 21(8), pp.2527–2540. Available from: https://doi.org/10.1105/tpc.108.065193.

Chinchilla, D., Zipfel, C., Robatzek, S., Kemmerling, B., Nürnberger, T., Jones, J.D.G., Felix, G. and Boller, T., 2007. A flagellin-induced complex of the receptor FLS2 and BAK1 initiates plant defence. *Nature* [Online], 448(7152), pp.497–500. Available from: https://doi.org/10.1038/nature05999.

Choi, J., Park, S.Y., Kim, B.R., Roh, J.H., Oh, I.S., Han, S.S. and Lee, Y.H., 2013. Comparative Analysis of Pathogenicity and Phylogenetic Relationship in Magnaporthe grisea Species Complex. *PLoS ONE* [Online], 8(2), pp.1–8. Available from: https://doi.org/10.1371/journal.pone.0057196.

Collier, S.M., Hamel, L.-P. and Moffett, P., 2011. Cell Death Mediated by the N-Terminal Domains of a Unique and Highly Conserved Class of NB-LRR Protein. *Molecular Plant-Microbe Interactions* [Online], 24(8), pp.918–931. Available from: https://doi.org/10.1094/MPMI-03-11-0050.

Cormack, B.P., Valdivia, R.H. and Falkow, S., 1996. FACS-optimized mutants of the green fluorescent protein (GFP). *Gene* [Online],

173(1), pp.33–38. Available from: https://doi.org/10.1016/0378-1119(95)00685-0.

Cotton, J.A., Lilley, C.J., Jones, L.M., Kikuchi, T., Reid, A.J., Thorpe, P., Tsai, I.J., Beasley, H., Blok, V., Cock, P.J., Eves-van den Akker, S., Holroyd, N., Hunt, M., Mantelin, S., Naghra, H., Pain, A., Palomares-Rius, J.E., Zarowiecki, M., Berriman, M., Jones, J.T. and Urwin, P.E., 2014. The genome and life-stage specific transcriptomes of Globodera pallida elucidate key aspects of plant parasitism by a cyst nematode. *Genome Biology* [Online], 15(3), R43. Available from: https://doi.org/10.1186/gb-2014-15-3-r43.

Creager, A.N., Scholthof, K.-B.G., Citovsky, V. and Scholthof, H.B., 1999. Tobacco Mosaic Virus: Pioneering Research for a Century. *The Plant Cell* [Online], 11(3), pp.301–308. Available from: https://doi.org/10.1105/tpc.11.3.301.

Crick, F.H.C., 1953. The packing of α-helices: simple coiled-coils. *Acta Crystallographica* [Online], 6(8), pp.689–697. Available from: https://doi.org/10.1107/s0365110x53001964.

Crocker, W. and Knight, L.I., 1935. Similarities in the effects of ethylene and the plant auxins. *Contributions of the Boyce Thompson Institute* 7. Chap. 3, pp.231–248.

Dangle, J.L. and Jones, J.D.G., 2001. Plant pathogens and integrated defence in plants. *Nature* [Online], 411(November), pp.826–833. Available from: www.nature.com.

Danot, O., Marquenet, E., Vidal-Ingigliardi, D. and Richet, E., 2009. Wheel of Life, Wheel of Death: A Mechanistic Insight into Signaling

by STAND Proteins. *Structure* [Online], 17(2), pp.172–182. Available from: https://doi.org/10.1016/j.str.2009.01.001.

Denoux, C., Galletti, R., Mammarella, N., Gopalan, S., Werck, D., De Lorenzo, G., Ferrari, S., Ausubel, F.M. and Dewdney, J., 2008. Activation of Defense Response Pathways by OGs and Flg22 Elicitors in Arabidopsis Seedlings. *Molecular Plant* [Online], 1(3), pp.423–445. Available from: https://doi.org/10.1093/mp/ssn019.

Dixon, C.H., 2017. *The DNA Binding Activity of the Potato NBLRR protein Rx1*. PhD thesis.

Dodds, P.N., Lawrence, G.J., Catanzariti, A.-M., Teh, T., Wang, C.-I.A., Ayliffe, M.A., Kobe, B. and Ellis, J.G., 2006. Direct protein interaction underlies gene-for-gene specificity and coevolution of the flax resistance genes and flax rust avirulence genes. *Proceedings of the National Academy of Sciences* [Online], 103(23) (), June, pp.8888–8893. Available from: https://doi.org/10.1073/pnas.0602577103.

Dollet, M., 1984. Plant Diseases Caused by Flagellate Protozoa (Phytomonas). *Annual Review of Phytopathology* [Online], 22(1), pp.115–132. Available from: https://doi.org/10.1146/annurev.py.22.090184.000555.

Du, L., Ali, G.S., Simons, K.A., Hou, J., Yang, T., Reddy, A.S.N. and Poovaiah, B.W., 2009. Ca2+/calmodulin regulates salicylic-acid-mediated plant immunity. *Nature* [Online], 457(7233), pp.1154–1158. Available from: https://doi.org/10.1038/nature07612.

Duprat, A., Caranta, C., Revers, F., Menand, B., Browning, K.S. and Robaglia, C., 2002. The Arabidopsis eukaryotic initiation factor (iso)4E is dispensable for plant growth but required for susceptibility

to potyviruses. *Plant Journal* [Online], 32(6), pp.927–934. Available from: https://doi.org/10.1046/j.1365-313X.2002.01481.x.

Einstein, A., 1905. Über die von der molekularkinetischen Theorie der Wärme geforderte Bewegung von in ruhenden Flüssigkeiten suspendierten Teilchen. *Annalen der Physik* [Online], 322(8), pp.549–560. Available from: https://doi.org/10.1002/andp.19053220806.

Erzberger, J.P. and Berger, J.M., 2006. Evolutionary relationships and structural mechanisms of AAA+ proteins. *Annual Review of Biophysics and Biomolecular Structure* [Online], 35, pp.93–114. Available from: https://doi.org/10.1146/annurev.biophys.35.040405.101933.

Espinosa, A., Guo, M., Tam, V.C., Fu, Z.Q. and Alfano, J.R., 2003. The Pseudomonas syringae type III-secreted protein HopPtoD2 possesses protein tyrosine phosphatase activity and suppresses programmed cell death in plants. *Molecular Microbiology* [Online], 49(2), pp.377–387. Available from: https://doi.org/10.1046/j.1365-2958.2003.03588.x.

Felix, G. and Boller, T., 2003. Molecular sensing of bacteria in plants: The highly conserved RNA-binding motif RNP-1 of bacterial cold shock proteins is recognized as an elicitor signal in tobacco. *Journal of Biological Chemistry* [Online], 278(8), pp.6201–6208. Available from: https://doi.org/10.1074/jbc.M209880200.

Fenyk, S., San, A.D., Campillo, E., Pohl, E., Hussey, P.J. and Cann, M.J., 2012. A Nucleotide Phosphatase Activity in the Nucleotide Binding Domain of an Orphan Resistance Protein from Rice * â¡ [Online]. 287(6), pp.4023–4032. Available from: https://doi.org/10.1074/jbc.M111.314450.

Fenyk, S., Townsend, P.D., Dixon, C.H., Spies, G.B., De San Eustaquio Campillo, A., Slootweg, E.J., Westerhof, L.B., Gawehns, F.K.K., Knight, M.R., Sharples, G.J., Goverse, A., P??lsson, L.O., Takken, F.L.W. and Cann, M.J., 2015. The potato nucleotide-binding leucine-rich repeat (NLR) immune receptor Rx1 is a pathogen-dependent DNA-deforming protein. *Journal of Biological Chemistry* [Online], 290(41), pp.24945–24960. Available from: https://doi.org/10.1074/jbc.M115.672121.

Ferrari, S., Galletti, R., Denoux, C., De Lorenzo, G., Ausubel, F.M. and Dewdney, J., 2007. Resistance to Botrytis cinerea induced in arabidopsis by elicitors is independent of salicylic acid, ethylene, or jasmonate signaling but requires PHYTOALEXIN DEFICIENT3. *Plant Physiology* [Online], 144(1), pp.367–379. Available from: https://doi.org/10.1104/pp.107.095596.

Fischer, M. and Bacher, A., 2008. Biosynthesis of vitamin B2: Structure and mechanism of riboflavin synthase. *Archives of Biochemistry and Biophysics* [Online], 474(2), pp.252–265. Available from: https://doi.org/10.1016/j.abb.2008.02.008.

Gabriëls, S.H.E.J., Vossen, J.H., Ekengren, S.K., Ooijen, G.V., Abd-El-Haliem, A.M., Berg, G.C.M.V.D., Rainey, D.Y., Martin, G.B., Takken, F.L.W., Wit, P.J.G.M.D. and Joosten, M.H.A.J., 2007. An NB-LRR protein required for HR signalling mediated by both extra- and intracellular resistance proteins. *Plant Journal* [Online], 50(1), pp.14–28. Available from: https://doi.org/10.1111/j.1365-313X.2007.03027.x.

Geiss-Friedlander, R. and Melchior, F., 2007. Concepts in sumoylation: a decade on. *Nature Reviews Molecular Cell Biology* [Online], 8(12), pp.947–956. Available from: https://doi.org/10.1038/nrm2293.

Glazebrook, J., 2005. Contrasting Mechanisms of Defense Against Biotrophic and Necrotrophic Pathogens. *Annual Review of Phytopathology* [Online], 43(1), pp.205–227. Available from: https://doi.org/10.1146/annurev.phyto.43.040204.135923.

Gnanamanickam, S.S., 2009. Biological control of rice diseases, In: Progress in Biological Control edited by Hokkanen, Heikki M. T. *Springer* [Online], 8, pp.20–26. Available from: https://doi.org/10.1007/978-90-481-2465-7.

Gómez-Gómez, L., Felix, G. and Boller, T., 1999. A single locus determines sensitivity to bacterial flagellin in Arabidopsis thaliana. *Plant Journal* [Online], 18(3), pp.277–284. Available from: https://doi.org/10.1046/j.1365-313X.1999.00451.x.

Goritschnig, S., Steinbrenner, A.D., Grunwald, D.J. and Staskawicz, B.J., 2016. Structurally distinct Arabidopsis thaliana NLR immune receptors recognize tandem WY domains of an oomycete effector. *New Phytologist* [Online], 210(3), pp.984–996. Available from: https://doi.org/10.1111/nph.13823.

Grant, S.R., Fisher, E.J., Chang, J.H., Mole, B.M. and Dangl, J.L., 2006. Subterfuge and manipulation: type III effector proteins of phytopathogenic bacteria. *Annual review of microbiology* [Online], 60, pp.425–449. Available from: https://doi.org/10.1146/annurev.micro.60.080805.142251.

Griesbeck, O., Baird, G.S., Campbell, R.E., Zacharias, D.A. and Tsien, R.Y., 2001. Reducing the environmental sensitivity of yellow fluorescent protein. Mechanism and applications. *Journal of Biological Chemistry* [Online], 276(31), pp.29188–29194. Available from: https://doi.org/10.1074/jbc.M102815200.

Guan, R., Su, J., Meng, X., Li, S., Liu, Y., Xu, J. and Zhang, S., 2015. Multilayered regulation of ethylene induction plays a positive role in arabidopsis resistance against Pseudomonas syringae. *Plant Physiology* [Online], 169(1), pp.299–312. Available from: https://doi.org/10.1104/pp.15.00659.

Gutierrez, J.R., Balmuth, A.L., Ntoukakis, V., Mucyn, T.S., Gimenez-Ibanez, S., Jones, A.M.E. and Rathjen, J.P., 2010. Prf immune complexes of tomato are oligomeric and contain multiple Pto-like kinases that diversify effector recognition. *Plant Journal* [Online], 61(3), pp.507–518. Available from: https://doi.org/10.1111/j.1365-313X.2009.04078.x.

Hanania, U., Furman-Matarasso, N., Ron, M. and Avni, A., 1999. Isolation of a novel SUMO protein from tomato that suppresses EIX-induced cell death. *Plant Journal* [Online], 19(5), pp.533–541. Available from: https://doi.org/10.1046/j.1365-313X.1999.00547.x.

Hao, W., Collier, S.M., Moffett, P. and Chai, J., 2013. Structural basis for the interaction between the potato virus X resistance protein (Rx) and its cofactor ran GTPase-activating protein 2 (RanGAP2). *Journal of Biological Chemistry* [Online], 288(50), pp.35868–35876. Available from: https://doi.org/10.1074/jbc.M113.517417.

Heim, R. and Tsien, R.Y., 1996. Engineering green fluorescent protein for improved brightness, longer wavelengths and fluorescence resonance energy transfer. *Current Biology* [Online], 6(2), pp.178–182. Available from: https://doi.org/10.1016/S0960-9822(02)00450-5.

Hoepker, A.C., Wang, A., Le Marois, A., Suhling, K., Yan, Y. and Marriott, G., 2015. Genetically encoded sensors of protein hydrodynamics and molecular proximity. *Proceedings of the National Academy of Sciences of the United States of America* [Online], 112(20), E2569–E2574. Available from: https://doi.org/10.1073/pnas.1424021112.

Huber, R., 1979. Conformational flexibility and its functional significance in some protein molecules. *Trends in Biochemical Sciences* [Online], 4(12), pp.271–276. Available from: https://doi.org/10.1016/0968-0004(79)90298-6.

Huffaker, A., Pearce, G. and Ryan, C.A., 2006. An endogenous peptide signal in Arabidopsis activates components of the innate immune response. *Proceedings of the National Academy of Sciences of the United States of America* [Online], 103(26), pp.10098–10103. Available from: https://doi.org/10.1073/pnas.0603727103.

Humphry, M., Bednarek, P., Kemmerling, B., Koh, S., Stein, M., Göbel, U., Stüber, K., Piślewska-Bednarek, M., Loraine, A., Schulze-Lefert, P., Somerville, S. and Panstruga, R., 2010. A regulon conserved in monocot and dicot plants defines a functional module in antifungal plant immunity. *Proceedings of the National Academy of Sciences of the United States of America* [Online], 107(50), pp.21896–21901. Available from: https://doi.org/10.1073/pnas.1003619107.

Jabłoński, A., 1960. On the Notion of Emission Anisotropy. *Bulletin L'Académie Polonaise des Science, Série des Sciences Mathématiques, Astronomiques et Physiques*, 8(4), pp.259–264.

Jain, A., Sarsaiya, S., Wu, Q., Lu, Y. and Shi, J., 2019. A review of plant leaf fungal diseases and its environment speciation. *Bioengineered* [Online], 10(1), pp.409–424. Available from: https://doi.org/10.1080/21655979.2019.1649520.

Jha, G., Rajeshwari, R. and Sonti, R.V., 2005. Bacterial type two secretion system secreted proteins: Double-edged swords for plant pathogens. *Molecular Plant-Microbe Interactions* [Online], 18(9), pp.891–898. Available from: https://doi.org/10.1094/MPMI-18-0891.

Johal, G.S. and Briggs, S.P., 1992. Reductase activity encoded by the HM1 disease resistance gene in maize. *Science* [Online], 258(5084), pp.985–987. Available from: https://doi.org/10.1126/science.1359642.

Jones, J.D. and Dangl, J.L., 2006. The plant immune system. *Nature* [Online], 444(7117), pp.323–329. Available from: https://doi.org/10.1038/nature05286.

Jordan, D.B., Bacot, K.O., Carlson, T.J., Kessel, M. and Viitanen, P.V., 1999. Plant Riboflavin Biosynthesis. *Journal of Biological Chemistry* [Online], 274(31), pp.22114–22121. Available from: https://doi.org/10.1074/jbc.274.31.22114.

Kadota, Y., Amigues, B., Ducassou, L., Madaoui, H., Ochsenbein, F., Guerois, R. and Shirasu, K., 2008. Structural and functional analysis of SGT1-HSP90 core complex required for innate immunity in plants.

EMBO Reports [Online], 9(12), pp.1209–1215. Available from: https://doi.org/10.1038/embor.2008.185.

Kadota, Y., Shirasu, K. and Guerois, R., 2010. NLR sensors meet at the SGT1-HSP90 crossroad. *Trends in Biochemical Sciences* [Online], 35(4), pp.199–207. Available from: https://doi.org/10.1016/j.tibs.2009.12.005.

Kang, H.G., Oh, C.S., Sato, M., Katagiri, F., Glazebrook, J., Takahashi, H., Kachroo, P., Martin, G.B. and Klessig, D.F., 2010. Endosome-associated CRT1 functions early in Resistance gene-mediated defense signaling in Arabidopsis and tobacco. *Plant Cell* [Online], 22(3), pp.918–936. Available from: https://doi.org/10.1105/tpc.109.071662.

Kannan, V., Bastas, K. and Antony, R., 2015. Plant Pathogenic Bacteria: An Overview. *Sustainable Approaches to Controlling Plant Pathogenic Bacteria* [Online], (September), pp.1–16. Available from: https://doi.org/10.1201/b18892-2.

Kourelis, J. and Van Der Hoorn, R.A., 2018. Defended to the nines: 25 years of resistance gene cloning identifies nine mechanisms for R protein function. *Plant Cell* [Online], 30(2), pp.285–299. Available from: https://doi.org/10.1105/tpc.17.00579.

Kremers, G.J., Gilbert, S.G., Cranfill, P.J., Davidson, M.W. and Piston, D.W., 2011. Fluorescent proteins at a glance. *Journal of Cell Science* [Online], 124(15), p.2676. Available from: https://doi.org/10.1242/jcs.095059.

Lakowicz, J.R. and Gryczynski, I., 2002. Multiphoton Excitation of Biochemical Fluorophores. *Topics in Fluorescence Spectroscopy* [On-

line]. Boston, MA: Springer US, pp.87–144. Available from: https://doi.org/10.1007/0-306-47070-5_3.

Lee, J., O'Kane, D.J. and Visser, A.J., 1985. Spectral Properties and Function of Two Lumazine Proteins from Photobacterium. *Biochemistry* [Online], 24(6), pp.1476–1483. Available from: https://doi.org/10.1021/bi00327a028.

Leigh, J.A. and Coplin, D.L., 1992. Exopolysaccharides in Plant-Bacterial Interactions. *Annual Review of Microbiology* [Online], 46(1), pp.307–346. Available from: https://doi.org/10.1146/annurev.mi.46.100192.001515.

Leipe, D.D., Koonin, E.V. and Aravind, L., 2004. STAND, a class of P-loop NTPases including animal and plant regulators of programmed cell death: Multiple, complex domain architectures, unusual phyletic patterns, and evolution by horizontal gene transfer. *Journal of Molecular Biology* [Online], 343(1), pp.1–28. Available from: https://doi.org/10.1016/j.jmb.2004.08.023.

Lewis, J.D., Lee, A.H.Y., Hassan, J.A., Wana, J., Hurleya, B., Jhingree, J.R., Wang, P.W., Lo, T., Youn, J.Y., Guttman, D.S. and Desveaux, D., 2013. The Arabidopsis ZED1 pseudokinase is required for ZAR1-mediated immunity induced by the Pseudomonas syringae type III effector HopZ1a. *Proceedings of the National Academy of Sciences of the United States of America* [Online], 110(46), pp.18722–18727. Available from: https://doi.org/10.1073/pnas.1315520110.

Li, Y., Li, S., Bi, D., Cheng, Y.T., Li, X. and Zhang, Y., 2010. SRFR1 negatively regulates plant NB-LRR resistance protein accumulation

to prevent autoimmunity. *PLoS Pathogens* [Online], 6(9), pp.1–11. Available from: https://doi.org/10.1371/journal.ppat.1001111.

Libault, M., Wan, J., Czechowski, T., Udvardi, M. and Stacey, G., 2007. Identification of 118 Arabidopsis transcription factor and 30 ubiquitin-ligase genes responding to chitin, a plant-defense elicitor. *Molecular Plant-Microbe Interactions* [Online], 20(8), pp.900–911. Available from: https://doi.org/10.1094/MPMI-20-8-0900.

Liu, X., Grabherr, H.M., Willmann, R., Kolb, D., Brunner, F., Bertsche, U., Kühner, D., Franz-wachtel, M., Amin, B., Felix, G., Ongena, M., Nürnberger, T. and Gust, A.A., 2014. The LysM-RK CERK1 is also important for the perception of the fungal-derived PAMP chitin (Miya et al [Online], pp.1–24. Available from: https://doi.org/10.7554/eLife.01990.

Lombard, V., Golaconda Ramulu, H., Drula, E., Coutinho, P.M. and Henrissat, B., 2014. The carbohydrate-active enzymes database (CAZy) in 2013. *Nucleic Acids Research* [Online], 42(D1), pp.490–495. Available from: https://doi.org/10.1093/nar/gkt1178.

Lozano-Torres, J.L., Wilbers, R.H., Gawronski, P., Boshoven, J.C., Finkers-Tomczak, A., Cordewener, J.H., America, A.H., Overmars, H.A., Van 't Klooster, J.W., Baranowski, L., Sobczak, M., Ilyas, M., Van Der Hoorn, R.A., Schots, A., De Wit, P.J., Bakker, J., Goverse, A. and Smant, G., 2012. Dual disease resistance mediated by the immune receptor Cf-2 in tomato requires a common virulence target of a fungus and a nematode. *Proceedings of the National Academy of Sciences of the United States of America* [Online], 109(25), pp.10119–10124. Available from: https://doi.org/10.1073/pnas.1202867109.

Maekawa, T., Cheng, W., Spiridon, L.N., Töller, A., Lukasik, E., Saijo, Y., Liu, P., Shen, Q.H., Micluta, M.A., Somssich, I.E., Takken, F.L., Petrescu, A.J., Chai, J. and Schulze-Lefert, P., 2011. Coiled-coil domain-dependent homodimerization of intracellular barley immune receptors defines a minimal functional module for triggering cell death. *Cell Host and Microbe* [Online], 9(3), pp.187–199. Available from: https://doi.org/10.1016/j.chom.2011.02.008.

Maekawa, T., Kufer, T.A. and Schulze-Lefert, P., 2011. NLR functions in plant and animal immune systems: So far and yet so close. *Nature Immunology* [Online], 12(9), pp.818–826. Available from: https://doi.org/10.1038/ni.2083.

Matunis, M.J., Coutavas, E. and Blobel, G., 1996. A novel ubiquitin-like modification modulates the partitioning of the Ran-GTPase-activating protein RanGAP1 between the cytosol and the nuclear pore complex. *Journal of Cell Biology* [Online], 135(6), pp.1457–1470. Available from: https://doi.org/10.1083/jcb.135.6.1457.

Meier, I., 2007. Composition of the plant nuclear envelope: Theme and variations. *Journal of Experimental Botany* [Online], 58(1), pp.27–34. Available from: https://doi.org/10.1093/jxb/erl009.

Melotto, M., Underwood, W., Koczan, J., Nomura, K. and He, S.Y., 2006. Plant Stomata Function in Innate Immunity against Bacterial Invasion. *Cell* [Online], 126(5), pp.969–980. Available from: https://doi.org/10.1016/j.cell.2006.06.054.

Melville, B., Lucieer, A. and Aryal, J., 2006. *Principles of Fluorescence Spectroscopy*. Ed. by J.R. Lakowicz. Vol. 10, 2. Boston, MA: Springer

US. Available from: https://doi.org/10.1007/978-0-387-46312-4.

Merrick, W.C. and Pavitt, G.D., 2018. Protein Synthesis Initiation in Eukaryotic Cells. *Cold Spring Harbor Perspectives in Biology* [Online], 10(12), p.a033092. Available from: https://doi.org/10.1101/cshperspect.a033092.

Meyer, A., Pühler, A. and Niehaus, K., 2001. The lipopolysaccharides of the phytopathogen Xanthomonas campestris pv. campestris induce an oxidative burst reaction in cell cultures of Nicotiana tabacum. *Planta* [Online], 213(2), pp.214–222. Available from: https://doi.org/10.1007/s004250000493.

Mithöfer, A., Ebel, J. and Felle, H.H., 2005. Cation fluxes cause plasma membrane depolarization involved in β-glucan elicitor-signaling in soybean roots. *Molecular Plant-Microbe Interactions* [Online], 18(9), pp.983–990. Available from: https://doi.org/10.1094/MPMI-18-0983.

Mou, Z., Fan, W. and Dong, X., 2003. Inducers of plant systemic acquired resistance Regulate NPR1 function through redox changes. *Cell* [Online], 113(7), pp.935–944. Available from: https://doi.org/10.1016/S0092-8674(03)00429-X.

Navarro, L., Dunoyer, P., Jay, F., Arnold, B., Dharmasiri, N., Estelle, M., Voinnet, O. and Jones, J.D.G., 2006. A Plant miRNA Contributes to Antibacterial Resistance by Repressing Auxin Signaling. *Science* [Online], 312(5772), pp.436–439. Available from: https://doi.org/10.1126/science.1126088.

New England Biolabs, 2011. *Tm calculator* [Online]. Available from: https://tmcalculator.neb.com/%7B%5C#%7D!/main.

New England Biolabs, 2014. *NEBcloner* [Online]. Available from: https://nebcloner.neb.com/%7B%5C#%7D!/redigest.

Nicaise, V., Roux, M. and Zipfel, C., 2009. Recent advances in PAMP-triggered immunity against bacteria: pattern recognition receptors watch over and raise the alarm. *Plant Physiology* [Online], 150(4), pp.1638–1647. Available from: https://doi.org/10.1104/pp.109.139709.

Nicaise, V., German-Retana, S., Sanjuán, R., Dubrana, M.-p., Mazier, M., Maisonneuve, B., Candresse, T., Caranta, C. and LeGall, O., 2003. The Eukaryotic Translation Initiation Factor 4E Controls Lettuce Susceptibility to the Potyvirus Lettuce mosaic virus. *Plant Physiology* [Online], 132(3), pp.1272–1282. Available from: https://doi.org/10.1104/pp.102.017855.

Nühse, T.S., Peck, S.C., Hirt, H. and Boller, T., 2000. Microbial Elicitors Induce Activation and Dual Phosphorylation of the Arabidopsis thaliana MAPK 6. *Journal of Biological Chemistry* [Online], 275(11), pp.7521–7526. Available from: https://doi.org/10.1074/jbc.275.11.7521.

Nurnberger, T., Brunner, F., Kemmerling, B. and Piater, L., 2004. Innate immunity in plants and animals: striking similarities and obvious differences. *Immunological Reviews* [Online], 198(1), pp.249–266. Available from: https://doi.org/10.1111/j.0105-2896.2004.0119.x.

Nürnberger, T., Nennstiel, D., Jabs, T., Sacks, W.R., Hahlbrock, K. and Scheel, D., 1994. High affinity binding of a fungal oligopeptide elicitor to parsley plasma membranes triggers multiple defense responses. *Cell* [Online], 78(3), pp.449–460. Available from: https://doi.org/10.1016/0092-8674(94)90423-5.

O'Kane, D.J., Karle, V.A. and Lee, J., 1985. Purification of lumazine proteins from Photobacterium leiognathi and Photobacterium phosphoreum: bioluminescence properties. *Biochemistry* [Online], 24(6), pp.1461–1467. Available from: https://doi.org/10.1021/bi00327a026.

O'Reilly, D.E. and Peterson, E.M., 1970. Rotational correlation times and coefficients of viscosity of electrolytic solutions. *Journal of Physical Chemistry* [Online], 74(17), pp.3280–3285. Available from: https://doi.org/10.1021/j100711a022.

Okuyama, Y., Kanzaki, H., Abe, A., Yoshida, K., Tamiru, M., Saitoh, H., Fujibe, T., Matsumura, H., Shenton, M., Galam, D.C., Undan, J., Ito, A., Sone, T. and Terauchi, R., 2011. A multifaceted genomics approach allows the isolation of the rice Pia-blast resistance gene consisting of two adjacent NBS-LRR protein genes. *Plant Journal* [Online], 66(3), pp.467–479. Available from: https://doi.org/10.1111/j.1365-313X.2011.04502.x.

Papoulis, A., 1984. Expected Value; Dispersion; Moments. *Probability, random variables, and stochastic processes*. Second Edi. New York: McGraw-Hill. Chap. 5-4, pp.139–152.

Peart, J.R., Cook, G., Feys, B.J., Parker, J.E. and Baulcombe, D.C., 2002. An EDS1 orthologue is required for N âmediated resistance against tobacco mosaic virus. *The Plant Journal* [Online], 29(5) (), March,

pp.569–579. Available from: https://doi.org/10.1046/j.1365-313X.2002.029005569.x.

Pieterse, C.M., Van der Does, D., Zamioudis, C., Leon-Reyes, A. and Van Wees, S.C., 2012. Hormonal Modulation of Plant Immunity. *Annual Review of Cell and Developmental Biology* [Online], 28(1), pp.489–521. Available from: https://doi.org/10.1146/annurev-cellbio-092910-154055.

Ponmurugan, P., Saravanan, D. and Ramya, M., 2010. CULTURE AND BIOCHEMICAL ANALYSIS OF A TEA ALGAL PATHOGEN, CEPHALEUROS PARASITICUS1. *Journal of Phycology* [Online], 46(5), pp.1017–1023. Available from: https://doi.org/10.1111/j.1529-8817.2010.00879.x.

Preininger, A.M., Meiler, J. and Hamm, H.E., 2013. Conformational flexibility and structural dynamics in GPCR-mediated G protein activation: A perspective. *Journal of Molecular Biology* [Online], 425(13), pp.2288–2298. arXiv: NIHMS150003. Available from: https://doi.org/10.1016/j.jmb.2013.04.011.

Pruitt, R.N., Schwessinger, B., Joe, A., Thomas, N., Liu, F., Albert, M., Robinson, M.R., Chan, L.J.G., Luu, D.D., Chen, H., Bahar, O., Daudi, A., De Vleesschauwer, D., Caddell, D., Zhang, W., Zhao, X., Li, X., Heazlewood, J.L., Ruan, D., Majumder, D., Chern, M., Kalbacher, H., Midha, S., Patil, P.B., Sonti, R.V., Petzold, C.J., Liu, C.C., Brodbelt, J.S., Felix, G. and Ronald, P.C., 2015. The rice immune receptor XA21 recognizes a tyrosine-sulfated protein from a Gram-negative bacterium. *Science Advances* [Online], 1(6), pp.1–13. Available from: https://doi.org/10.1126/sciadv.1500245.

Rairdan, G.J., Collier, S.M., Sacco, M.a., Baldwin, T.T., Boettrich, T. and Moffett, P., 2008. The coiled-coil and nucleotide binding domains of the Potato Rx disease resistance protein function in pathogen recognition and signaling. *The Plant cell* [Online], 20(3), pp.739–751. Available from: https://doi.org/10.1105/tpc.107.056036.

Ramachandran, H., Herfurth, K., Grosschedl, R., Schäfer, T. and Walz, G., 2015. SUMOylation blocks the ubiquitin-mediated degradation of the nephronophthisis gene product Glis2/NPHP7. *PLoS ONE* [Online], 10(6), pp.1–16. Available from: https://doi.org/10.1371/journal.pone.0130275.

Ranf, S., 2016. Immune Sensing of Lipopolysaccharide in Plants and Animals: Same but Different. *PLoS Pathogens* [Online], 12(6), pp.1–7. Available from: https://doi.org/10.1371/journal.ppat.1005596.

Ranf, S., 2017. Sensing of molecular patterns through cell surface immune receptors. *Current Opinion in Plant Biology* [Online], 38, pp.68–77. Available from: https://doi.org/10.1016/j.pbi.2017.04.011.

Ravensdale, M., Bernoux, M., Ve, T., Kobe, B., Thrall, P.H., Ellis, J.G. and Dodds, P.N., 2012. Intramolecular Interaction Influences Binding of the Flax L5 and L6 Resistance Proteins to their AvrL567 Ligands. *PLoS Pathogens* [Online], 8(11) (), November. Ed. by J.-R. Xu, e1003004. Available from: https://doi.org/10.1371/journal.ppat.1003004.

Ren, J., Gao, X., Jin, C., Zhu, M., Wang, X., Shaw, A., Wen, L., Yao, X. and Xue, Y., 2009. Systematic study of protein sumoylation: Development of a site-specific predictor of SUMOsp 2.0. *PROTEOMICS*

[Online], 9(12), pp.3409–3412. Available from: https://doi.org/10.1002/pmic.200800646.

Robatzek, S., Bittel, P., Chinchilla, D., Kchner, P., Felix, G., Shiu, S.H. and Boller, T., 2007. Molecular identification and characterization of the tomato flagellin receptor LeFLS2, an orthologue of Arabidopsis FLS2 exhibiting characteristically different perception specificities. *Plant Molecular Biology* [Online], 64(5), pp.539–547. Available from: https://doi.org/10.1007/s11103-007-9173-8.

Römer, P., Hahn, S., Jordan, T., Strauß, T., Bonas, U. and Lahaye, T., 2007. Plant Pathogen Recognition Mediated by Promoter Activation of the Pepper Bs3 Resistance Gene. *Science* [Online], 318(5850), pp.645–648. Available from: https://doi.org/10.1126/science.1144958.

Ron, M. and Avni, A., 2004. The Receptor for the Fungal Elicitor Ethylene-Inducing Xylanase Is a Member of a Resistance-Like Gene Family in Tomato. *The Plant Cell* [Online], 16(6), pp.1604–1615. Available from: https://doi.org/10.1105/tpc.022475.

Ruffel, S., Dussault, M.H., Palloix, A., Moury, B., Bendahmane, A., Robaglia, C. and Caranta, C., 2002. A natural recessive resistance gene against potato virus Y in pepper corresponds to the eukaryotic initiation factor 4E (eIF4E). *Plant Journal* [Online], 32(6), pp.1067–1075. Available from: https://doi.org/10.1046/j.1365-313X.2002.01499.x.

Ryder, L.S. and Talbot, N.J., 2015. Regulation of appressorium development in pathogenic fungi. *Current Opinion in Plant Biology* [Online],

26, pp.8–13. Available from: https://doi.org/10.1016/j.pbi.2015.05.013.

Saleh, A., Withers, J., Mohan, R., Marqués, J., Gu, Y., Yan, S., Zavaliev, R., Nomoto, M., Tada, Y. and Dong, X., 2015. Posttranslational Modifications of the Master Transcriptional Regulator NPR1 Enable Dynamic but Tight Control of Plant Immune Responses. *Cell Host & Microbe* [Online], 18(2), pp.169–182. Available from: https://doi.org/10.1016/j.chom.2015.07.005.

Sarris, P.F., Cevik, V., Dagdas, G., Jones, J.D.G. and Krasileva, K.V., 2016. Comparative analysis of plant immune receptor architectures uncovers host proteins likely targeted by pathogens. *BMC Biology* [Online], 14(1) (), December, p.8. Available from: https://doi.org/10.1186/s12915-016-0228-7.

Sarris, P.F., Duxbury, Z., Huh, S.U., Ma, Y., Segonzac, C., Sklenar, J., Derbyshire, P., Cevik, V., Rallapalli, G., Saucet, S.B., Wirthmueller, L., Menke, F.L., Sohn, K.H. and Jones, J.D., 2015. A plant immune receptor detects pathogen effectors that target WRKY transcription factors. *Cell* [Online], 161(5), pp.1089–1100. Available from: https://doi.org/10.1016/j.cell.2015.04.024.

Sato, Y., Shimizu, S., Ohtaki, A., Noguchi, K., Miyatake, H., Dohmae, N., Sasaki, S., Odaka, M. and Yohda, M., 2010. Crystal structures of the lumazine protein from Photobacterium kishitanii in complexes with the authentic chromophore, 6,7-dimethyl-8-(1â^2 − *D* − *ribityl*)*lumazine*, *anditsanalogues*, *ribo f lavinand f lavinmononucleotide*, *athighresolution*. *Journal of Bacteriology* [Online], 192(1), pp.127–133. Available from: https://doi.org/10.1128/JB.01015-09.

Schie, C.C. van and Takken, F.L., 2014. Susceptibility Genes 101: How to Be a Good Host. *Annual Review of Phytopathology* [Online], 52(1), pp.551–581. Available from: https://doi.org/10.1146/annurev-phyto-102313-045854.

Schlaich, N.L., 2007. Flavin-containing monooxygenases in plants: looking beyond detox. *Trends in Plant Science* [Online], 12(9), pp.412–418. Available from: https://doi.org/10.1016/j.tplants.2007.08.009.

Schleifenbaum, F., Elgass, K., Sackrow, M., Caesar, K., Berendzen, K., Meixner, A.J. and Harter, K., 2010. Fluorescence intensity decay shape analysis microscopy (FIDSAM) for quantitative and sensitive live-cell imaging: A novel technique for fluorescence microscopy of endogenously expressed fusion-proteins. *Molecular Plant* [Online], 3(3), pp.555–562. Available from: https://doi.org/10.1093/mp/ssp110.

Schmitt-Keichinger, C., 2019. Manipulating cellular factors to combat viruses: A case study from the plant eukaryotic translation initiation factors eIF4. *Frontiers in Microbiology* [Online], 10(FEB), pp.1–8. Available from: https://doi.org/10.3389/fmicb.2019.00017.

Sela, H., Spiridon, L.N., Petrescu, A.J., Akerman, M., Mandel-Gutfreund, Y., Nevo, E., Loutre, C., Keller, B., Schulman, A.H. and Fahima, T., 2012. Ancient diversity of splicing motifs and protein surfaces in the wild emmer wheat (Triticum dicoccoides) LR10 coiled coil (CC) and leucine-rich repeat (LRR) domains. *Molecular Plant Pathology* [Online], 13(3), pp.276–287. Available from: https://doi.org/10.1111/j.1364-3703.2011.00744.x.

Seto, D., Koulena, N., Lo, T., Menna, A., Guttman, D.S. and Desveaux, D., 2017. Expanded type III effector recognition by the ZAR1 NLR protein using ZED1-related kinases. *Nature Plants* [Online], 3(March), pp.25–28. Available from: https://doi.org/10.1038/nplants.2017.27.

Shao, F., Merritt, P.M., Bao, Z., Innes, R.W. and Dixon, J.E., 2002. A Yersinia effector and a Pseudomonas avirulence protein define a family of cysteine proteases functioning in bacterial pathogenesis. *Cell* [Online], 109(5), pp.575–588. Available from: https://doi.org/10.1016/S0092-8674(02)00766-3.

Shimomura, O., Johnson, F.H. and Saiga, Y., 1962. Extraction, Purification and Properties of Aequorin, a Bioluminescent Protein from the Luminous Hydromedusan,Aequorea. *Journal of Cellular and Comparative Physiology* [Online], 59(3), pp.223–239. Available from: https://doi.org/10.1002/jcp.1030590302.

Skelly, M.J., Malik, S.I., Le Bihan, T., Bo, Y., Jiang, J., Spoel, S.H. and Loake, G.J., 2019. A role for S-nitrosylation of the SUMO-conjugating enzyme SCE1 in plant immunity. *Proceedings of the National Academy of Sciences of the United States of America* [Online], 116(34), pp.17090–17095. Available from: https://doi.org/10.1073/pnas.1900052116.

Slootweg, E.J., Spiridon, L.N., Roosien, J., Butterbach, P., Pomp, R., Westerhof, L., Wilbers, R., Bakker, E., Bakker, J., Petrescu, A.-J., Smant, G. and Goverse, A., 2013. Structural Determinants at the Interface of the ARC2 and Leucine-Rich Repeat Domains Control the Activation of the Plant Immune Receptors Rx1 and Gpa2. *PLANT*

PHYSIOLOGY [Online], 162(3) (), July, pp.1510–1528. Available from: https://doi.org/10.1104/pp.113.218842.

Slootweg, E., Roosien, J., Spiridon, L.N., Petrescu, A.-J., Tameling, W., Joosten, M., Pomp, R., Schaik, C. van, Dees, R., Borst, J.W., Smant, G., Schots, A., Bakker, J. and Goverse, A., 2010. Nucleocytoplasmic distribution is required for activation of resistance by the potato NB-LRR receptor Rx1 and is balanced by its functional domains. *The Plant cell* [Online], 22(12), pp.4195–215. Available from: https://doi.org/10.1105/tpc.110.077537.

Spanu, P., Grosskopf, D.G., Felix, G. and Boller, T., 1994. The Apparent Turnover of 1-Aminocyclopropane-1-Carboxylate Synthase in Tomato Cells Is Regulated by Protein Phosphorylation and Dephosphorylation. *Plant physiology* [Online], 106(2), pp.529–535. Available from: https://doi.org/106/2/529[pii].

Stadler, C., Rexhepaj, E., Singan, V.R., Murphy, R.F., Pepperkok, R., Uhlén, M., Simpson, J.C. and Lundberg, E., 2013. Immunofluorescence and fluorescent-protein tagging show high correlation for protein localization in mammalian cells. *Nature Methods* [Online], 10(4), pp.315–323. Available from: https://doi.org/10.1038/nmeth.2377.

Steinbrenner, A.D., 2015. *Recognition, Activation, and Signaling Functions of the Arabidopsis NLR receptor RPP1*. PhD thesis.

Sukarta, O.C., Townsend, P.D., Llewelyn, A., Dixon, C.H., Slootweg, E.J., Pålsson, L.-O., Takken, F.L., Goverse, A. and Cann, M.J., 2020. A DNA-Binding Bromodomain-Containing Protein Interacts with and Reduces Rx1-Mediated Immune Response to Potato Virus X.

Plant Communications [Online], 1(4) (), July, p.100086. Available from: https://doi.org/10.1016/j.xplc.2020.100086.

Swiderski, M.R., Birker, D. and Jones, J.D.G., 2009. The TIR domain of TIR-NB-LRR resistance proteins is a signaling domain involved in cell death induction. *Molecular Plant-Microbe Interactions* [Online], 22(2), pp.157–165. Available from: https://doi.org/10.1094/MPMI-22-2-0157.

Takken, F.L.W. and Tameling, W.I.L., 2009. To nibble at plant resistance proteins. *Science (New York, N.Y.)* [Online], 324(5928), pp.744–746. Available from: https://doi.org/10.1126/science.1171666.

Takken, F.L.W. and Goverse, A., 2012. How to build a pathogen detector: Structural basis of NB-LRR function. *Current Opinion in Plant Biology* [Online], 15(4), pp.375–384. Available from: https://doi.org/10.1016/j.pbi.2012.05.001.

Talbot, N.J., 2003. On the Trail of a Cereal Killer: Exploring the Biology of Magnaporthe grisea. *Annual Review of Microbiology* [Online], 57(1), pp.177–202. Available from: https://doi.org/10.1146/annurev.micro.57.030502.090957.

Tameling, W.I.L. and Baulcombe, D.C., 2007. Physical association of the NB-LRR resistance protein Rx with a Ran GTPase-activating protein is required for extreme resistance to Potato virus X. *The Plant cell* [Online], 19(5), pp.1682–1694. Available from: https://doi.org/10.1105/tpc.107.050880.

Tameling, W.I.L., Elzinga, S.D.J., Darmin, P.S., Vossen, J.H., Takken, F.L.W., Haring, M.A. and Cornelissen, B.J.C., 2002. The Tomato

[Online]. 14(November), pp.2929–2939. Available from: https://doi.org/10.1105/tpc.005793.motif.

Tameling, W.I., Nooijen, C., Ludwig, N., Boter, M., Slootweg, E., Goverse, A., Shirasu, K. and Joosten, M.H., 2010. RanGAP2 mediates nucleocytoplasmic partitioning of the NB-LRR immune receptor rx in the solanaceae, thereby dictating Rx function. *Plant Cell* [Online], 22(12), pp.4176–4194. Available from: https://doi.org/10.1105/tpc.110.077461.

Tameling, W.I., Vossen, J.H., Albrecht, M., Lengauer, T., Berden, J.A., Haring, M.A., Cornelissen, B.J. and Takken, F.L., 2006. Mutations in the NB-ARC domain of I-2 that impair ATP hydrolysis cause autoactivation. *Plant Physiology* [Online], 140(4), pp.1233–1245. Available from: https://doi.org/10.1104/pp.105.073510.

Tamura, K., Imamura, M., Yoneyama, K., Kohno, Y., Takikawa, Y., Yamaguchi, I. and Takahashi, H., 2002. Role of phaseolotoxin production by Pseudomonas syringae pv. actinidiae in the formation of halo lesions of kiwifruit canker disease. *Physiological and Molecular Plant Pathology* [Online], 60(4), pp.207–214. Available from: https://doi.org/10.1006/pmpp.2002.0405.

Testa, O.D., Moutevelis, E. and Woolfson, D.N., 2009. CC+: A relational database of coiled-coil structures. *Nucleic Acids Research* [Online], 37(SUPPL. 1), pp.315–322. Available from: https://doi.org/10.1093/nar/gkn675.

Thompson, M. and Woodbury, N.W., 2001. Thermodynamics of specific and nonspecific DNA binding by two DNA-binding domains conjugated to fluorescent probes. *Biophysical Journal* [Online], 81(3),

pp.1793–1804. Available from: https://doi.org/10.1016/S0006-3495(01)75830-4.

Tör, M., Lotze, M.T. and Holton, N., 2009. Receptor-mediated signalling in plants: Molecular patterns and programmes. *Journal of Experimental Botany* [Online], 60(13), pp.3645–3654. Available from: https://doi.org/10.1093/jxb/erp233.

Townsend, P.D., Dixon, C.H., Slootweg, E.J., Sukarta, O.C., Yang, A.W., Hughes, T.R., Sharples, G.J., Pålsson, L.O., Takken, F.L., Goverse, A. and Cann, M.J., 2018. The intracellular immune receptor Rx1 regulates the DNA-binding activity of a Golden2-like transcription factor. *Journal of Biological Chemistry* [Online], 293(9), pp.3218–3233. Available from: https://doi.org/10.1074/jbc.RA117.000485.

Truman, W., De Zabala, M.T. and Grant, M., 2006. Type III effectors orchestrate a complex interplay between transcriptional networks to modify basal defence responses during pathogenesis and resistance. *Plant Journal* [Online], 46(1), pp.14–33. Available from: https://doi.org/10.1111/j.1365-313X.2006.02672.x.

Van Der Hoorn, R.A.L. and Kamoun, S., 2008. From guard to decoy: A new model for perception of plant pathogen effectors. *Plant Cell* [Online], 20(8), pp.2009–2017. Available from: https://doi.org/10.1105/tpc.108.060194.

Ve, T., Williams, S.J. and Kobe, B., 2015. Structure and function of Toll/interleukin-1 receptor/resistance protein (TIR) domains. *Apoptosis* [Online], 20(2), pp.250–261. Available from: https://doi.org/10.1007/s10495-014-1064-2.

Velásquez, A.C., Chakravarthy, S. and Martin, G.B., 2009. Virus-induced gene silencing (VIGS) in Nicotiana benthamiana and tomato. *Journal of Visualized Experiments* [Online], (28), pp.20–23. Available from: https://doi.org/10.3791/1292.

Vidhyasekaran, P., 2015. Ethylene Signaling System in Plant Innate Immunity [Online], pp.195–244. Available from: https://doi.org/10.1007/978-94-017-9285-1_4.

Vivian, J.T. and Callis, P.R., 2001. Mechanisms of tryptophan fluorescence shifts in proteins. *Biophysical journal* [Online], 80(5), pp.2093–2109. Available from: https://doi.org/10.1016/S0006-3495(01)76183-8.

Voinnet, O., Rivas, S., Mestre, P. and Baulcombe, D., 2003. Retracted: An enhanced transient expression system in plants based on suppression of gene silencing by the p19 protein of tomato bushy stunt virus. *The Plant Journal* [Online], 33(5), pp.949–956. Available from: https://doi.org/10.1046/j.1365-313X.2003.01676.x.

Vossen, J.H., Arkel, G. van, Bergervoet, M., Jo, K.-R., Jacobsen, E. and Visser, R.G.F., 2016. The Solanum demissum R8 late blight resistance gene is an Sw-5 homologue that has been deployed worldwide in late blight resistant varieties. *Theoretical and Applied Genetics* [Online], 129(9) (), September, pp.1785–1796. Available from: https://doi.org/10.1007/s00122-016-2740-0.

Walia, A., Guleria, S., Mehta, P., Chauhan, A. and Parkash, J., 2017. Microbial xylanases and their industrial application in pulp and paper biobleaching: a review. *3 Biotech* [Online], 7(1), pp.1–12. Available from: https://doi.org/10.1007/s13205-016-0584-6.

Wang, G., Roux, B., Feng, F., Guy, E., Li, L., Li, N., Zhang, X., Lautier, M., Jardinaud, M.F., Chabannes, M., Arlat, M., Chen, S., He, C., Noël, L.D. and Zhou, J.M., 2015. The Decoy Substrate of a Pathogen Effector and a Pseudokinase Specify Pathogen-Induced Modified-Self Recognition and Immunity in Plants. *Cell Host and Microbe* [Online], 18(3), pp.285–295. Available from: https://doi.org/10.1016/j.chom.2015.08.004.

Wang, J., Hu, M., Wang, J., Qi, J., Han, Z., Wang, G., Qi, Y., Wang, H.W., Zhou, J.M. and Chai, J., 2019. Reconstitution and structure of a plant NLR resistosome conferring immunity. *Science* [Online], 364(6435). Available from: https://doi.org/10.1126/science.aav5870.

Wang, J., Wang, J., Hu, M., Wu, S., Qi, J., Wang, G., Han, Z., Qi, Y., Gao, N., Wang, H.W., Zhou, J.M. and Chai, J., 2019. Ligand-triggered allosteric ADP release primes a plant NLR complex. *Science* [Online], 364(6435). Available from: https://doi.org/10.1126/science.aav5868.

Wendehenne, D., Lamotte, O., Frachisse, J.M., Barbier-Brygoo, H. and Pugin, A., 2002. Nitrate efflux is an essential component of the cryptogein signaling pathway leading to defense responses and hypersensitive cell death in tobacco. *Plant Cell* [Online], 14(8), pp.1937–1951. Available from: https://doi.org/10.1105/tpc.002295.

Whitfield, A.E., Falk, B.W. and Rotenberg, D., 2015. Insect vector-mediated transmission of plant viruses. *Virology* [Online], 479-480, pp.278–289. Available from: https://doi.org/10.1016/j.virol.2015.03.026.

Williams, S.J., Sohn, K.H., Wan, L., Bernoux, M., Sarris, P.F., Segonzac, C., Ve, T., Ma, Y., Saucet, S.B., Ericsson, D.J., Casey, L.W., Lonhienne, T., Winzor, D.J., Zhang, X., Coerdt, A., Parker, J.E., Dodds, P.N., Kobe, B. and Jones, J.D.G., 2014. Structural Basis for Assembly and Function of a Heterodimeric Plant Immune Receptor. *Science* [Online], 344(6181), pp.299–303. Available from: https://doi.org/10.1126/science.1247357.

Williams, S.J., Sornaraj, P., DeCourcy-Ireland, E., Menz, R.I., Kobe, B., Ellis, J.G., Dodds, P.N. and Anderson, P.A., 2011. An Autoactive Mutant of the M Flax Rust Resistance Protein Has a Preference for Binding ATP, Whereas Wild-Type M Protein Binds ADP. *Molecular Plant-Microbe Interactions* [Online], 24(8), pp.897–906. Available from: https://doi.org/10.1094/MPMI-03-11-0052.

Xue, J.Y., Wang, Y., Wu, P., Wang, Q., Yang, L.T., Pan, X.H., Wang, B. and Chen, J.Q., 2012. A primary survey on bryophyte species reveals two novel classes of nucleotide-binding site (NBS) genes. *PloS one* [Online], 7(5). Available from: https://doi.org/10.1371/journal.pone.0036700.

Yu, X., Feng, B., He, P. and Shan, L., 2017. From Chaos to Harmony: Responses and Signaling upon Microbial Pattern Recognition. *Annual review of phytopathology* [Online], 55, pp.109–137. Available from: https://doi.org/10.1146/annurev-phyto-080516-035649.

Yue, J.X., Meyers, B.C., Chen, J.Q., Tian, D. and Yang, S., 2012. Tracing the origin and evolutionary history of plant nucleotide-binding site-leucine-rich repeat (NBS-LRR) genes. *New Phytologist* [Online], 193(4), pp.1049–1063. Available from: https://doi.org/10.1111/j.1469-8137.2011.04006.x.

Zhang, J., Li, W., Xiang, T., Liu, Z., Laluk, K., Ding, X., Zou, Y., Gao, M., Zhang, X., Chen, S., Mengiste, T., Zhang, Y. and Zhou, J.M., 2010. Receptor-like cytoplasmic kinases integrate signaling from multiple plant immune receptors and are targeted by a Pseudomonas syringae effector. *Cell Host and Microbe* [Online], 7(4), pp.290–301. Available from: https://doi.org/10.1016/j.chom.2010.03.007.

Zhao, H., Tan, Z., Wen, X. and Wang, Y., 2017. An improved syringe agroinfiltration protocol to enhance transformation efficiency by combinative use of 5-azacytidine, ascorbate acid and tween-20. *Plants* [Online], 6(1), p.444. Available from: https://doi.org/10.3390/plants6010009.

Zhong, Z., Marcel, T.C., Hartmann, F.E., Ma, X., Plissonneau, C., Zala, M., Ducasse, A., Confais, J., Compain, J., Lapalu, N., Amselem, J., McDonald, B.A., Croll, D. and Palma-Guerrero, J., 2017. A small secreted protein in Zymoseptoria tritici is responsible for avirulence on wheat cultivars carrying the Stb6 resistance gene. *New Phytologist* [Online], 214(2), pp.619–631. Available from: https://doi.org/10.1111/nph.14434.

Zhou, H., Li, S., Deng, Z., Wang, X., Chen, T., Zhang, J., Chen, S., Ling, H., Zhang, A., Wang, D. and Zhang, X., 2007. Molecular analysis of three new receptor-like kinase genes from hexaploid wheat and evidence for their participation in the wheat hypersensitive response to stripe rust fungus infection. *Plant Journal* [Online], 52(3), pp.420–434. Available from: https://doi.org/10.1111/j.1365-313X.2007.03246.x.

Zhu, M., Jiang, L., Bai, B., Zhao, W., Chen, X., Li, J., Liu, Y., Chen, Z., Wang, B., Wang, C., Wu, Q., Shen, Q., Dinesh-Kumar, S.P. and

Tao, X., 2017. The intracellular immune receptor Sw-5b confers broad-spectrum resistance to tospoviruses through recognition of a conserved 21-amino acid viral effector epitope. *Plant Cell* [Online], 29(9), pp.2214–2232. Available from: https://doi.org/10.1105/tpc.17.00180.

Zipfel, C., Kunze, G., Chinchilla, D., Caniard, A., Jones, J.D.G., Boller, T. and Felix, G., 2006. Perception of the Bacterial PAMP EF-Tu by the Receptor EFR Restricts Agrobacterium-Mediated Transformation. *Cell* [Online], 125(4), pp.749–760. Available from: https://doi.org/10.1016/j.cell.2006.03.037.

Zipfel, C. and Oldroyd, G.E., 2017. Plant signalling in symbiosis and immunity. *Nature* [Online], 543(7645), pp.328–336. Available from: https://doi.org/10.1038/nature22009.

Zipfel, C., Robatzek, S., Navarro, L., Oakeley, E.J., Jones, J.D., Felix, G. and Boller, T., 2004. Bacterial disease resistance in Arabidopsis through flagellin perception. *Nature* [Online], 428(6984), pp.764–767. Available from: https://doi.org/10.1038/nature02485.